AN EXPERIMENTAL STUDY OF PRESSURE DROP CHARACTERISTICS IN VERTICAL UPWARD TWO PHASE AND THREE PHASE FLOWS

SRI SAILA MALLIKARJUNAN KUTTUVA RAMALINGAM VIJAYAKUMAR

(*B.Eng., Anna University*)

A THESIS SUBMITTED FOR THE DEGREE OF MASTER OF ENGINEERING

DEPARTMENT OF MECHANICAL ENGINEERING

NATIONAL UNIVERSITY OF SINGAPORE

2014

DECLARATION

I hereby declare that the thesis is my original work and it has been written by me in its entirety. I have duly acknowledged all the sources of information which have been used in the thesis.

This thesis has also not been submitted for any degree in any university previously.

Sri Saila Mallikarjunan

07 July 2014

ACKNOWLEDGEMENTS

It is my pleasure to express my sincere appreciation and gratitude to my supervisors, Prof. Nhan Phan-Thien and Prof. Khoo Boo Cheong for their able guidance throughout the course of my research work. Their wise counsel and consistent support during my study helped me to transform into an independent researcher.

I wish to thank Dr. Lin Yuan, Dr. Hien Luong and Dr. Karri Badarinath for guiding me in handling the rheometer and high-speed camera without which this research work would have been impossible.

I wish to thank Assoc. Prof. Lim Siak Piang and Assoc. Prof. S H Winoto for appointing me as their Graduate Tutor, which helped me in honing my interpersonal skills and financially supporting my Masters' Program.

I am also indebted to all staff of Fluid Mechanics lab II especially Mr. Yap, Mr. Tan, Ms. Cheng Fong and Ms. Iris for their help during my experimental work.

I would like to thank my parents and my roommates for providing me a conducive environment to work.

Table of Contents

ABSTRACT

The flow of multiphase mixture is encountered in numerous industrial, energy transfer process and especially in oil and gas transportation sector. Transportation of multiphase oil and gas mixture form wellbore to onshore production facility has many issues associated with it. One of the main issues associated with multiphase transportation is pressure drop. In this current work, a small scale three phase test loop was designed and constructed. The test loop is capable of conducting two phase (liquid-liquid) and three phase (liquid-liquid-gas) pressure drop measurement in vertical pipe. The two phase pressure drop experiment was conducted focusing on the phase inversion phenomenon. The three phase pressure drop experiment was conducted in slug flow and churn flow regimes and the effects of gas superficial velocity on the components of pressure drop (frictional and hydrostatic) was examined. Flow visualization technique using high-speed camera is used for identification of flow regime and to deduce essential information such as slug length, bubble rise velocity and slug frequency. Rheological characterization of emulsion sample for different oil concentration was performed using HAAKE MARS III Rheometer.

List of Tables

List of Figures

List of Symbols

η_r – relative viscosity

ϕ – volume fraction of dispersed phase

K - ratio of dispersed phase viscosity to continuous phase viscosity

ϕ_m – maximum packing fraction of dispersed phase

ε_o^l – oil holdup at inversion point

μ - dynamic viscosity of oil phase

ρ - density

D – internal diameter of pipe

C_o, C_w, n_o, n_w - parameters from Blasius friction factor equation

d_{32} – Sauter mean diameter

s – wetted perimeter

θ – water wettability angle

σ - oil–water interfacial tension

χ – Lockhart-Martinelli parameter

$\frac{dP}{dz}$ – pressure gradient

f - friction factor

G_T – mass velocity based on total flow rate of liquid plus gas

R – local volume fraction of liquid

ϵ – volume fraction of oil phase

τ_{wo} – wall shear stress

γ_w – wall shear rate

Q – volume flow rate

$\dot{x}$ – multiphase mixture quality

Subscript

o – oil phase

w – aqueous phase

m – oil-water mixture

L – liquid phase

G – gas phase

T – Total

B – body force

f – friction force

Chapter 1

Introduction

1.1 Multiphase flow - general

In general a fluid flow can be classified into two broad types based upon the number of immiscible phases that are considered into study: single phase flow and multiphase flow. A single phase flow is the one in which the entire flow is composed of same fluid whereas a multiphase flow is the simultaneous flow of materials with different phases or materials with different physical properties but in the same state such as in liquid-liquid systems (emulsions). In some cases, the system although composed of more than one phase can be treated as homogeneous and some properties can be averaged in a simple manner in such a way that it is most widely accepted. However in nature and in a multitude of other settings, the flow is multiphase such as air flow in the atmosphere in which particulate suspensions are dispersed in a random fashion wherein the system can be treated as a single phase system and in some cases like blood flow in veins, mere approximation into single phase approximation leads to a Newtonian fluid, whereas the suspension may display some viscoelastic properties, for example.

1.2 Background of the study

Multiphase pipeline flows are frequently encountered in oil and gas transportation, fluidized bed reactors, refrigerant coils, scrubbers, dryers, etc. Multiphase pipeline flow is often characterized by the flow of liquids and gases

simultaneously. In some scenarios, suspended particles (sand grains) may also be carried along the fluid flow. During the early stages of a production well, the well produces single phase crude oil however, within a short span of production life, the well starts to produce water and natural gas along with the crude oil. Thus if the multiphase flow mechanics are well understood, subsea production from satellite installation and subsequent transportation of unprocessed oil and gas to nearby platforms or directly to onshore facilities could be handled more appropriately.

For depleting oil wells, where the natural reservoir pressure is insufficient to drive the crude oil to the surface, artificial lift techniques such as gas lift technique is employed to recover the oil from the reservoir. The power required to lift oil, optimal gas injection pressure and flow rate can be predicted within acceptable range of accuracy if the pressure drop profile of the gas lift well is known before handed (Tek (1961)).

1.3 Problems associated with multiphase flows:

Problems associated with the simultaneous flow of two or more phases in transport pipeline are of long standing interest in the oil and gas transport industry. Some of the common problems associated with multiphase transportation are slugging, hydrate formation, unpredictable pressure drop during flow, etc.

1.3.1 Slugging:

The problem of slug flow persists in many industrial processes such as oil and gas production wells and during their transportation to onshore facilities, steam production in geothermal wells, transportation and handling of cryogenic fluids, boiling and condensation processes in power generation facilities as well as in chemical plants and refineries and coolant pipelines in nuclear reactors. Slug flow in pipelines can be broadly classified in to hydrodynamic slug flow and severe slug flow. The mechanism of formation of above two differs significantly. In general, hydrodynamic slug flow is a result of Kelvin-Helmholtz instability that induces fluctuation in the interface between gas and liquid (Wallis and Dodson (1973). However the formation of riser based slugging (or) severe slugging is mainly due to the undulations in the pipeline which forces the liquid to accumulate at the low points and block the flow of gas until the pressure drop over the pipeline overcomes the hydrostatic head of the liquid in the riser which pushes the liquid slug out of the system (Schmidt et al. (1979)).

Slug flow causes undesirable effects such as intermittent periods of without liquid and gas followed by very high liquid and gas flow rates into the production system. Thus it leads to flow starvation of the production facility during slug accumulation and flooding during blowout (Storkaas et al. (2001)). These undesirable effects cause significant loss due to reduced production.

Table 1.1 Commonly followed slug mitigation practices and their drawbacks

Sl. No	Method	Drawbacks
1.	Installation of slug catchers (Haandrikman et al. (1999))	Leads to inappropriate design changes which cannot be employed to compact separation units
2.	Feed-forward control (Skogestad and Havre (1996))	Separator unit is used as buffer instead of actual separation and it is not very robust due to model uncertainty
3.	Pipeline choke (Xu et al. (1997))	Due to closing of choke too many number of times, the slug returns to the bottom of the pipe and even larger slug is formed

1.3.2 Pressure drop in pipelines:

In fluid transportation pipelines, pressure drop (or) head loss is mainly attributed to viscosity of the flowing fluid, velocity of flow, internal surface roughness of the pipe, length and diameter of the pipeline. All these factors can be put together in the Hagen-Poiseuille equation. This equation is valid only for Newtonian fluid in steady state, fully developed laminar flow.

For the case of multiphase flow, some properties like viscosity and holdup cannot be estimated by mere averaging properties since these properties are strongly dependent on the flow regime. The interaction between the phases is too complex that there is no single unified model to predict such properties over the whole

range of flow regimes. Additional complexities include non-Newtonian behavior, stability of emulsion, etc.

1.4 Objectives of current work:

The objectives of the current experimental work are to design and construct a three phase test loop to facilitate pressure gradient measurement in vertical pipeline system. The effects of liquid and gas superficial velocity on the components of pressure gradient are examined. In order to study the pressure gradient characteristics, the rheological characterization of the oil-water sample is to be ascertained. In order to identify the type of flow regime occurring for a given experimental conditions, flow visualization has to be done.

1.5 Scope of the current work:

In the current work, an experimental investigation of pressure drop characteristics in vertical upward two-phase and three-phase flow is conducted in a small scale test loop. The two-phase pressure gradient experiment was conducted focusing on the phase inversion phenomenon. The experiment is conducted with emulsions having wide range of viscosity, controlled by varying the concentration of oil and aqueous phase. Pressure gradient measurements are logged for various flow rates. The three-phase pressure gradient experiment was conducted in slug flow and churn flow regimes. Slug flow regime was observed and identified by characteristics Taylor bubbles and churn flow regime is identified by the characteristics upwash-down wash phenomenon. The identification was done with the help of high-speed photography technique. Rheological characterization of

emulsion sample for different oil concentration was performed using HAAKE MARS III Rheometer. All the measurements were done at room temperature (28^{o}C).

1.6 Organization of the thesis:

Chapter 1 draws a general outline of multiphase flow systems, problems associated with them, reasons for complexities and some mitigation measures. In Chapter 2, a detailed review of literature pertaining to flow regime in vertical gas-liquid flow, characteristics of slug and churn flow, viscosity models, pressure drop prediction models and phase inversion prediction models is presented. In Chapter 3, details of experimental facility, equipment and instrumentation are described. In Chapter 4, rheometry results, pressure gradient measurement in liquid-liquid and liquid-liquid-gas systems and flow visualization results are presented and discussed. Finally based on the results of Chapter 4, some conclusions are derived in Chapter 5.

Chapter 2

Literature Review

This chapter gives a general overview of common flow patterns that occur in concurrent flow of liquid and gas in vertical conduits, models capturing viscosity of suspensions and emulsions, phase inversion phenomenon and pressure drop prediction in two and three phase systems. The first viscosity prediction model was proposed by Einstein (1906) for infinitely dilute solid dispersions in liquid media. Subsequently many researchers developed models for liquid-liquid systems. Another interesting phenomenon occurring in simultaneous flow of two or more immiscible phases is the phase inversion, which can be viewed as a form of instability of the system with least stability at inversion point. Under-estimating this fact would lead to inaccurate estimation of energy loss in piping systems. Pressure drop prediction in multiphase systems has been studied by researchers for past six decades. Lockhart and Martinelli (1949) were the first to come up with a model for two phase, two component flow in pipes. Pressure gradient studies in vertical pipes were studied by Govier and Short (1958), Brown et al. (1960), Ueda (1958) and so on.

2.1 Flow regimes in vertical conduits

Some of the common flow regimes observed in vertical ducts are Dispersed bubble flow, Slug flow, Churn flow, Annular flow and Annular-mist flow. Besides these five common flow regimes, there are several other flow regimes

that exist in vertical ducts as well, depending upon the superficial velocities, pressure and temperature of gas and liquid.

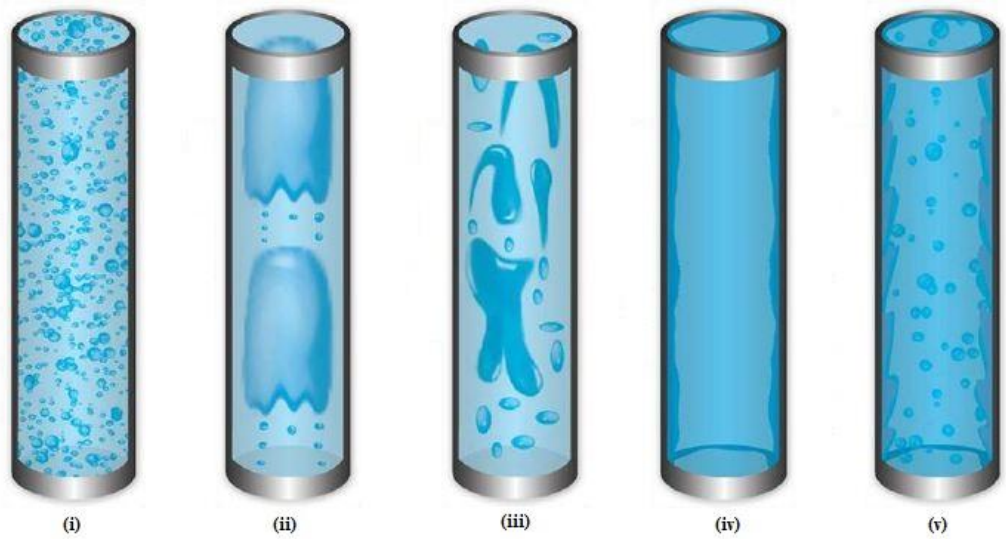

Figure 2.1 Gas-liquid flow regimes in vertical pipes ((i) Dispersed bubble flow, (ii) Slug flow, (iii) Churn flow, (iv) Annular flow and (v) Annular-mist flow) Bratland (2010)

2.1.1 General characteristics of slug flow

Gas-liquid slug flow can be defined as a sequence of pressure driven Taylor bubbles. These Taylor bubbles are elongated-bullet shaped with a thin film of liquid layer between the Taylor bubble and the pipe wall falling downwards and a liquid bridge flows between successive slugs. The length of the gas slug depends upon the gas flow rate. The slug length attains a maximum length at its transition to churn flow. According to Jayanti and Hewitt (1992), transition to churn flow depends four major criteria as follows: Entrance effect mechanism, Flooding mechanism, Wake effect mechanism and Bubble coalescence mechanism.

2.1.2 General characteristics of churn flow

This type of flow occurs in between slug and annular flow regimes. As the superficial velocity of the gas phase is increased, the Taylor bubble breaks down and the motion is random and unstable. In this type of flow, intermittent upward and downward flow of liquid phase can also be visualized. This is due to the balance of shear force of vapor phase and the combined effects of imposed pressure gradient gravitational force and falling liquid film attached to the pipe walls flowing downwards. In churn flow regime, as a result of the characteristic up wash-downwash phenomenon, there is an enormous variation in pressure gradient.

2.2 Flow pattern map for vertical gas-liquid flow

Flow pattern maps are pictorial description of the dependence of flow regimes on superficial quantities of gas and liquid such as mass flux, momentum flux, volume flux or any other quantity depending upon the author. A boundary between different flow regimes exist as the flow regime changes from one type to another due to growth of instabilities. Hence there exist a marginal error in such flow pattern map and shall be taken as a guideline in determining the flow regime. These patterns are generally developed using photographic visualization technique where both the phases are transparent and using spectral analysis of pressure field or void fraction fluctuation analysis for other cases. Fig. 2.2 shows flow pattern map for vertical air-water flow in 2.5 cm diameter pipe.

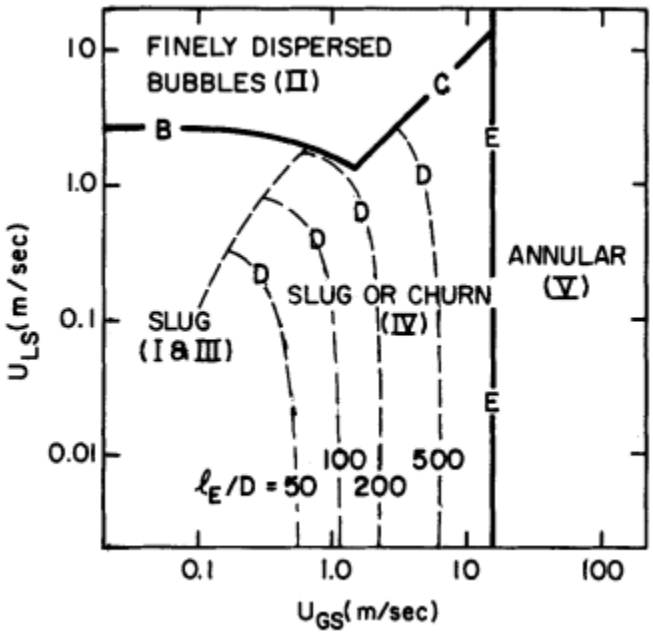

Figure 2.2 Flow pattern map for vertical gas-liquid flow presented by Taitel et al. (1980)

2.3 Experimental studies on multiphase flow

Some of the significant experimental studies conducted in flow of upward and/or downward oil-water systems are as follows as. Mukherjee et al. (1981) studied about the pressure gradient and water holdup in inclined pipes and reported about the sensitivity of inclination angle on maximum pressure gradient during phase inversion. Flores et al. (1998) conducted series of experiments pertaining to oil-water flow in vertical and inclined pipelines. They developed a model to predict the water holdup in vertical well bores using drift-flux model. Luo et al. (1997) studied about the influence of shear rate, temperature and effective viscosity of emulsion on pressure gradient in vertical pipeline flow. Abduvayt et al. (2004) studied about the flow pattern and water holdup in horizontal and slightly inclined pipelines whose inclination angle is in the range of 0.5^o and 3^o. They identified

some new flow patterns in hilly terrain profiles. Descamps et al. (2006) studied about the effects of gas injection in two phase system. Their studies shows at certain gas injection rates, the pressure gradient exceeds that of the two phase system. They also presented the results of bubble size on the adverse effects of pressure gradient. Hu and Angeli (2006) employed conductivity and HFA probes to study about the phase inversion region. In their study they proved with the help of drop size measurements that the interfacial energies of emulsion before and after phase inversion are not equal. Jana et al. (2007) conducted experimental study to test the validity of prediction models such as homogeneous model, drift-flux model and separated flow model.

2.4 Viscosity prediction model

Viscosity of a fluid is a measure of the amount of internal friction. It is primarily due to the cohesive forces between the molecules. It exists during fluid flow and it is essentially a friction force between different layers of fluid as they move past one another. When a tangential force is applied to a fluid particle, it begins to deform at a strain rate inversely proportional to the coefficient of dynamic viscosity of the fluid. This coefficient of dynamic viscosity (or perhaps simply viscosity) may or may not be constant throughout the range of applied shear stress or deformation. It is mainly this property that classifies entire family of liquids into Newtonian and non-Newtonian. There are fluids with constant viscosities but yet not Newtonian.

A wide range of literature is available for the prediction of apparent viscosity of emulsions. In general emulsions can be broadly classified into two types: oil-in-water type in which oil droplets are dispersed in water and water-in-oil type in which water droplets are dispersed in oil. The apparent viscosity of emulsions are viscosity and the density of continuous phase and dispersed phase, the phase volume fraction, the dispersed phase packing fraction, etc.

Einstein (1906) derived a model (Eq. 2.1) for predicting the apparent viscosity of infinitely dilute (~1-2%) suspensions. This model was basically derived for solid particles suspended in liquid media. But this model can be successfully applied to emulsions provided that the phase volume fraction (ϕ) tends to zero and there is no hydrodynamic interaction between the suspended droplets,

$$\eta_r = 1 + 2.5\phi. \tag{2.1}$$

Taylor (1932) extended Einstein's work of predicting apparent viscosity by considering actual liquid droplets suspended in another liquid media. The effect of surface tension of liquid droplet was also included in this model. In the following equation (Eq. 2.2), *K* is the ratio of dispersed phase viscosity to continuous phase viscosity. This expression reduces to Eq. 2.1 as $K \rightarrow \infty$:

$$\eta_r = 1 + \phi\left[\frac{5K+2}{2K+2}\right]. \tag{2.2}$$

Guth and Simha (1936) developed a model (Eq. 2.3) incorporating the droplet-droplet interaction. This model was basically an extension of Einstein's viscosity model as described in Eq. 2.1. This model also considers aspects such as

electroviscosity, wall effects, inertial effects and the influence of Brownian motion,

$$\boldsymbol{\eta_r = 1 + 2.5\phi + 14.1\phi^2}. \quad 2.3$$

Mooney (1951) developed a semi-empirical relation (Eq. 2.4) to predict the apparent viscosity of dilute suspension considering the effects of space-crowding of suspended spherical droplets and it can predict the non-Newtonian behavior of finite dilute suspensions and the range of empirical constant '*k*' is $1.35 < k < 1.91$. This model is an extension of Richardson (1933) model and agrees well with the experimental data at higher concentrations.

$$\boldsymbol{\eta_r = exp\left(\frac{2.5\phi}{1-k\phi}\right)}. \quad 2.4$$

Brinkman (1952) developed a model (Eq. 2.5) for relative viscosity by extending Einstein's viscosity model for highly concentrated suspensions of varied size distribution. This method is developed based on the assumption that the result of infinite dilution is known. This model is based on Vand (1948) hypothesis that collision of droplets suspended in the continuous media may also lead to the rise in apparent viscosity of the system,

$$\boldsymbol{\eta_r = (1-\phi)^{-2.5}}. \quad 2.5$$

Pal and Rhodes (1989) proposed as viscosity model (Eq. 2.6) especially for non-Newtonian emulsions if the shear rate is known from experimental data. This model also includes electroviscous effects. In their work they explained non-Newtonian behavior emulsions as described in Fig. 2.3. This model is applicable for emulsions in which the dispersed phased concentration is less than 74%. In the

following expression, $\phi(100)$ is the concentration of dispersed phase when the relative viscosity is 100,

$$\eta_r = \left[1 - \frac{0.8415}{\phi(100)}\phi\right]^{-2.5}. \quad 2.6$$

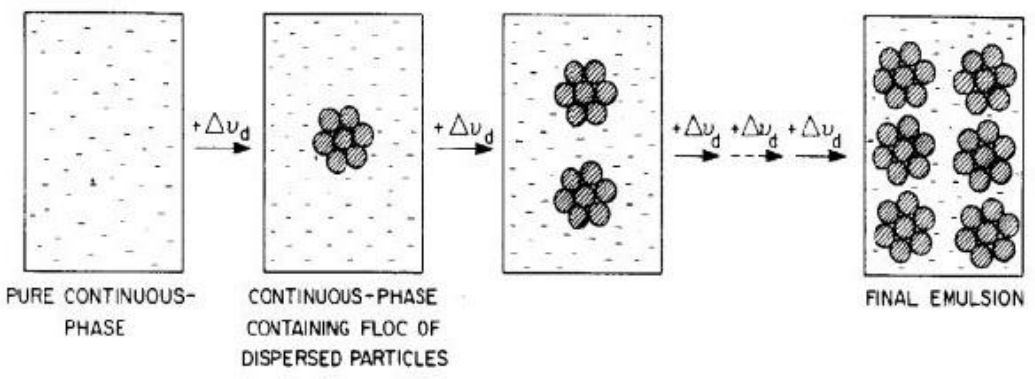

Figure 2.3 Schematic illustration of the process of non-Newtonian emulsion formation as described by Pal and Rhodes (Pal and Rhodes 1989)

Phan-Thien and Pham (1997) developed a viscosity model (Eq. 2.7) based on differential scheme for polydispersed suspensions and particulate solids. This model is constructed based on effective-medium theory which incorporates the local inhomogeneity. This model is an extension of Einstein's model to fit the low concentration emulsions.

$$\eta_r \left[\frac{2\eta_r + 5K}{2 + 5K}\right]^{1.5} = (1 - \phi)^{-2.5}. \quad 2.7$$

Pal (2000) proposed a viscosity model (Eq. 2.8) which fits the concentrated emulsions that covers a broad range of dispersed-phase to continuous-phase viscosity ratios (K). This model holds good for $4.15 \times 10^{-3} < K < 1.17 \times 10^{3}$. This model takes into consideration of the presence of surfactant which was ignored by previously proposed theoretical models. By considering this fact, the model takes into account of hydration of droplets due to the absorption of surfactants,

$$\eta_r \left[\frac{2\eta_r+5K}{2+5K}\right]^{1.5} = \left(1-\frac{\phi}{\phi_m}\right)^{-2.5}. \quad 2.8$$

Pal (2001) developed a viscosity model based on effective-medium theory. In this approach, the addition of an infinitesimal amount of particles leads to the next stage in which the suspensions are treated homogenous and thus lead to an effective increase in viscosity which follows Einstein's equation. This model takes into consideration of crowding effect by including maximum packing fraction term and the Model 1 described in Eq. 2.9 reduces to the Mooney equation (Eq. 2.4) as $K \rightarrow \infty$ and to Arrhenius equation when $\phi_m \rightarrow \infty$ and $K \rightarrow \infty$. In developing model 2 as described in Eq. 2.10, he assumes that as the concentration of dispersed phase is increased, the packing fraction also increases leading to increase in viscosity as described by Krieger and Dougherty (1959). This model can be simplified to Krieger and Dougherty's model as $K \rightarrow \infty$ and to Phan-Thien and Pham's model as $\phi_m = 1$:

$$\eta_r \left[\frac{2\eta_r+5K}{2+5K}\right]^{1.5} = exp\left(\frac{2.5\phi}{1-\phi/\phi_m}\right); \quad 2.9$$

$$\eta_r \left[\frac{2\eta_r+5K}{2+5K}\right]^{1.5} = \left(1-\frac{\phi}{\phi_m}\right)^{-2.5\phi_m}. \quad 2.10$$

2.5 Phase inversion prediction model

Phase inversion is a phenomenon in liquid-liquid dispersed systems, in which the external phase (continuous) inverts from oil to water spontaneously and vice versa. The reason behind this phenomenon is basically due to the instability of the dispersed phase droplets which coalesce and break-up at a critical packing fraction to invert into continuous phase. Another mechanism postulated for phase inversion phenomenon is that the system always tends to minimize the total free energy, which takes into account of gravitational potential energy and interfacial energy. The effects of dynamic forces may also eventually lead to inversion of phases.

The theory behind phase inversion in liquid-liquid dispersed systems has been studied by many authors in the past. According to Yeh et al. (1964), if no force other than surface tension is present between the two immiscible phases of the system, then inversion would have occurred at 50% of phase volume fraction. But due to the presence of other influential parameters such as density difference, viscosity difference, geometry, etc., in general, phase inversion would not occur at 50% phase volume fraction. Assuming zero shear at the interface of two immiscible phases, Yeh et al. (1964) proposed the following relationship between phase volume fraction at the point of inversion (ε_o^l) and the viscosities of the two immiscible liquids.

$$\boldsymbol{\varepsilon_o^l} = \frac{\left(\frac{\mu_o}{\mu_w}\right)^{0.5}}{1+\left(\frac{\mu_o}{\mu_w}\right)^{0.5}} . \qquad 2.11$$

The major limitation of this model is that, it is applicable only if both the liquids are Newtonian; it is not applicable if the density differences between the phases are not too high and the hydrodynamic behavior of the system should be dominated by inertial forces rather than viscous forces.

Arirachakaran et al. (1989) proposed a logarithmic relationship between input water/oil fractions required to invert the emulsion under laminar flow conditions as stated in Eq. 2.12. In their studies, they have described the inversion process as shown in Fig. 2.4,

$$\varepsilon_o^l = 0.5 + 0.1108\, log\left(\frac{\mu_o}{\mu_w}\right). \qquad 2.12$$

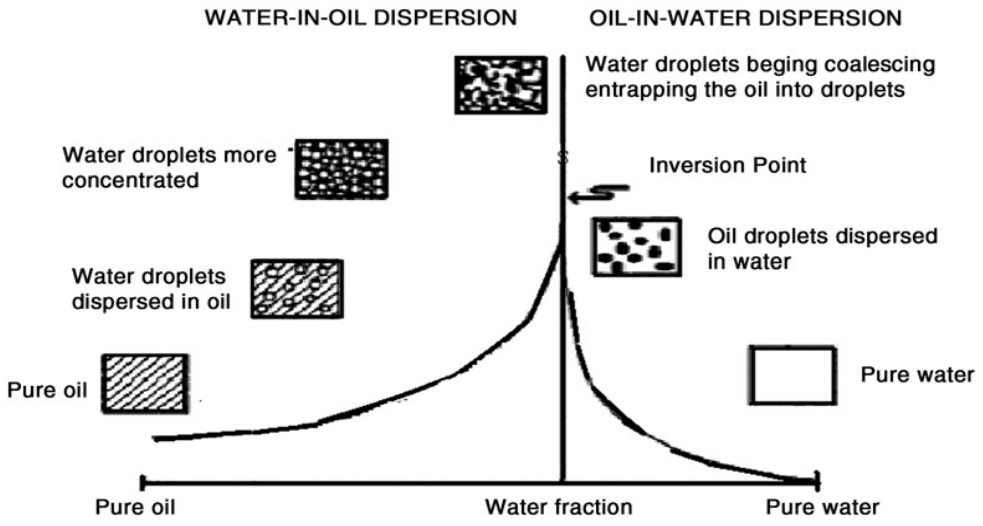

Figure 2.4 Phase inversion process in oil-water system as described by Arirachakaran et al.

The major limitation of this model is that, it can be applied only if both oil and aqueous phases flow in laminar flow regime. In the above formulation, the effects of interfacial tension, drop size distribution, and flow regime have not been considered.

Nädler and Mewes (1997) obtained an empirical correlation (Eq. 2.13) for critical oil holdup at which the system inverts. This model is based on the momentum equations for stratified flow. The assumption is that, there is no slip between the two immiscible phases and negligible interfacial shear between the two layers.

$$\varepsilon_o^l = 1 - \frac{1}{1+k_1\left[\frac{C_o\rho_o^{(1-n_o)}\mu_o^{n_o}}{C_w\rho_w^{(1-n_w)}\mu_w^{n_w}}(DU_m)^{(n_w-n_o)}\right]^{1/k_2}}. \quad 2.13$$

In the above expression, C_o, C_w, n_o, n_w are parameters from Blasius friction factor equation which is given by $f = CRe_m^{-n}$ and k_1 and k_2 are empirical parameters that reflects the in-situ contact perimeters and flow regime respectively. The above expression can be reduced to Eq. 2.11 by assuming k_1=1 and k_2=2.

Brauner and Ullmann (2002) developed a model (Eq. 2.14) by extending the Kolmogorov-Hinze model for the break-up of droplets in turbulent flow to the case of dense dispersions and combining with criterion of minimization of the total system energy. This model takes into consideration of free energy of continuous phase, dispersed phase as well as that at interface, wettability, effects of hysteresis loop and the existence of ambivalence region. This model is applicable for pipe flows and static mixers as well.

$$\varepsilon_o^l = \frac{[\sigma/d_{32}]_{w/o}+\frac{s}{6}\cos\theta}{[\sigma/d_{32}]_{w/o}+[\sigma/d_{32}]_{o/w}}, \quad 2.14$$

where θ is the water wettability angle, σ the oil–water interfacial tension, d_{32} the Sauter mean diameter which is the measure of the fineness of droplets. It can also be defined as the mean diameter wherein the ratio of volume to surface area is same as the entire ensemble and s the wetted perimeter of hydrophilic surface.

If the oil-water surface tension is assumed to be same before and after inversion, and if the effect of solid-liquid wettability is neglected, Eq. 2.14 can be reduced to the following expression,

$$\varepsilon_o^l = \frac{\left(\frac{\rho_o}{\rho_w}\right)\left(\frac{\mu_o}{\mu_w}\right)^{0.4}}{1+\left(\frac{\rho_o}{\rho_w}\right)\left(\frac{\mu_o}{\mu_w}\right)^{0.4}}. \quad 2.15$$

Poesio and Beretta (2008) proposed a model (Eq. 2.16) for prediction of phase inversion in liquid-liquid system in pipe flow based on minimal dissipation rate. This method is based upon estimation of two pressure drop curves (assuming oil as continuous phase and water as continuous phase) against all values of holdup ignoring the fact that the continuous phase system will not exist as continuous phase itself beyond a certain holdup value. The holdup value, at which these two curves intersect, is the critical holdup value for phase inversion.

$$\varepsilon_o^l = \frac{1-\left(\frac{\mu_o}{\mu_w}\right)^{-2/5k}+k\left(\frac{\mu_o}{\mu_w}\right)^{-2/5k}}{1+\left(\frac{\mu_o}{\mu_w}\right)^{-2/5k}} \quad 2.16$$

However, this prediction methodology could not capture the existence of ambivalent range in which either of the phases can exist as continuous phase and dispersed phase as well.

2.6 Pressure drop prediction model

Predicting pressure drop in multiphase flows has drawn more attention ever since long distance fluid transportation came to existence. Experimental works pertaining to pressure drop prediction models can be broadly categorized into models independent of flow regime and models dependent on flow regime. Early

studies were mainly focused on two phase flow systems comprising of air and water. Developing a model for accurate prediction of pressure drop may involve one or many of the following techniques.

1. Empirical or semi-empirical correlation
2. Correlations based on dimensional analysis
3. Correlations based on similarity analysis and model theory
4. Correlations using mass, momentum and energy conservation equations with approximate boundary conditions and empirical relation for turbulent transport terms
5. Mathematical analysis resulting in relating influential properties or terms

Lockhart and Martinelli (1949) presented a correlation for predicting pressure drop in pipe of two fluid two component flows. In their model, four different flow mechanisms in multiphase flows in pipe were correlated using a parameter (χ) which equals to the square root of ratio of pressure gradient of liquid to that of gas. In their model $\left(\frac{dP}{dz}\right)_f$ is the pressure drop in the pipeline if gas alone is flowing through it and ϕ_f^2 is the term, which is a function of non-dimensional parameter χ which is described previously,

$$\left(\frac{dP}{dz}\right)_F = \left(\frac{dP}{dz}\right)_f \phi_f^2. \tag{2.17}$$

$$\phi_f^2 = 1 + \frac{C}{\chi} + \frac{1}{\chi^2} \qquad C = \begin{cases} 5; laminar\ liquid - laminar\ vapor \\ 10; turbulent\ liquid - laminar\ vapor \\ 12; laminar\ liquid - turbulent\ vapor \\ 20;\ turbulet\ liquid - turbulent\ vapor \end{cases} \tag{2.18}$$

$$\chi^2 = \frac{(dP/dz)_l}{(dP/dz)_f} \quad 2.19$$

For two phase flows, in which the liquid phase is non-Newtonian, Farooqi and Richardson (1982) proposed a modified Lockhart-Martinelli parameter, which is obtained by multiplying a factor with χ. This factor takes care of the non-Newtonian shear thinning behavior of the liquid phase.

Dukler et al. (1964) developed a pressure drop prediction correlation based on similarity analysis starting with dynamic similarity in two phase flows. In this method parameters for two phase flows were developed using single phase flow parameters such as Reynolds number and Euler number. In this model, $\alpha(\lambda)$ is the ratio of the volumetric flow rate of liquid to the total volumetric flow rate as defined by Eq. 2.22 and β is the dimensionless group defined by Eq. 2.21

$$\frac{\partial P}{\partial z} = \frac{2G_T^2 f_o}{g_c D \rho_m} \alpha(\lambda)\beta, \quad 2.20$$

$$\beta = \frac{\rho_L}{\rho_m}\frac{\lambda^2}{R_L} + \frac{\rho_G}{\rho_m}\frac{(1-\lambda)^2}{R_G}, \quad 2.21$$

$$\alpha(\lambda) = 1 + \frac{-ln\,\lambda}{1.281 - 0.478(-ln\,\lambda) + 0.444(-\ln\lambda)^2 - 0.094(-\ln\lambda)^3 + 0.00843(-\ln\lambda)^4}. \quad 2.22$$

Hagedorn and Brown (1964) developed a model (Eq. 2.23) for predicting the pressure drop in vertical tubing from the data measured for a wide range of tubing size, gas-liquid ratio and properties such as density, mass flow rate and friction factor. This model does not take into consideration of different flow regime generated due to the injection of third phase. In this method, the holdup value

used to calculate the average mixture density was determined using the relation proposed by Griffith and Wallis (1961),

$$\mathbf{144}\frac{dP}{dz} = \bar{\rho}_m + \frac{f q_L^2 M^2}{2.96*10^{11} d^5 \bar{\rho}_m} + \bar{\rho}_m \frac{\bar{V}^2/2g_c}{dz}. \quad 2.23$$

Orkiszewski (1967) developed a model (Eq. 2.24) incorporating gas entrainment in liquid slug and liquid entrained in gas bubble. This model overcomes the difficulty faced by Griffith model at higher flow rates in slug regime,

$$\left(\frac{dP}{dz}\right)_F = 1.294 * 10^{-3} f \frac{\rho_l}{d}\left(\frac{V_{sl}}{\varepsilon_l}\right)^2. \quad 2.24$$

In this model the friction factor '*f* ' is determined from Moody diagram based on Reynolds number given by Eq. 2.25.

$$N_{Re} = \frac{\rho_l d}{\mu_l}\frac{V_{sl}}{\varepsilon_l} \quad 2.25$$

Friedel (1979) developed a correlation similar to Lockhart and Martinelli. In this model, a two phase multiplier is used to incorporate the effects of surface tension and viscosity. The surface tension effect is introduced by including liquid Weber number in Eq. 2.27 and the effects of viscosity is included by defining dimensionless factor *H*,

$$\left(\frac{dP}{dz}\right)_F = \left(\frac{dP}{dz}\right)_f \phi_{fr}^2, \quad 2.26$$

$$\phi_{fr}^2 = E + \frac{3.24FH}{Fr_H^{0.045} We_L^{0.035}}. \quad 2.27$$

In the above expression, *E, F, H,* Fr_H are dimensionless group as defined in Eq. 2.29, 2.30, 2.31 and 2.28 respectively

$$\boldsymbol{Fr_H = \frac{\dot{m}_{total}^2}{g d \rho_H^2}}, \quad 2.28$$

$$\boldsymbol{E = (1-x)^2 + x^2 \frac{\rho_L f_G}{\rho_G f_L}}, \quad 2.29$$

$$\boldsymbol{F = x^{0.78}(1-x)^{0.224}}, \quad 2.30$$

$$\boldsymbol{H = \left(\frac{\rho_L}{\rho_G}\right)^{0.91} \left(\frac{\mu_G}{\mu_L}\right)^{0.19} \left(1 - \frac{\mu_G}{\mu_L}\right)^{0.7}}. \quad 2.31$$

According to Hewitt and Whalley (1980), the above described correlation can be used with reasonable accuracy when $\mu_L/\mu_G < 1000$ and mass velocity less than 2000 kg/m^{2}s (The mass flow rate of fluid per unit area of cross-section).

Müller-Steinhagen and Heck (1986) proposed a correlation (Eq. 2.32) based on the single phase flow pressure drop. In this model the value of *C* was estimated from curve fitting of experimental data. The terms *A* and *B* denote the single phase pressure drop of liquid and gas respectively.

$$\boldsymbol{\left(\frac{dP}{dz}\right)_T = G(1-\dot{x})^{1/C} + B\dot{x}^C}, \quad 2.32$$

$$\boldsymbol{G = A + 2(B-A)\dot{x}}. \quad 2.33$$

Chapter 3

Experimental Facility, Material, Equipment and Instrumentation

3.1 Experimental test loop

Two phase and three phase flow experiments were conducted in a small scale flow loop at Fluid Mechanics Laboratory, National University of Singapore. The test section (refer to Fig. 3.1) consists of a 2 m long vertical transparent Perspex pipe of internal diameter 25 mm. The bottom end of the vertical test section is connected to a T-junction. Liquid phase (oil-water mixture) is injected from one side of T-junction and gas phase is injected from the other side. Liquid phase is stored in a tank of dimension 40 x 40 x 40 cm. A flexible impeller pedestal pump, supplied by JABSCO is used to pump the liquid mixture at desired flow rate into the test section. A FLOMEC positive displacement flow meter is installed between the pump and the T-junction to estimate the flow rate of liquid mixture flowing through the test section. After passing through the test section, liquid phase is discharged to the buffer tank to get rid of aeration problems. From the buffer tank, the liquid mixture which is free of air is transferred to the storage tank via a short pipeline with a globe valve. An in-house twin cylinder reciprocating air compressor is used to supply compressed air at desired pressure. The flow rate and pressure of compressed air is controlled using a Rota meter and a pressure regulator respectively. Pressure drop measurements were taken using a capacitive

type wet-wet differential pressure transducer supplied by Setra. The schematic of experimental flow loop is as follows.

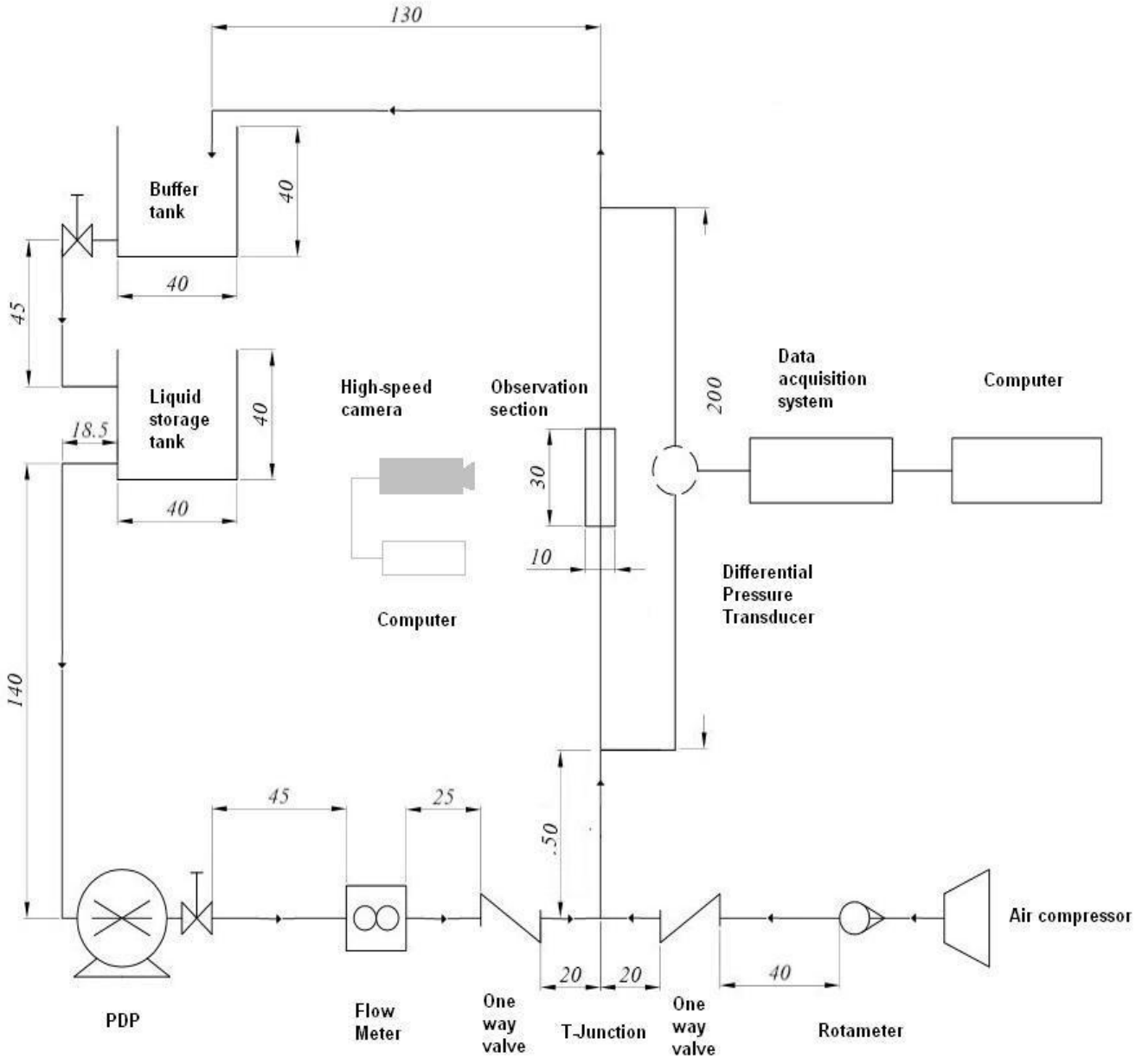

Figure 3.1 Schematic of three phase test loop facility (all dimensions in cm)

Extensive review work of Durst et al. (2005) on flow development length is shown in pictorial form in Fig. 3.2. The ratio of development length to pipe diameter is a function of Reynolds number. The value of constant 'C' basically depends upon the assumption and method used to arrive at. Although the authors have claimed that these results are applicable only for Re → 0 and Re → ∞, the authors have developed their own analytical correlation for flow development length (Eq. 3.1)

$$\frac{L}{D} = [0.619^{1.6} + (0.0567\ Re)^{1.6}]^{1/1.6} \qquad 3.1$$

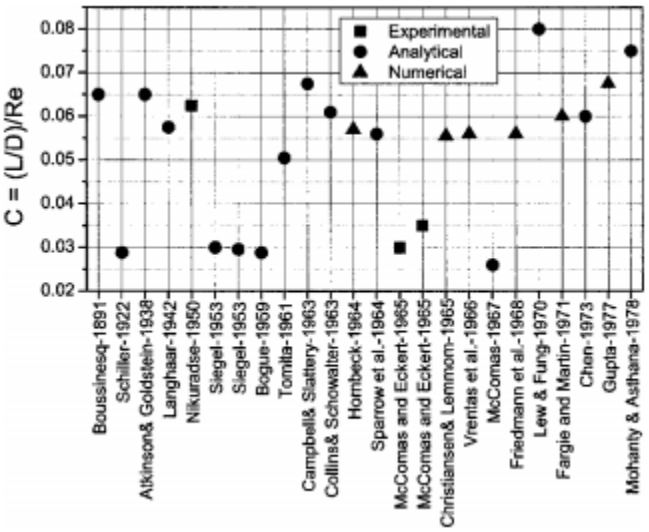

Figure 3.2 The constants C relationship between Re and the ratio of development length and pipe diameter

Thus for fluid flow of low Reynolds number (50 ≤ Re ≤ 300), the L/D ratio is in the range of 5 to 16. In our experimental setup, the high port of pressure transducer is connected to the tapping at 0.5 m (~20D) from T-junction. Hence the assumption of fully developed flow is valid.

3.2 Equipment

3.2.1 Materials

The oil phase used in this experiment is hydraulic oil (Tellus S2 M 68) supplied by Shell. The dynamic viscosity of oil is 0.12 Pa.s at 28^{o}C and density is 886 kg/m^{3} at 15^{o}C. The viscosity index of the oil determined according to ISO 2909 standard is 97. Normal tap water of dynamic viscosity 0.001 Pa.s at 20^{o}C and density of 1000 kg/m^{3} at 28^{o}C is used as aqueous phase. All the experiments were conducted without addition of any surfactants. For visualization purpose, Shell Tonna S2 M 68 was used as it is more transparent than Tellus S2 M 68.

3.2.2 Flow meter

The volumetric flow rate of pumped liquid mixture is measured using a FLOMEC oval gear medium capacity positive displacement flow meter. The flow of liquid inside the casing causes the oval gears to rotate in opposite directions. With each rotation of the gear, a fixed volume of liquid is displaced passing through the meter. Thus liquid travels around the crescent shaped chambers created by the rotational movement of the rotors. The rotors are embedded with magnets, which generates pulsed output depending upon the speed of rotation of the rotors. The range of this flow meter is 15 – 250 liters per minute with nominal size of 40 mm. The flow meter is equipped with an LED display, which reads us the value of flow rate. The accuracy of this flow meter is ± 0.25%.

3.2.3 Pump

Flexible impeller positive displacement pump is used to pump the liquid mixture in the test loop. The vanes of the impeller are flexible and it is mounted eccentrically inside the pump casing. The impeller is made of nitrile with a maximum discharge of 82 liters per minute at 1400 rpm. The pump can generate a maximum head of 18 m. Nitrile impeller is chosen in order to handle high viscous oil mixture. The pump is powered by a 1.1 kW single phase electric motor supplied by ELEKTRIM Motors and it is provided with a forced cooling fan. The volume flow rate of the pump is controlled by a Frequency converter supplied by WATT DRIVE ANTRIEBSTECHNIK GmbH. The volume flow rate is varied by controlling the speed of impeller.

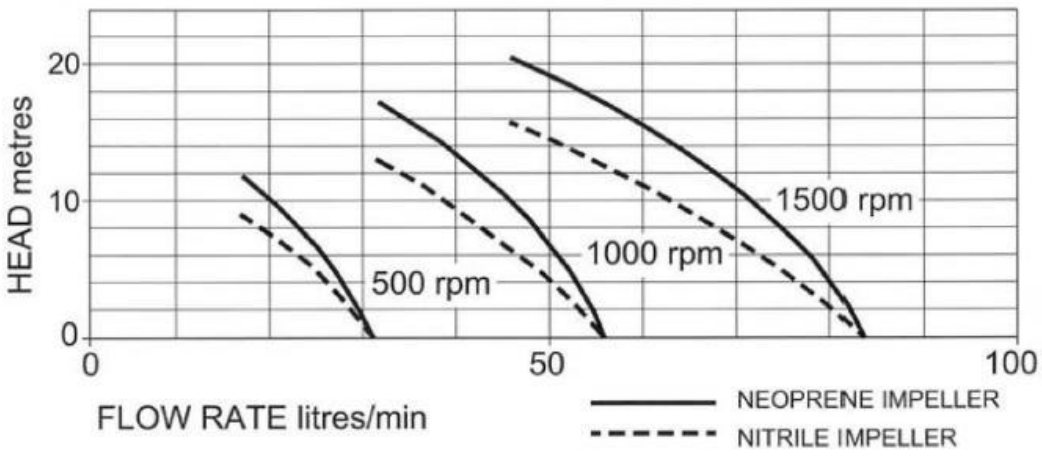

Figure 3.3 Performance curve of the flexible impeller pump

3.2.4 Mechanical homogenizer

A mechanical disperser supplied by IKA – Werke GmbH & Co. was used to prepare emulsion samples that were to be tested using Rheometer. It can be used

to homogenize samples up to 2 l. The speed range of the rotor is 3400 -25000 rpm. The dispersing element has a stator of diameter 18 mm and rotor of diameter 13.4 mm, which can handle viscosities up to 5000 mPas. The rotor acts as a centrifugal pump to recirculate the liquid and suspended solids through the generator, where shear, impact, collision, and cavitation provide rapid homogenization. It can produce fine emulsion in the range of 1 to 10 µm.

3.2.5 Differential Pressure Transducer

Pressure difference along the length of the test section is measured using a capacitive type wet-wet differential pressure transducer supplied by Setra. It works on the principle that as the pressure is applied on the electrode, the distance between the two electrodes decrease, which gives rise to variation in capacitance. This change in distance between electrodes is correlated to the change in pressure. The range of Setra M 230 transducer is 0 – 10 psi (0 – 68.94 kPa) with corresponding linear output of 4 – 20 mA. The transducer is equipped with inbuilt signal conditioning circuitry and hence no external signal conditioning is required. The transducer is connected to a desktop computer via NI data acquisition system for logging purpose. The frequency of data logging is 2 Hz. The transducer is energized with 20 V DC external power supply. The connecting tubes of the transducer are bleeded off air before initiating the measurements. This is done with the help of bleed screws provides at the back of the transducer.

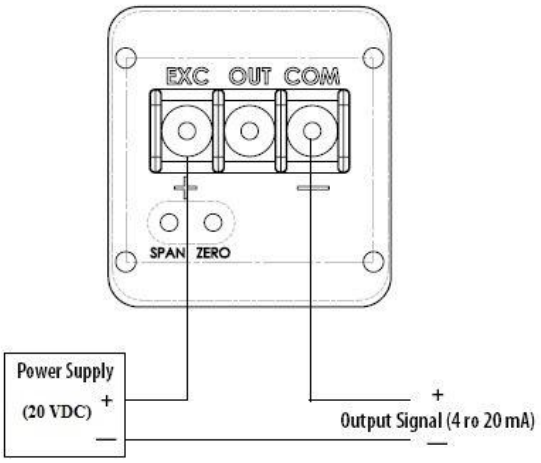

Figure 3.4 Wiring diagram of pressure transducer

3.2.5.1 Calibration of pressure transducer

Calibration of differential pressure transducer is done using 'Pipe Friction Flow rig' which is equipped with a mercury manometer. The range of mercury manometer is 0 – 50 cm of Hg (0 – 66.67 kPa). The procedure for calibration is as follows: The flow rig is operated at different flow rates and the corresponding head loss is initially estimated with mercury manometer and then the electrical output in terms of mA is logged with pressure transducer for corresponding flow rates. By comparing the corresponding head loss and recorded electrical signal for various flow rates, calibration graph can be plotted. Regression analysis of the plot shows that the output from the transducer is linear with regression factor (R^2) 0.9981. As we can see from the graph above (Fig. 3.5), the linear relationship between pressure difference and current output can be approximated as y = 4.818x – 17.458.

Table 3.1 Calibration table for pressure transducer

Sl. No	Flow rate (lpm)	Mercury Manometer Reading (cm)		Difference in height (cm)	Current output (mA)	Equivalent pressure in kPa	Equivalent pressure in psi
		A	B				
1	17	51.7	48	3.7	4.833	4.933	0.715
2	25.6	53.8	45.7	8.1	5.851	10.799	1.566
3	37.3	57.6	41.8	15.8	7.652	21.065	3.054
4	46.7	61.5	38	23.5	9.850	31.331	4.543
5	56.4	65.5	33.9	31.6	12.712	42.130	6.109
6	60.5	68.2	31	37.2	14.119	49.596	7.191
7	68.2	72.7	26.3	46.4	16.387	61.861	8.970
8	71.2	74.8	24.2	50.6	17.526	67.461	9.782

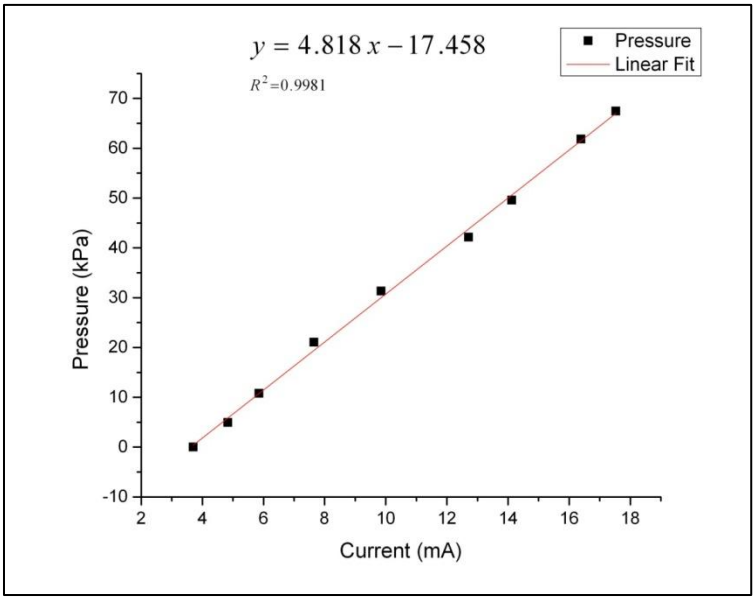

Figure 3.5 Calibration graph for pressure transducer

3.3 High-speed camera

High speed image/video recording is done using Photron FASTCAM SA5. The images/videos are captured at 5000 fps with shutter speed of 1/15000 s. The image/video resolution is 1024x1024. Backlit lighting was provided with Neon

lamp, supplied by Sumita Fiber Optics (Model: LS-M350) and the lighting source is dispersed using tracing paper. A square shaped hollow box filled with water is fabricated surrounding the visualization test section for avoiding image distortion. Image processing software, Photron Fastcam Viewer version .350 is used for measuring parameters such as slug length, slug frequency and bubble rise velocity and identification of flow regimes.

Figure 3.6 Photron FASTCAM-High speed camera

3.4 HAAKE MARS III Rheometer

The viscometric measurements were done using HAAKE MARS III Rheometer. This rheometer can be operated either in controlled stress (CS) mode or controlled shear rate (CR) mode. In this study all the measurements were taken in controlled shear rate (CR) mode.

Here a torque (M_d) applied to the measuring shaft and the rotational speed (the angular velocity Ω) of spindle are related to shear stress and rate of deformation by shear factor A and M respectively. These shear factors depends upon the geometries of rotor and spindle. The torque applied to the measuring shaft is

correlated to the current supplied to the drive motor (Drag-cup type) which has an extremely low moment of inertia of about 10 μNms^2. The torque measurement range is between 0.05μNm and 200 mNm with a resolution of 0.5 nNm. The motor shaft is supported by two radial bearings which prevent the shaft from tilting and one axial bearing for axial stiffness. The angular velocity is measured using optical technique. A line disc is attached to the drive spindle and an optical encoder is used to detect the impulses generated by the rotating disc per revolution. This generated impulse generated per revolution is correlated to the angular velocity. The minimum angular velocity in CR mode is 10^{-4} min^{-1} and maximum angular velocity is 1500 min^{-1} with an angular resolution of 12 nrad. Couette geometry is used for viscosity measurements and temperature was maintained at 28^oC throughout the experiment. The rheometer is equipped with Peltier temperature control module which can be used to control temperature in the range of -40^oC to 200^oC with an accuracy of ±0.1^oC.

Figure 3.7 HAAKE MARS III Rheometer

3.5 Experimental procedure

Pressure drop measurements were taken for two phase liquid-liquid flows and three phase liquid-liquid-gas flows in slug and churn flow regime. The experiment is started by filling hydraulic oil and tap water in the liquid storage tank without any premixing. Formation of well dispersed emulsion is induced by flow shear itself by allowing it to flow in a closed loop for a given amount of time. Russell et al. (1959), in their works had stated that the turbulent shear induced mixing in pipelines and associated piping components can well disperse the initially separated immiscible liquids. Homogenization of the mixture is ensured by density matching technique. For this, samples of mixture are taken from the tank and their densities are measured and compared with the theoretical value based up

on volume fraction of mixture. A density measuring bottle made of borosilicate glass along with an electronic weighing balance is used to measure the density of emulsion. The bottle volume has an accuracy of ± 0.001 mL of that of actual volume of the bottle. Measurements were initiated only when the difference between measured and theoretical densities are less than 5%. The range of liquid and gas flow rate for different flow regimes are provided in the following table.

Table 3.2 Superficial velocity specification for present experimental study

Sl. No	Type of Experiment	Liquid superficial velocity (m/s)	Gas superficial velocity (m/s)
1	Two phase flow	0.24 – 1.61	---
2	Three phase flow- Slug flow	0.24 – 1.00	0. 34– 0.85
3	Three phase flow- Churn flow	0.24	1.36 – 3.39

Pressure loss due to non-return valve on the gas end is analyzed and it is found to be negligible (14 Pa for maximum gas flow rate). Hence its effect on actual flow rate is assumed to be negligible. The pressure loss is calculated using $f = sg\left(\frac{Q}{C_v}\right)^2$. The value of C_v is supplied by the manufacturer. The pressure loss chart and C_v for various diameters has been provided in Appendix C.

Chapter 4

Experimental Results and Discussion

4.1 Rheological Characterization of emulsions:

Emulsion samples were prepared in batches of 50 mL using mechanical homogenizer and viscosity measurements were done using HAAKE MARS III Rheometer with couette geometry. Emulsions with different phase fractions (from 20% oil to 90% oil) were homogenized with at a speed of 6000 rpm for 10 minutes and were then transferred to the rheometer for viscosity measurement. Emulsion samples were subjected to shear rates between 0.1 s^{-1} and 1900 s^{-1} and temperature was maintained at 28 ± 0.1^{o}C.

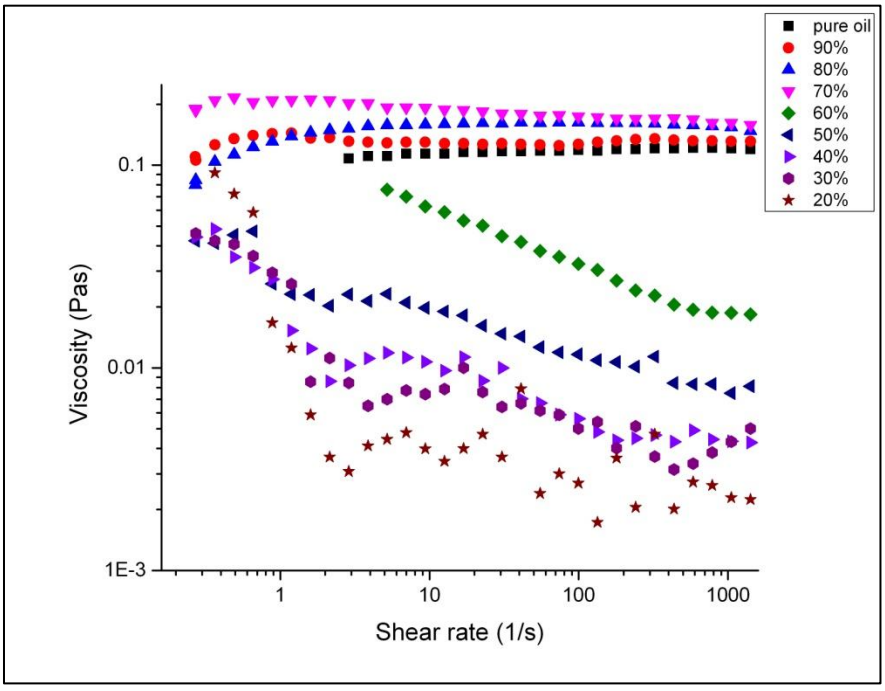

Figure 4.1 Rheogram of Emulsion of different concentration at T = 28^{o}C

From the rheogram (Fig. 4.1), it can be seen that pure oil shows Newtonian behavior, i.e., viscosity is independent of shear rate whereas for oil concentrations greater than 60% and lesser than 90%, the emulsion shows low degree of shear thinning behavior and for oil concentrations below 60%, the emulsion shows high degree of shear thinning behavior, i.e., viscosity sharply decreases with increase in shear rate. It can also be noted that, as the water cut is increased up to 30%, the viscosity increases and further increase in water cut results in huge fall in viscosity. The reason behind this phenomenon is phase inversion. Thus it can be noticed that the emulsion samples have different rheological properties based upon the phase fraction of dispersed and continuous phase. The results of apparent viscosity measurement in the rheometer are compared with that of flow rig in section 4.2.3.

4.2 Results of two phase flow experiment

The results of pressure gradient measurements in two phase liquid-liquid system are presented in this section. In this experiment, the two immiscible phases namely the aqueous and oil phase are initially stored in the liquid storage tank without any premixing. The mixture is emulsified and hence breakdown of molecules is induced entirely due to the shear of the pump. From Fig. 4.2 and Fig. 4.4, it can be seen that for a given concentration of emulsion, the piezometric and frictional pressure gradient increases gradually as the liquid flow rate is increased. It can also be noted from Fig. 4.3 and Fig. 4.5 that the frictional and hence piezometric pressure gradient of 60% emulsion is greater than 70% and the trend follows as 60% > 70% > 80% > 90%. In these concentrations of oil, the emulsion

is of water in oil (W/O) type where water droplets are dispersed in the oil phase. The apparent viscosity of the emulsion is increased as the concentration of dispersed phase is increased. This is due to increase in dissipative forces.

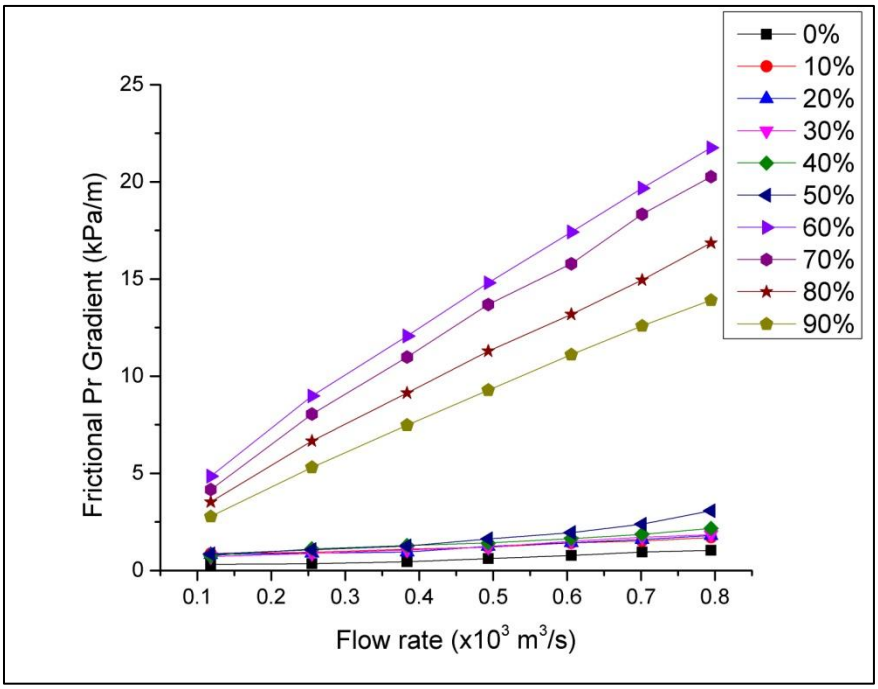

Figure 4.2 Plot of frictional pressure drop vs flow rate for different emulsion concentration

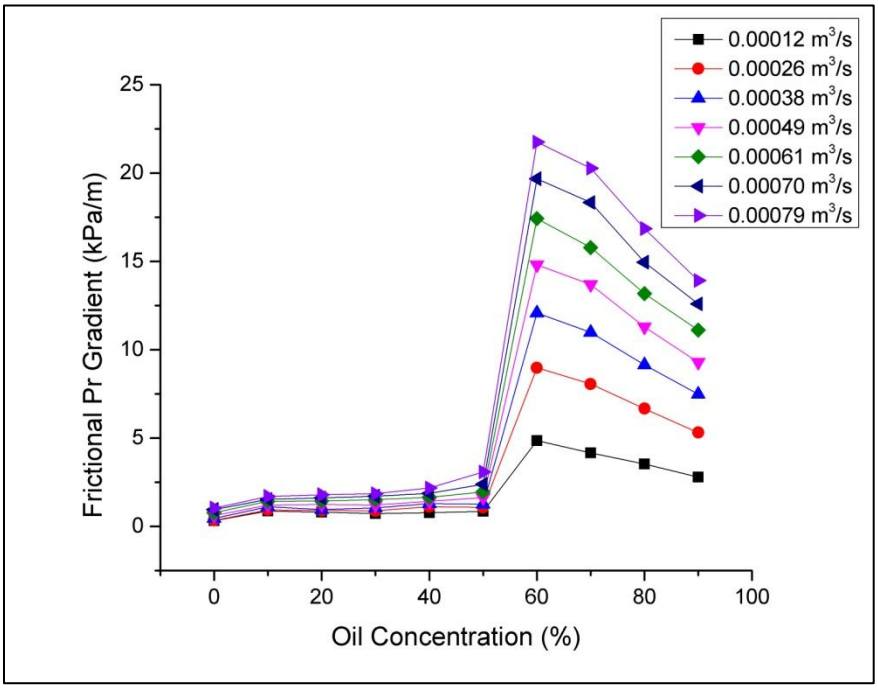

Figure 4.3 Plot of frictional pressure drop vs different emulsion concentration for different flow rate

For vertical upward fluid flow in pipelines, the total pressure gradient is attributed to body forces, frictional losses and acceleration component. Assuming the flow to be fully developed, the acceleration component tends to be zero. Thus total pressure drop is a combination of body force term and frictional loss term.

$$\left(\frac{dP}{dl}\right)_T = \left(\frac{dP}{dl}\right)_B + \left(\frac{dP}{dl}\right)_f \quad 4.1$$

where $\left(\frac{dP}{dl}\right)_f$ is the frictional pressure gradient that represents the energy required to overcome the drag of the fluids on the walls of pipeline and the energy required to overcome the slippage of phases and $\left(\frac{dP}{dl}\right)_B$ is the gravitational pressure drop (or) static energy gradient which is used to represent the energy required to support the fluid column in the pipeline, which is given by

$$\left(\frac{dP}{dl}\right)_B = \rho_m g \quad 4.2$$

where ρ_m is the oil-water mixture density based on the concentration of each phase and is given by,

$$\rho_m = \epsilon\rho_o + (1-\epsilon)\rho_w \quad 4.3$$

where ρ_o is the oil density, ρ_w is the water density and ϵ is the oil concentration. The reason behind sudden raise in pressure gradient value as the oil concentration is increased from 50 to 60% is that phase inversion has had happened. For oil concentrations less than 50%, the emulsion is of oil in water (O/W) type where the oil is dispersed phase and water is continuous phase whereas for oil concentrations greater than 60%, the emulsion is of water in oil (O/W) type where the water droplets are dispersed in the continuous oil phase. Thus when the emulsion type is switched from water continuous to oil continuous, apparent viscosity of the emulsion increases sharply which leads to higher fluid friction and eventually to higher pressure drop. This is supported by the results obtained by Arirachakaran et al. (1989). Lower pressure gradient for oil concentrations less than 60% is not only attributed to lower apparent viscosity of oil in water type of emulsion, but also high degree of shear thinning effect experienced by this type of emulsion at higher shear rates. This is supported by the discussion about rheogram in section 4.1.

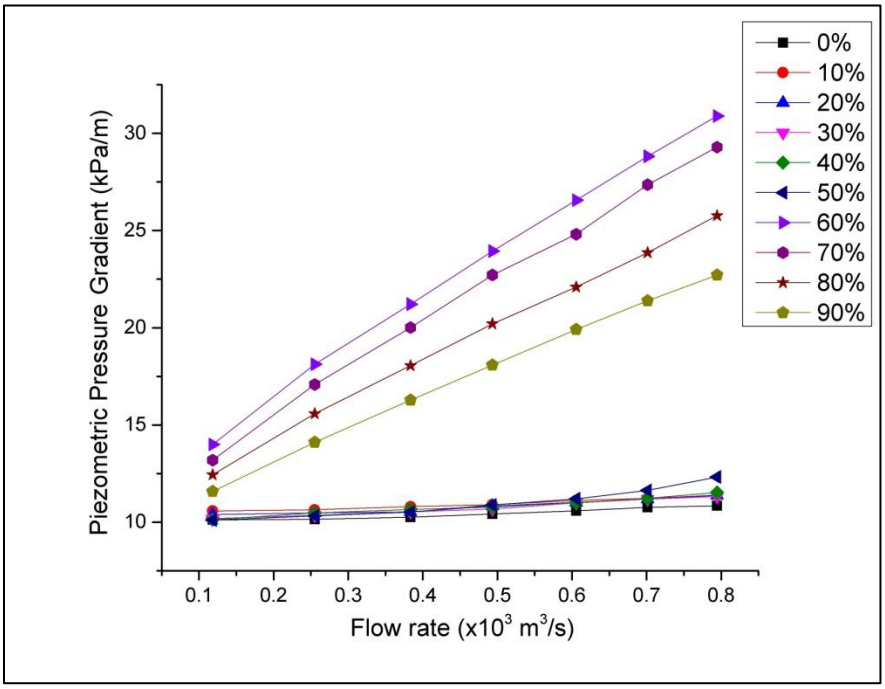

Figure 4.4 Plot of piezometric pressure drop vs flow rate for different emulsion concentration

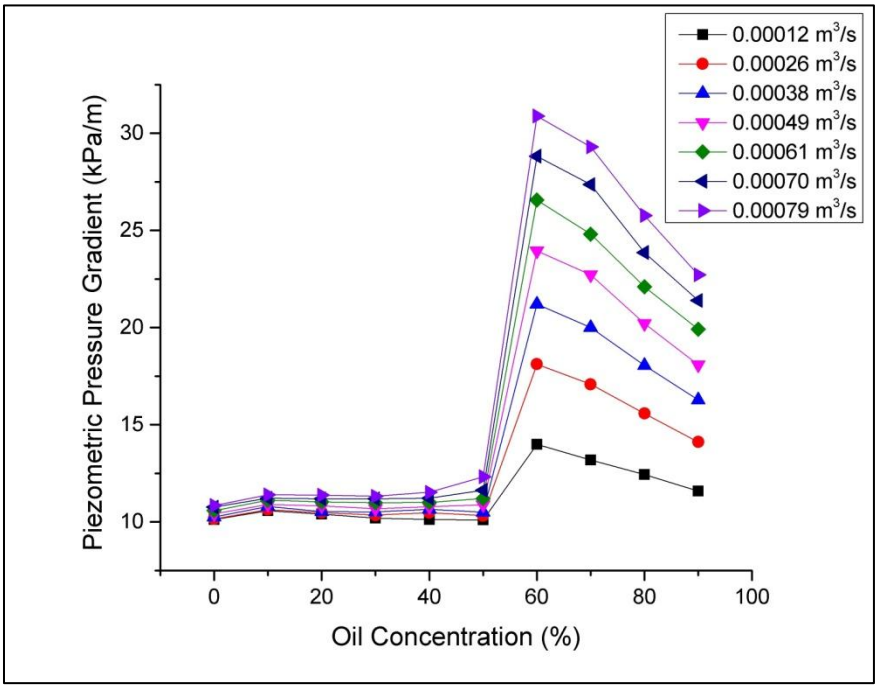

Figure 4.5 Plot of piezometric pressure drop vs different emulsion concentration for different flow rate

4.2.1 Significance of hydrostatic and frictional pressure drop in two phase system

For a two phase liquid-liquid system, if the piezometric pressure drop is resolved into hydrostatic and frictional pressure drop, significance of each component could be studied. From Fig. 4.6, it can be seen that for oil in water system, i.e. for oil concentrations less than 60%, hydrostatic pressure gradient is dominant than frictional pressure gradient and for water in oil system, i.e. for oil concentration greater than 60%, frictional component assumes more significance than hydrostatic component.

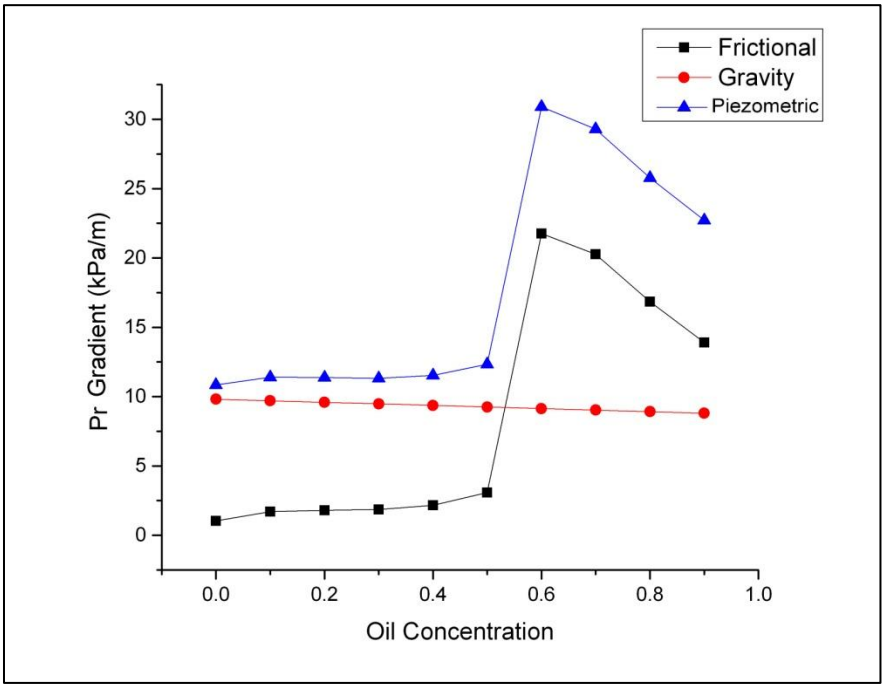

Figure 4.6 Components of two phase pressure drop at U_m = 1.61 m/s

4.2.2 Wall shear stress for two phase liquid-liquid flows

The expression for wall shear stress can be derived from Newton's second law of motion, which states that,

$$\boldsymbol{F_x = \frac{d(mV_x)}{dt}} \quad 4.4$$

Since we know that, for a fully developed flow, the acceleration of fluid particle tends to zero, the above equation can be written as $F_x = 0$. Thus it is merely a balance of all forces acting on the fluid particle.

Consider an inclined fluid cylinder, as shown in Fig. 4.7. The pressure force act on top and bottom end of the cylinder with cross sectional area πr^2, the component of body force ($W \sin\theta$) acts downward and viscous forces act along the circumferential area of the cylinder ($2\pi rdl$). Thus the force balance equation can be written as,

$$\boldsymbol{p_1\pi r^2 - (p_1 - dp)\pi r^2 - 2\pi r dl\tau(r) - \gamma\pi r^2 dl \sin\theta = 0} \quad 4.5$$

$$\boldsymbol{\frac{dp - \gamma dl \sin\theta}{dl} = \frac{2\tau(r)}{r}} \quad 4.6$$

Here, shear stress (τ) is a strong function of radial coordinate r. At the centerline of the pipe ($r = 0$), shear stress is zero and it has a maximum value at the pipe wall ($r = \frac{D}{2}$). Thus shear stress at $r = D/2$ is denoted as wall shear stress (τ_w).

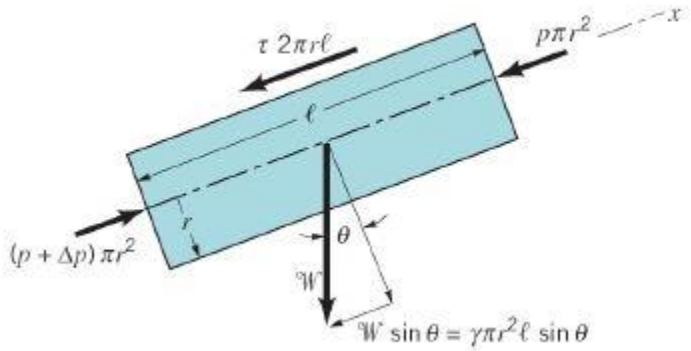

Figure 4.7 A schematic of cylindrical fluid element depicting various forces acting on it.

For vertical pipes (θ = 90^o), in addition to pressure forces acting on the cross sectional area, body forces also act downwards and thus Eq. 4.6 can be written as

$$\frac{dP}{dl} = \frac{4\tau_w}{D} + \rho_m g \qquad 4.7$$

where τ_{wo} is the wall shear stress and ρ_m the liquid mixture density.

The wall shear stress can be deduced from the velocity dependent pressure drop data from the following expression.

$$\tau_w(U) = \frac{D}{4}\left[\frac{dP}{dl}(U) - \frac{dP}{dl}(U = 0)\right] \qquad 4.8$$

where $\frac{dP}{dl}(U = 0)$ is the static pressure head along the liquid column.

From Fig. 4.8, it can be seen that wall shear stress is directly proportional to liquid flow rate. At higher liquid flow rates, the fluid experiences a higher drag, which is also a function of apparent viscosity of the emulsion.

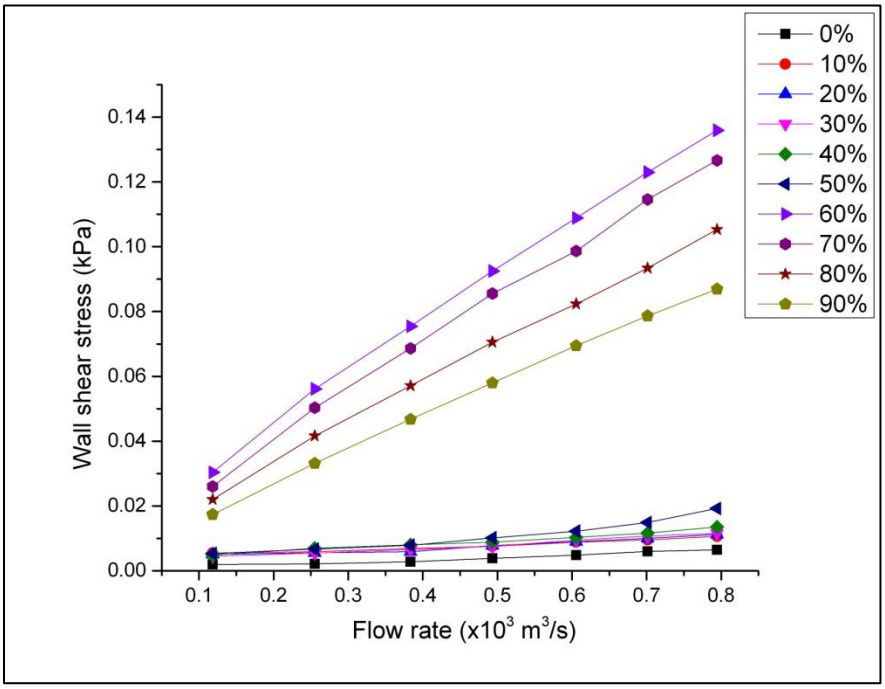

Figure 4.8 Plot of wall shear stress vs flow rate for different emulsion concentration

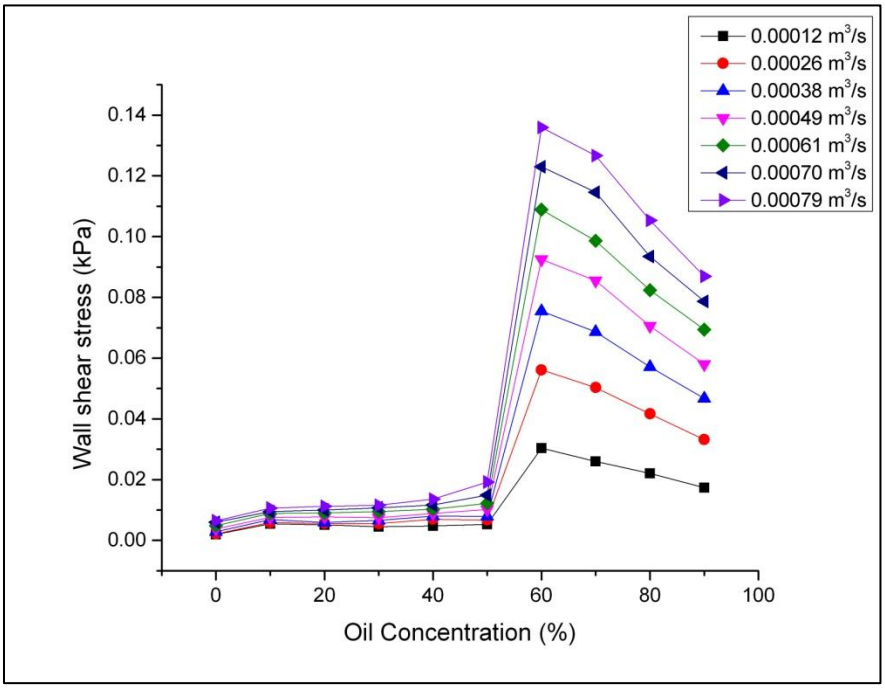

Figure 4.9 Plot of wall shear stress vs different emulsion concentration for different flow rate

4.2.3 Wall shear rate for circular pipes

For a time independent homogeneous non-Newtonian fluid, the shear stress is function of shear rate only. The variation of shear stress with respect to radial coordinate is given by the following relation

$$\frac{\tau_{rx}}{\tau_w} = \frac{r}{R} \qquad 4.9$$

For pipe flow, the relation between wall shear rate and volumetric flow rate is given by Rabinowitsch-Mooney equation.

$$\gamma_w = \xi\left[\frac{3}{4} + \frac{1}{4}\frac{d(\ln \xi)}{d(ln\tau_w)}\right] \qquad 4.10$$

In the above expression, $\xi = \frac{8v_{avg}}{D}$, where V_{avg} is the average flow velocity in m/s, R is the radius of the pipe in m, $\frac{d(\ln \xi)}{d(ln\tau_w)}$ is the inverse of the slope of wall shear stress vs. ξ.

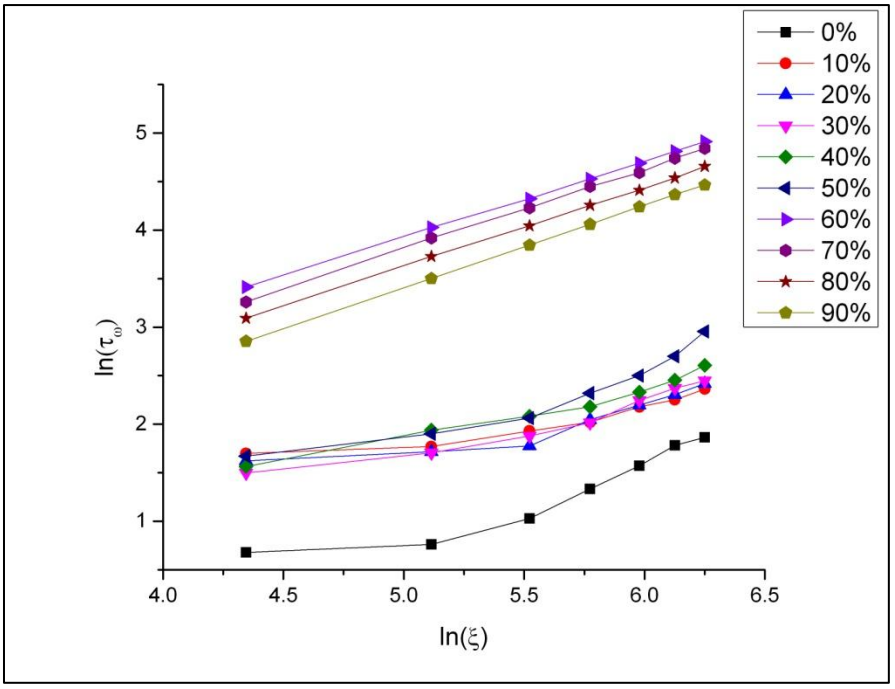

Figure 4.10 Plot of ln (τ_w) vs. ln (ξ)

Thus, wall shear rate is deduced from Eq. 4.10 including Rabinowitsch correction factor. Now, apparent viscosity is calculated using wall shear stress and wall shear rates discussed in the previous section. Experimental result shows that the shear rate experienced by the emulsion during pipe flow is between 73.840 $s^{-1}$and 1393.069 s^{-1}. From Fig. 4.11, it can be seen that as the shear rate is increased, the apparent viscosity of emulsion decreases gradually, implying non-Newtonian shear thinning behavior. This result is similar to the one obtained using the rheometer (Fig. 4.1). The variation of apparent viscosity with respect to oil concentration for different flow rate is presented in Fig. 4.12. It can also be noted from Fig. 4.12 that for same oil concentration, the apparent viscosity differs with respect to flow rate. This is because, at different flow rates, the emulsion experiences different shear rate as governed by Eq. 4.10 and hence different values of apparent viscosity.

Table 4.1 Wall shear rate values for various flow rates and concentration

Flow rate (m^3/s)	Wall shear rate (s^{-1})							
	20%	30%	40%	50%	60%	70%	80%	90%
0.000118	207.213	85.211	94.372	73.840	82.408	81.177	81.504	80.554
0.000255	447.205	183.903	203.672	159.360	177.851	175.195	175.195	173.851
0.000384	672.605	276.593	306.327	239.681	267.492	263.497	264.560	261.475
0.000493	864.779	355.620	393.850	308.161	343.918	338.782	340.149	336.182
0.000606	1061.756	436.622	483.559	378.353	422.255	415.949	417.627	412.757
0.000701	1229.646	505.663	560.022	438.180	489.024	481.721	483.665	478.024
0.000795	1393.069	572.867	634.451	496.415	554.016	545.742	547.945	541.555

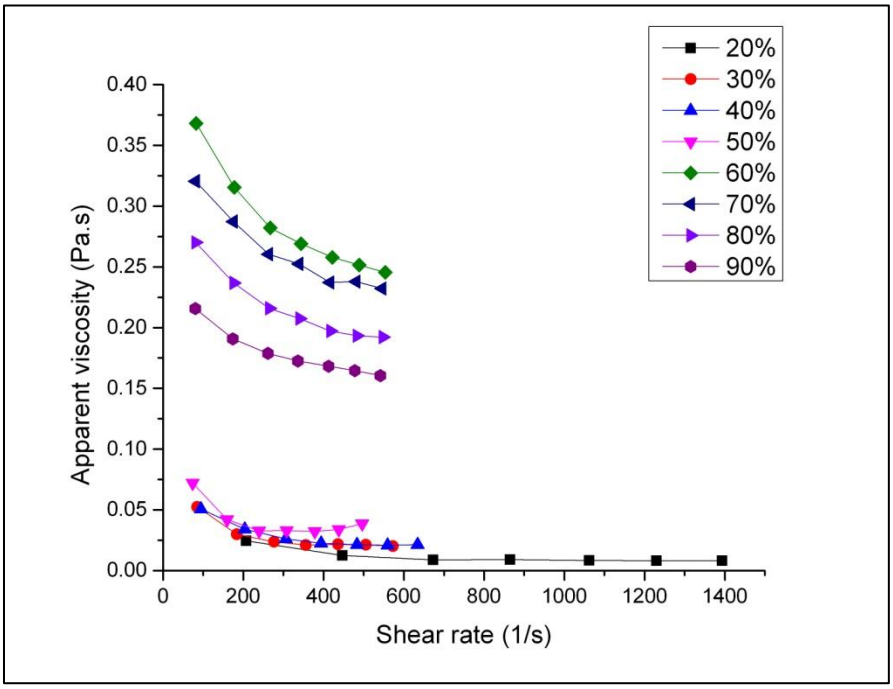

Figure 4.11 Plot of apparent viscosity (estimated from Eq. 4.8 and Eq. 4.10) vs shear rate for different emulsion flow rate

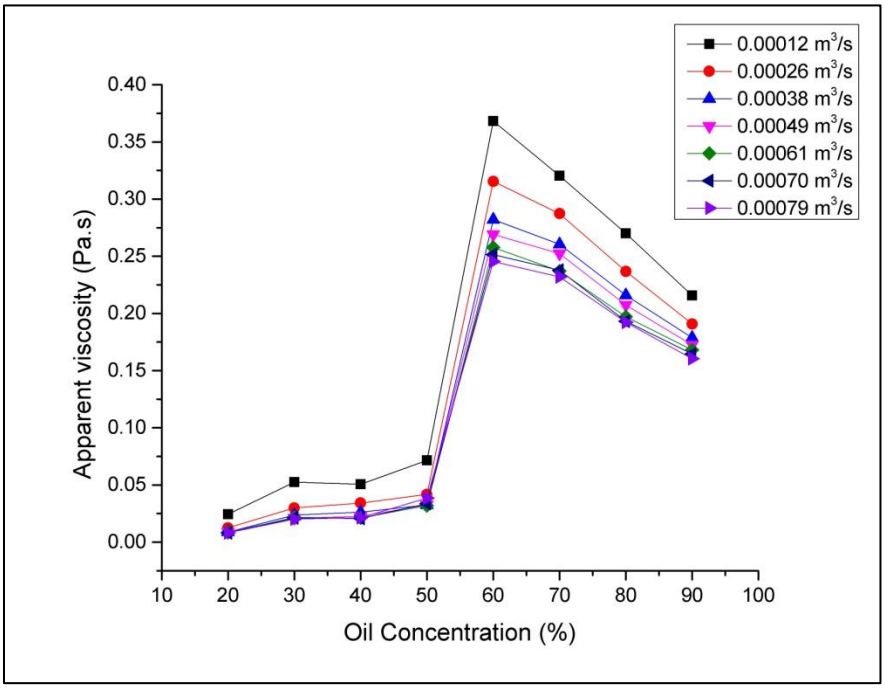

Figure 4.12 Plot of apparent viscosity (estimated from Eq. 4.8 and Eq. 4.10) vs emulsion concentration for different emulsion flow rate

On comparing Fig. 4.11 with Fig. 4.13 and Fig. 4.12 with Fig. 4.14, similar trend in viscosity profile can be observed. Difference in viscosity values arises due to the fact that effect of local turbulence is not captured in the rheometer as the rate of shearing is uniform and steady. Another notable fact is that in the pipe flow system, the phase inversion has occurred at oil concentration greater than 50% (Refer Fig. 4.12) whereas in the rheometer, phase inversion has occurred at oil concentration greater than 60% (Refer Fig. 4.14). This suggests the existence of ambivalent region where the oil and aqueous phase can exist as either continuous phase or dispersed phase.

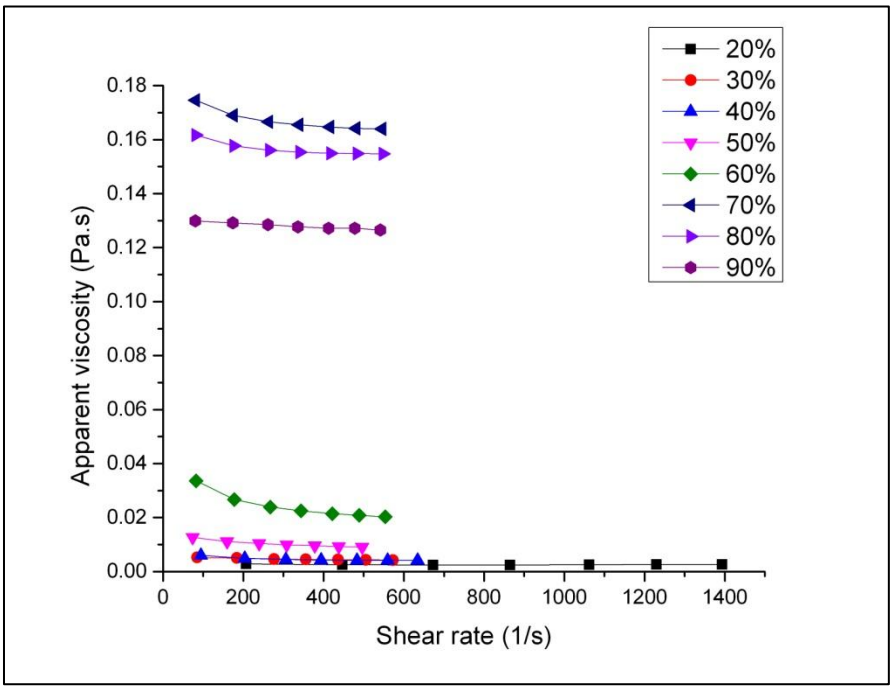

Figure 4.13 Plot of apparent viscosity (estimated from the rheometer) vs shear rate for different emulsion flow rate

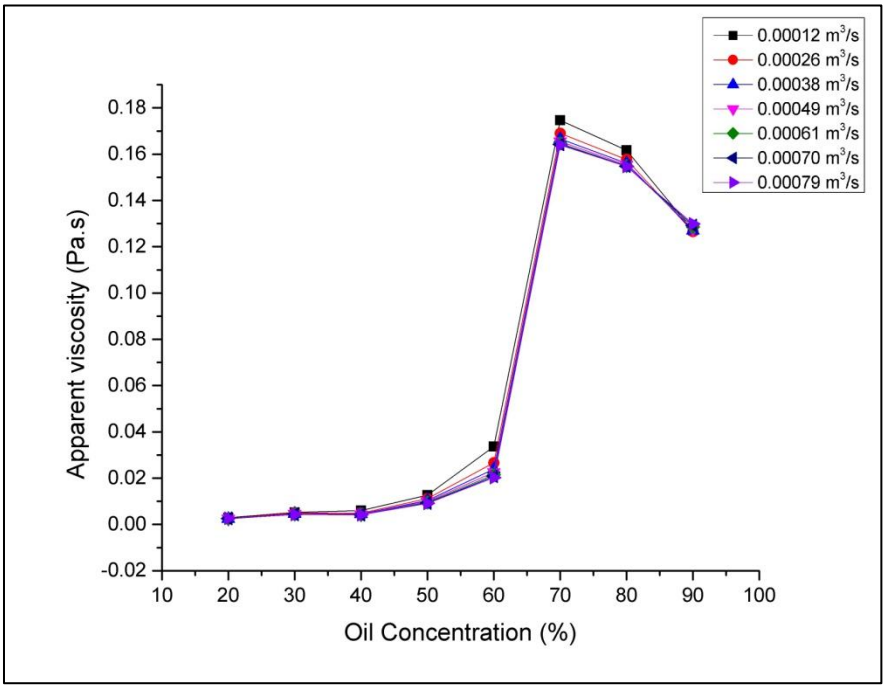

Figure 4.14 Plot of apparent viscosity (estimated from the rheometer) vs emulsion concentrations for different emulsion flow rate

Some of the phase inversion models available in the literature have been evaluated for the current experimental conditions and presented in Table 4.2.

Table 4.2 Evaluation of phase inversion prediction models

Sl. No	Author	Model	Predicted value
1.	Yeh et al. (Yeh et al. 1964)	$\varepsilon_o^l = \frac{\left(\frac{\mu_o}{\mu_w}\right)^{0.5}}{1+\left(\frac{\mu_o}{\mu_w}\right)^{0.5}}$	0.91
2.	Arirachakaran et al. (Arirachakaran et al. 1989)	$\varepsilon_o^l = 0.5 + 0.1108\, log\left(\frac{\mu_o}{\mu_w}\right)$	0.73
3.	Brauner and	$\varepsilon_o^l = \frac{\left(\frac{\rho_o}{\rho_w}\right)\left(\frac{\mu_o}{\mu_w}\right)^{0.4}}{1+\left(\frac{\rho_o}{\rho_w}\right)\left(\frac{\mu_o}{\mu_w}\right)^{0.4}}$	0.85

	Ullman (Brauner and Ullmann 2002)		
4.	Poesio and Bertlta (Poesio and Beretta 2008)	$\varepsilon_o^l = \frac{1 - \left(\frac{\mu_o}{\mu_w}\right)^{-2/5k} + k\left(\frac{\mu_o}{\mu_w}\right)^{-2/5k}}{1 + \left(\frac{\mu_o}{\mu_w}\right)^{-2/5k}}$	0.87

4.2.4 Friction factor for two phase liquid-liquid system

The friction factor for pipeline flows can be deduced from Darcy-Weisbach equation, in which head loss is related to the length, the diameter and the velocity of flow.

$$\boldsymbol{h_L = \frac{\Delta P}{\rho g} = f \frac{L}{D} \frac{U^2}{2g}} \qquad 4.11$$

The two phase friction factor for various liquid concentrations and at different liquid superficial velocity is calculated using the following expression. In the following expression, the effect of fluid viscosity is taken care by pressure gradient.

$$\boldsymbol{f = \left(\frac{\Delta P}{l}\right) \frac{2\,D}{\rho_m U_m^2}} \qquad 4.12$$

In the above expression, the term $\left(\frac{\Delta P}{l}\right)$ represents pressure gradient, which includes hydrostatic component as well. For single phase water flow, the flow regime is completely turbulent as the Reynolds number is in the range of 13,208 to 40,894.

Table 4.3 Comparison of friction factor

Sl. No	Velocity (m/s)	Reynolds Number	f_{exp}	$f_{th} = \frac{1.325}{\left[ln\left(\frac{1}{3.7}\frac{\varepsilon}{D} + \frac{5.74}{Re^{0.9}}\right)\right]^2}$	$f_{\text{moody's chart}}$
1.	0.52	13208	0.06328	0.02872	0.029
2.	0.78	19812	0.03679	0.02586	0.026
3.	1.0	25400	0.03023	0.02432	0.024
4.	1.23	31242	0.02545	0.02314	0.023
5.	1.41	36068	0.02354	0.02237	0.022
6.	1.61	40894	0.01988	0.02173	0.022

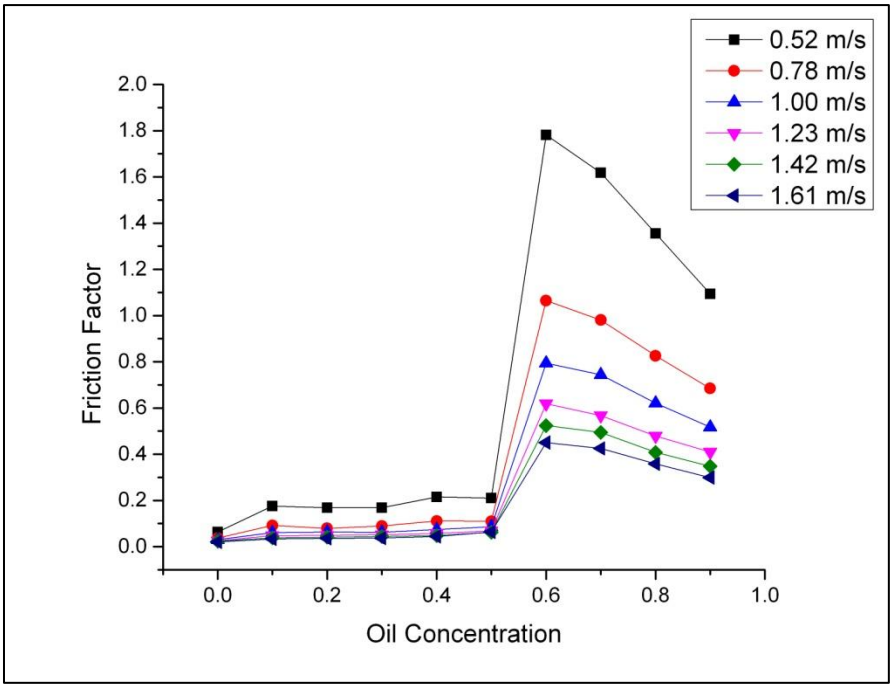

Figure 4.15 Variation of friction factor with respect to oil concentration

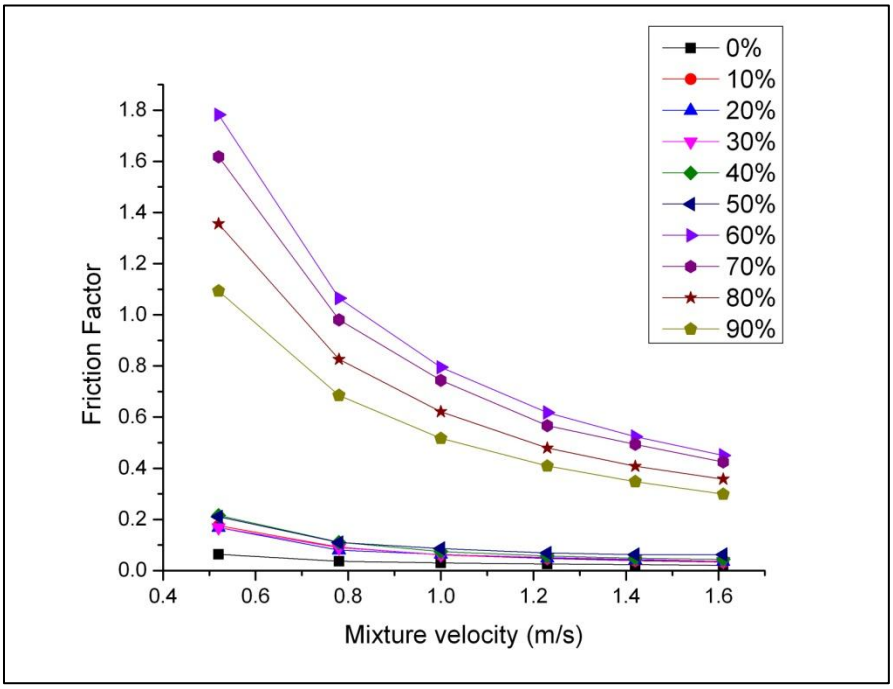

Figure 4.16 Variation of friction factor with respect to mixture velocity

For Newtonian fluid, the friction factor does not vary significantly with respect to mean velocity but for non-Newtonian fluids, as such in our case (for oil concentration between 10% and 90%), the friction factor assumes an asymptotic shape as shown in Fig. 4.16. Similar friction factor profile has been reported in previous study conducted by Meriem-Benziane and Bou-Saïd (2013) (Fig. 4.17). Modified Phan Thien-Tanner (MPTT) model best captures this phenomenon.

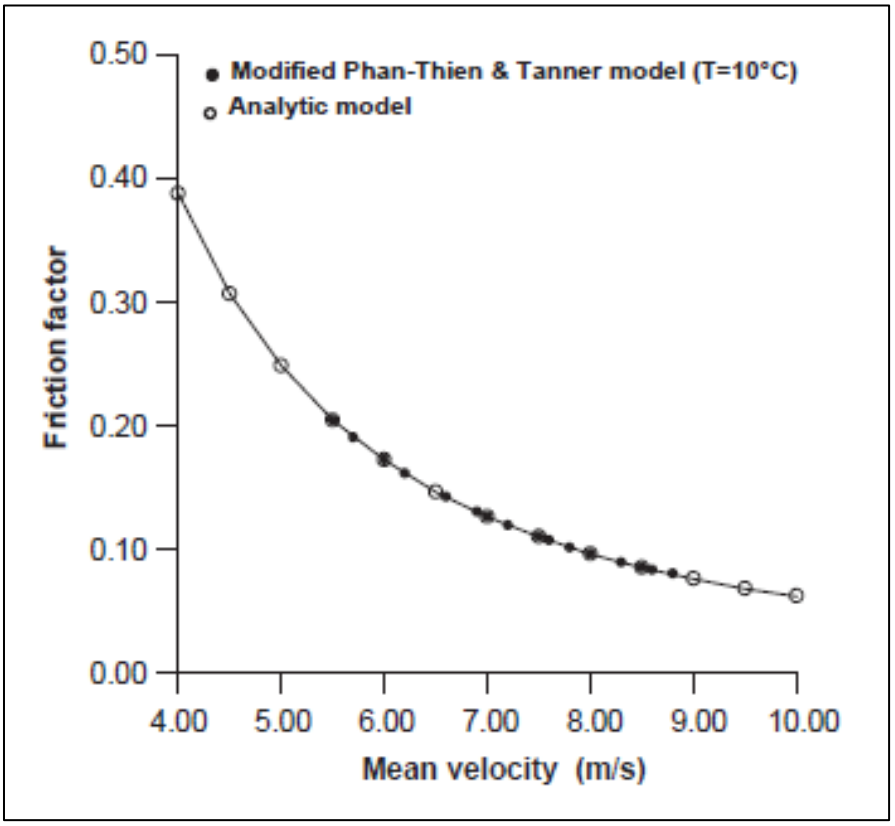

Figure 4.17 Variation of friction factor w.r.t mean velocity from Bou-Said et al.

4.3 Results of three phase flow experiment

The results of three phase pressure gradient measurements for liquid-liquid-gas flows are presented in this section. Here the third phase is compressed air at 1 bar gauge supplied from the air compressor. Two distinct flow regimes viz. slug and churn flow regime were able to generate by varying the air flow rate.

Similar to two phase flow, the piezometric pressure drop is attributed to body forces and frictional losses,

$$\left(\frac{dP}{dl}\right)_{3\emptyset} = \left(\frac{dP}{dl}\right)_{B-3\emptyset} + \left(\frac{dP}{dl}\right)_{f-3\emptyset} \qquad 4.13$$

where, $\left(\frac{dP}{dl}\right)_{B-3\emptyset}$ is the body force term and it is a function of the in-situ gas fraction (α_g)

$$\left(\frac{dP}{dl}\right)_{B-3\emptyset} = (1-\alpha_g)\rho_m g \quad 4.14$$

and frictional pressure gradient is the sum of two phase pressure gradient and pressure gradient due to air injection,

$$\left(\frac{dP}{dl}\right)_{f-3\emptyset} = F_l + F_{g-l} \quad 4.15$$

4.3.1 Results of three phase slug flow experiments:

Slug flow is one of the common types of flow regime in a multi-phase fluid flow, where the superficial liquid and gas velocities are in the range of 0-5 m/s. It is characterized by alternate liquid and gas slugs with some gas entrained in the liquid slug and some liquid entrained in the gas slug. In the present study, slug flow regime is generated at the following liquid and gas superficial velocities: $0.282 < U_{SL} < 0.938$ m/s and $0.385 < U_{SG} < 0.978$ at 1 bar gauge. The superficial velocities stated above are chosen based on the flow pattern map discussed in Fig. 2.2 as a guideline and fine tuning of the superficial velocities are done with the help of high-speed photography/videography. The slug flow visualization using high-speed camera is presented in Fig. 4.23 to Fig. 4.26.

The introduction of third phase in slug flow regime significantly reduces the piezometric pressure gradient and frictional pressure gradient as well. This is because, in addition to the reduction in apparent density, apparent viscosity is also reduced due to the introduction of third phase. This can be seen on from Fig. 4.18

and Fig. 4.22. Detailed Pressure-time history is presented in Appendix E to Appendix L.

In Fig. 4.22, it can be seen that for lower liquid velocities, the pressure transducer has recorded negative signal. This is because at lower liquid flow rate, although there is a net upward flow, the liquid film attached to the walls of the pipe tends to move downwards (Ghosh and Cui (1999). This concept is explained schematically in Fig. 4.19. Since the transducer is connected to the pressure tappings at the wall, where the direction of flow is opposite to that of net flow, it gives a negative signal. Such negative pressure gradient has been noted by several other authors as well (Liu et al. (2005), Wilkens and Jepson (1996)).

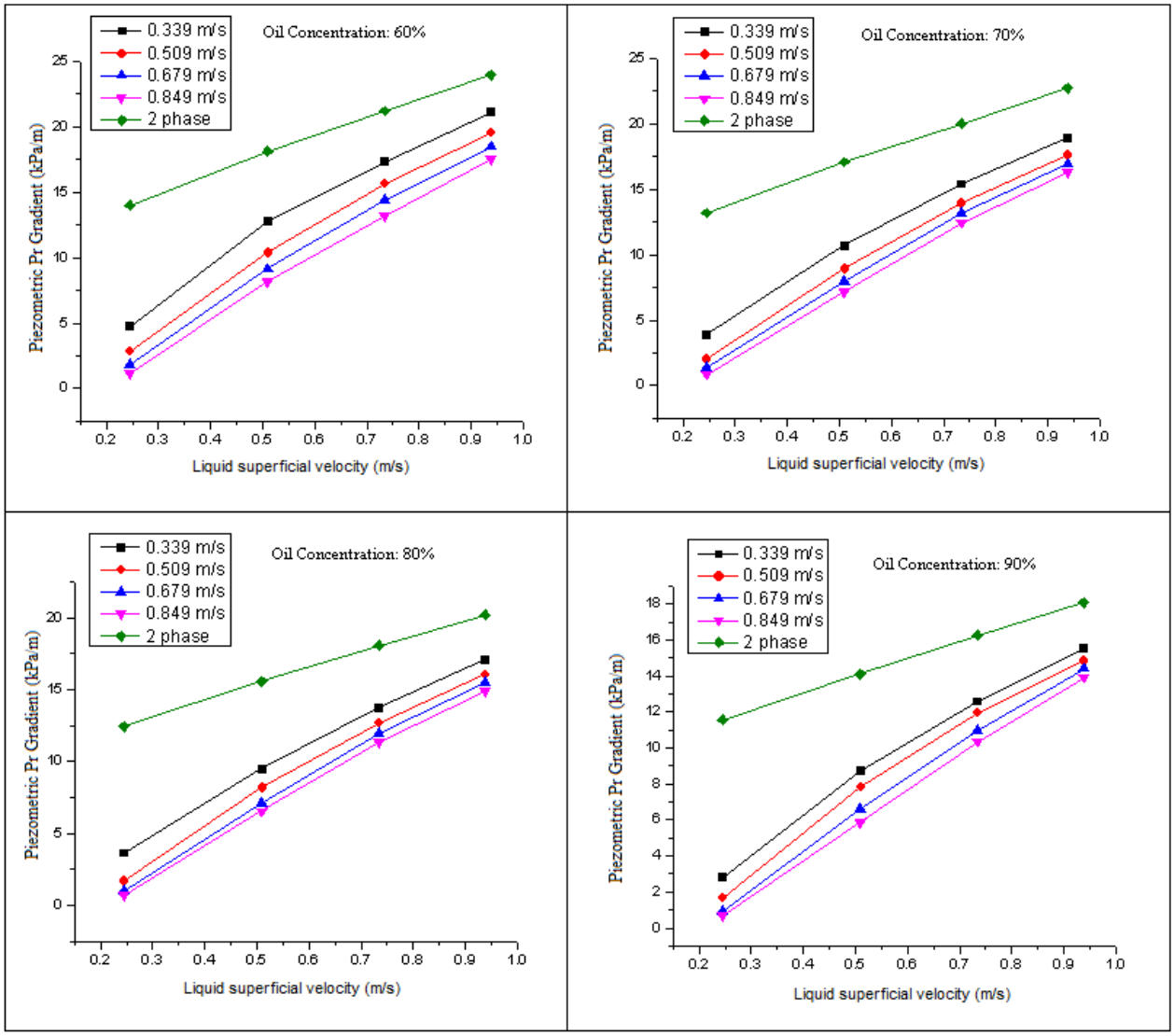

Figure 4.18 Effect of liquid superficial velocity on total pressure drop for different oil concentrations

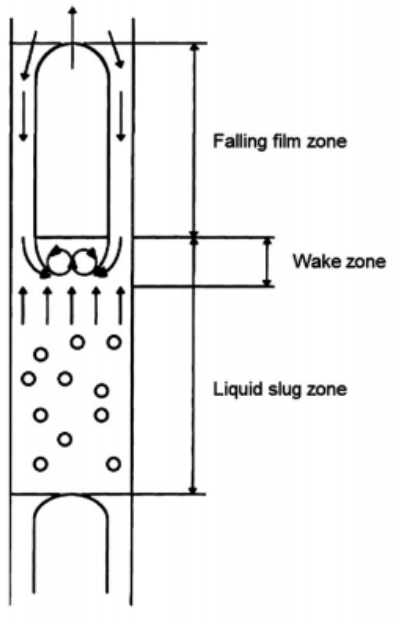

Figure 4.19 Different zones in slug flow regime as described by Ghosh and Cui

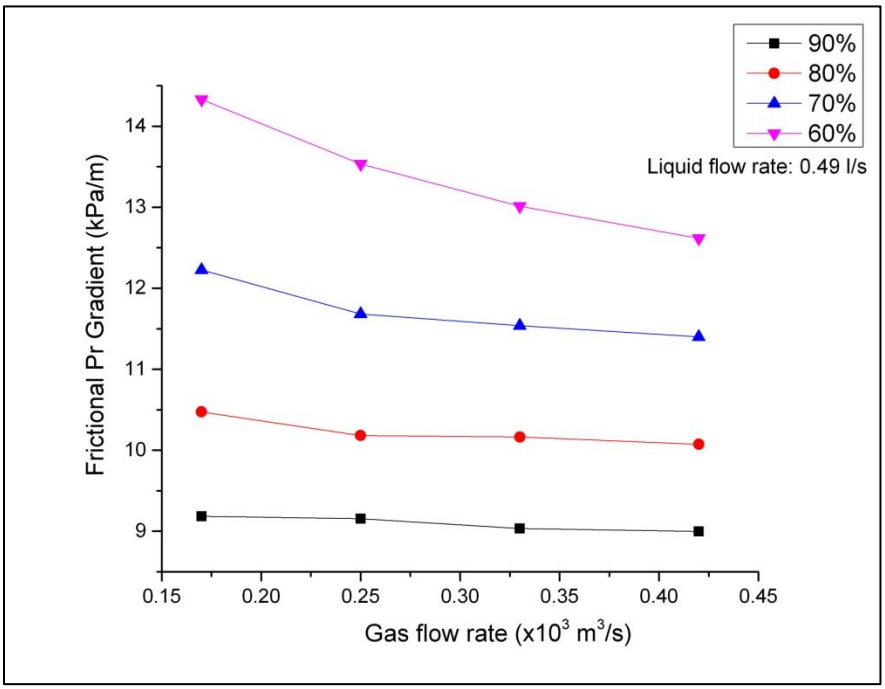

Figure 4.20 Effect of gas flow rate on frictional pressure drop in slug flow regime

From Fig. 4.20 and 4.21, it can also be noticed that for a given liquid superficial velocity, as the gas superficial velocity is increased, piezometric and frictional

pressure gradient reduces significantly for emulsions with oil concentrations near phase inversion region and reduces slightly for emulsions whose oil concentration is away from inversion region.

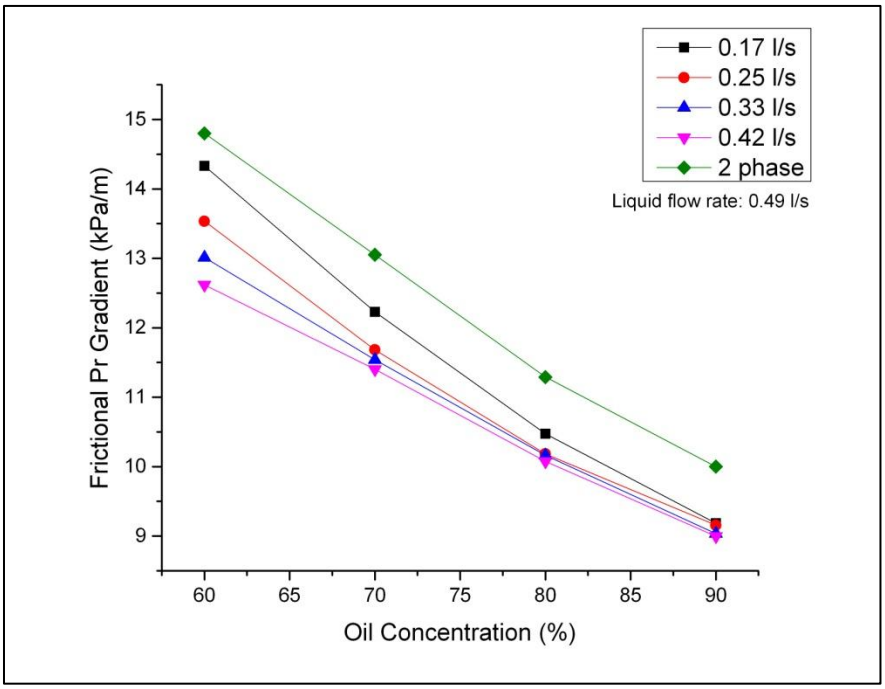

Figure 4.21 Effect of oil concentration on frictional pressure drop in slug flow regime

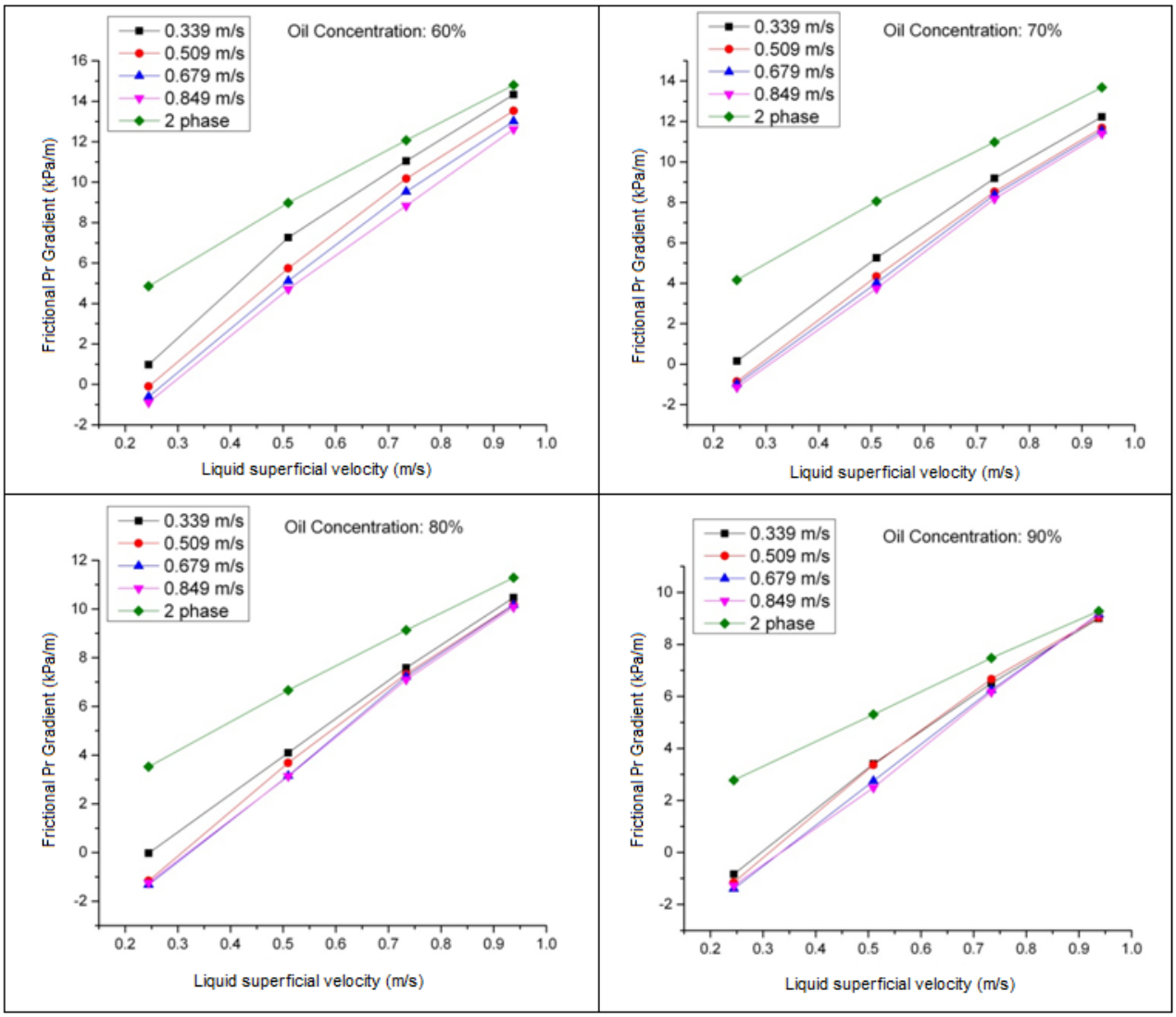

Figure 4.22 Effect of liquid superficial velocity on frictional pressure drop for different oil concentrations

4.3.1.1 Slug flow visualization using high-speed camera

Flow visualization is done using the state-of-the-art High speed camera discussed in Section 3.3. The slug flow is characterized with distinctive liquid and gas slugs flowing concurrently. As the oil-water emulsion is highly opaque in nature, images/videos are captured in air-oil system and presented in this section. The dynamic viscosity of the oil (Shell Tonna S3 M 68) used for visualization purpose

is 0.12 Pa.s. From the images/videos captured, parameters such as slug length, slug frequency and bubble rise velocities are estimated using image processing software PFV viewer (supplied with high speed camera). The images of gas slugs in both oil and water are presented in Fig. 4.23 to Fig.4.26.

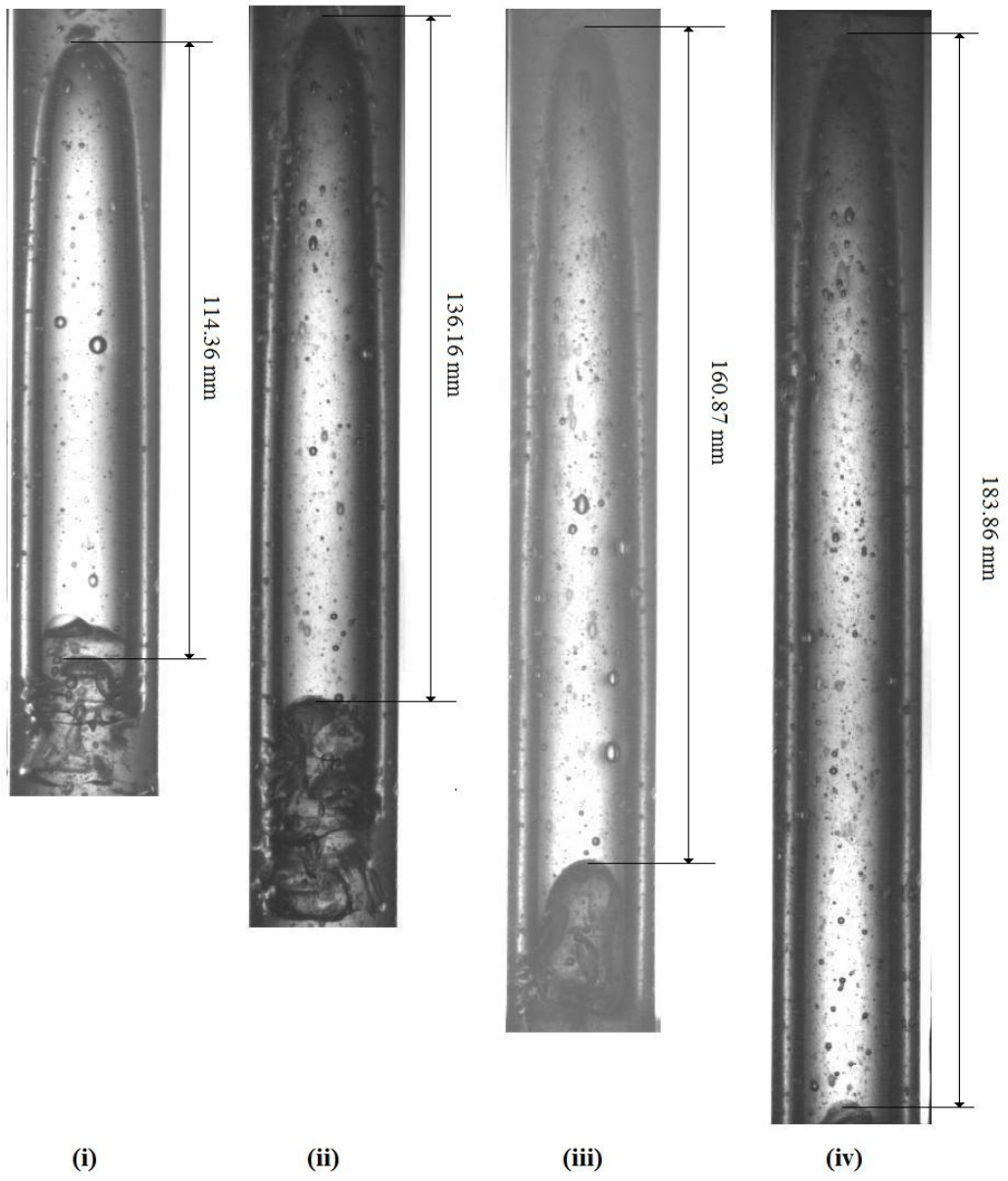

Figure 4.23 Slug flow visualization in viscous liquid. (V_{sl} = 0.244 m/s; V_{sg} = (i) 0.339 m/s; (ii) 0.509 m/s; (iii) 0.679 m/s; (iv) 0.849 m/s)

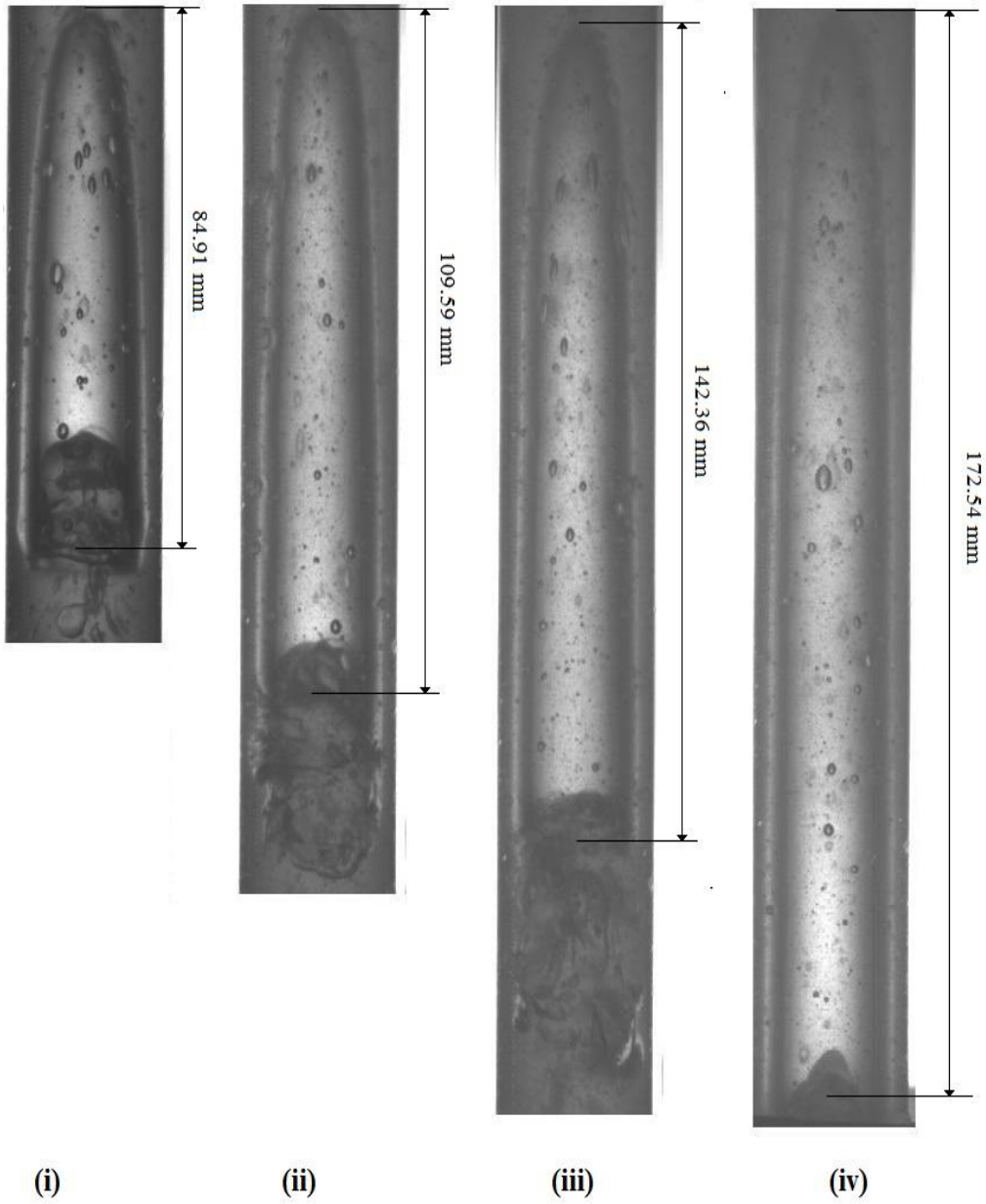

Figure 4.24 Slug flow visualization in viscous liquid. (V_{sl} = 0.509 m/s; V_{sg} = (i) 0.339 m/s; (ii) 0.509 m/s; (iii) 0.679 m/s; (iv) 0.849 m/s)

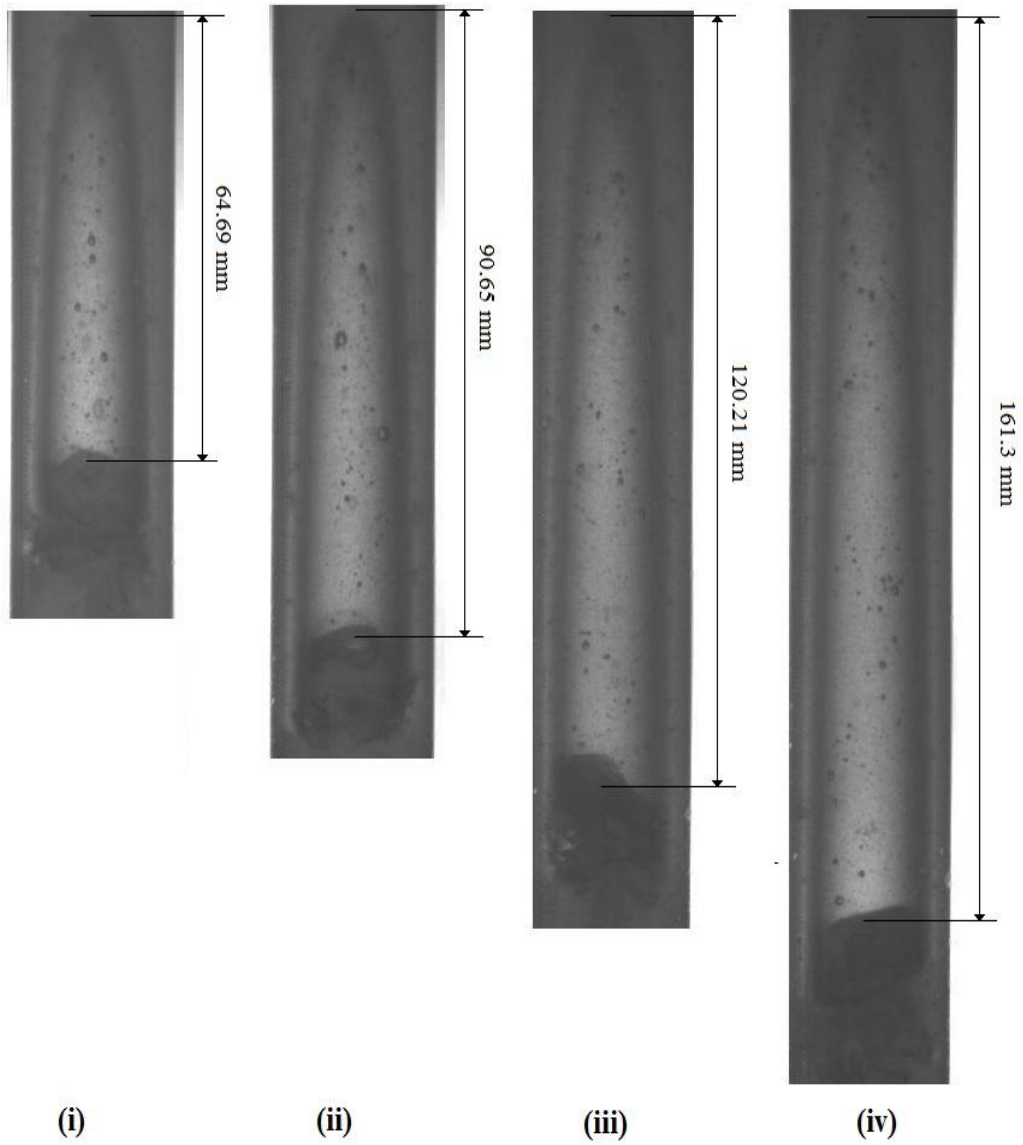

Figure 4.25 Slug flow visualization in viscous liquid. (V_{sl} = 0.733 m/s; V_{sg} = (i) 0.339 m/s; (ii) 0.509 m/s; (iii) 0.679 m/s; (iv) 0.849 m/s)

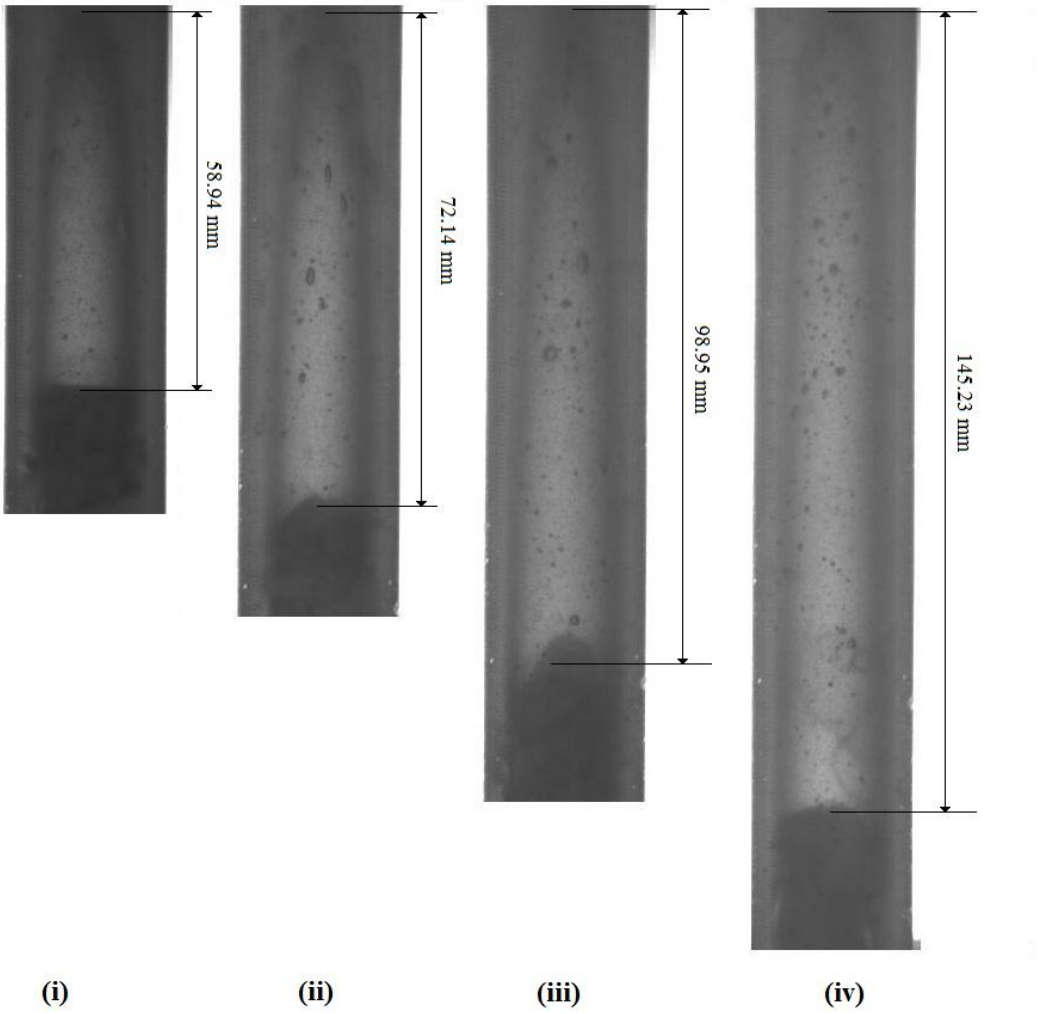

Figure 4.26 Slug flow visualization in viscous liquid. (V_{sl} = 0.937 m/s; V_{sg} = (i) 0.339 m/s; (ii) 0.509 m/s; (iii) 0.679 m/s; (iv) 0.849 m/s)

4.3.1.2 Slug length

In vertical multiphase flow, liquid and gas superficial velocity has great impact on slug length, bubble rise velocity and slug frequency. The variation of slug length with respect to gas and liquid superficial velocity is presented in Fig. 4.27 and Fig. 4.28 respectively. For a given liquid superficial velocity, increasing gas superficial velocity increases the slug length and as the slug length reaches a critical value, instabilities cause the breakdown of the smaller gas slugs of irregular shape with liquid chunks separating them (transition to churn flow).

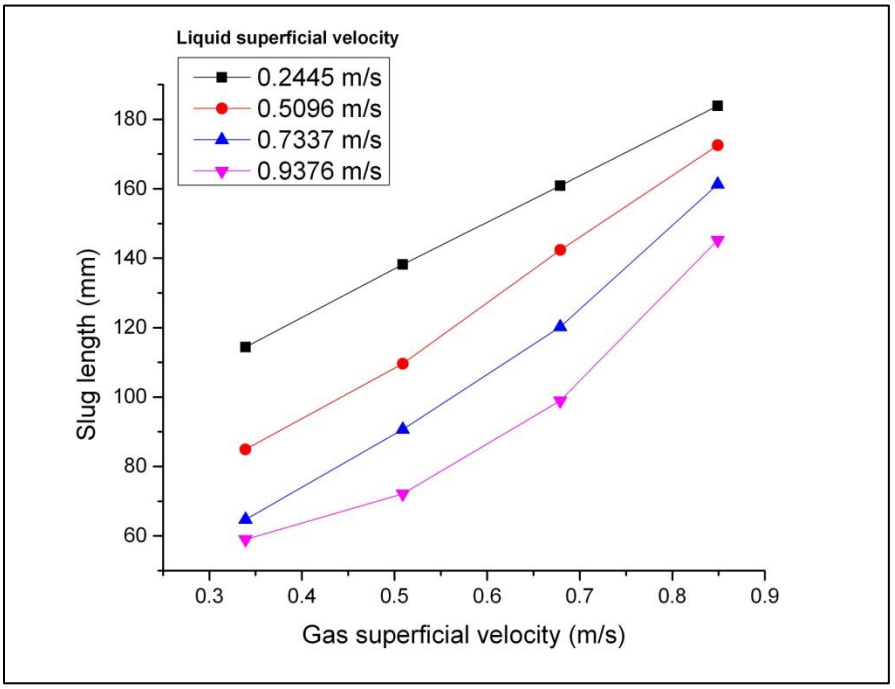

Figure 4.27 Effect of gas superficial velocity on slug length in viscous oil

On the other hand, for a given gas superficial velocity, increasing liquid superficial velocity decreases the slug length (Fig. 4.28). The limiting case for this trend is the transition to dispersed bubbly flow, where the gas bubbles attain spherical shape due to surface tension effects.

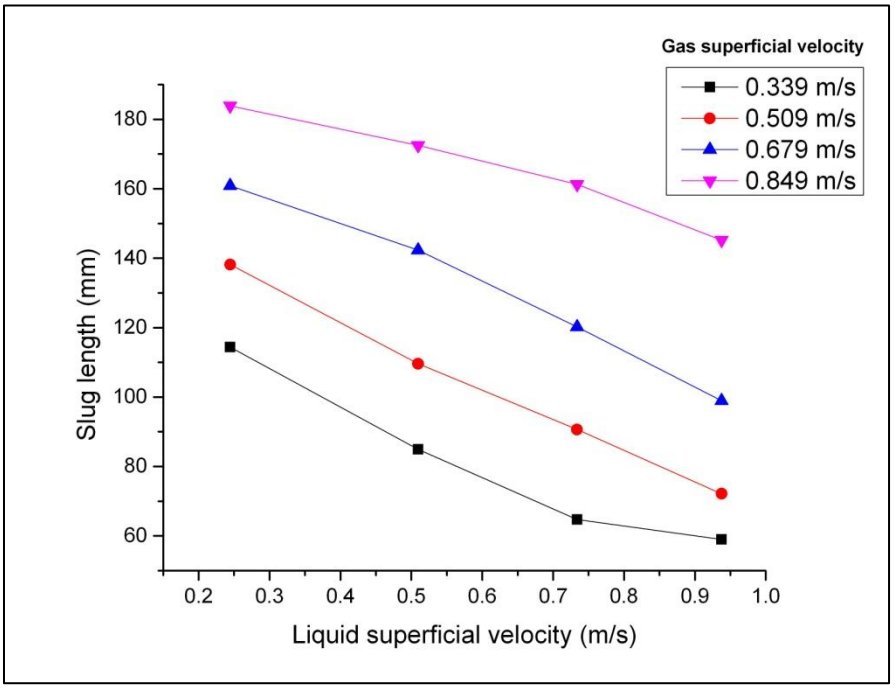

Figure 4.28 Effect of liquid superficial velocity on slug length in viscous oil

4.3.1.3 Bubble rise velocity

In a multiphase fluid system, the fluid with lesser density tends to rise continuously due to buoyancy. In case of a bubble rising in a stagnant liquid, the rise velocity is given by $v_B = C\sqrt{gD}$ (Davies and Taylor 1950). The value of C varies from 0.33 to 0.35. Bubble rise velocity in concurrent gas-liquid flow is empirically given by $w = \sqrt{gD}\left(a + b(v_{SG} + v_{SL})\right)$ (Street and Tek 1965). The values of coefficient 'a' and 'b' strictly depend upon the system considered. Bubble rise velocity is deduced from high-speed photography by estimating the

number of frames for the bubble to traverse through a pre-specified distance. The time interval taken to traverse the pre-specified distance is correlated with the frame rate at which the video is shot. Experimental result shows that the rise velocity increases as the liquid and gas superficial velocity is increased (Fig. 4.29 and Fig. 4.30).

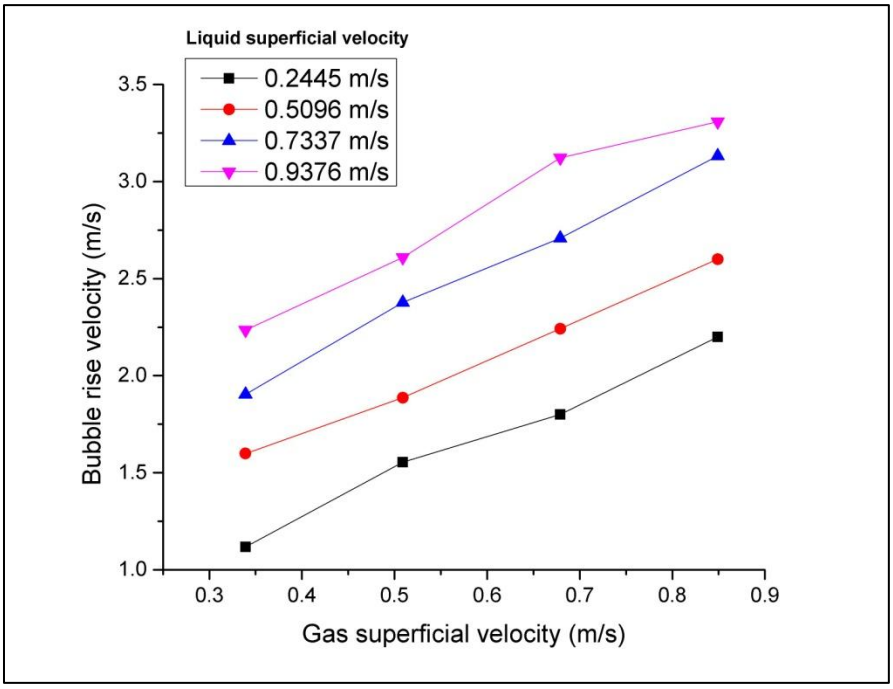

Figure 4.29 Effect of gas superficial velocity on bubble rise velocity in viscous oil

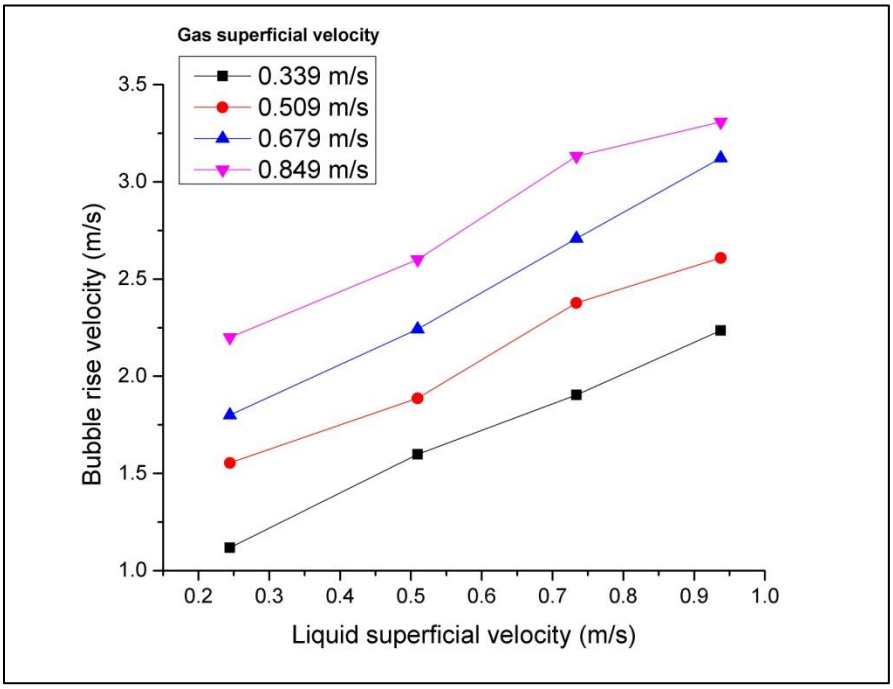

Figure 4.30 Effect of liquid superficial velocity on bubble rise velocity in viscous oil

4.3.1.4 Slug frequency

Slug frequency is defined as the inverse of time taken by to consecutive gas and liquid slug to traverse a specific point along the length of the pipeline. Mechanistic models pertaining to the prediction on slug frequency in horizontal are available in the literature. However, models to correlate slug frequency in vertical pipeline system such as risers are very scarce. Experimental observations in vertical system are compared with the available data in horizontal system.

From Fig. 4.31, it can be observed that, increasing gas superficial velocity decreases the slug frequency. One possible explanation to this trend is that, as the gas superficial velocity is increased, the slug length increases (Fig. 4.27), which takes higher time to completely traverse a specific point along the length of the pipeline. Similar trend is observed in horizontal flow as well (Fig. 4.32).

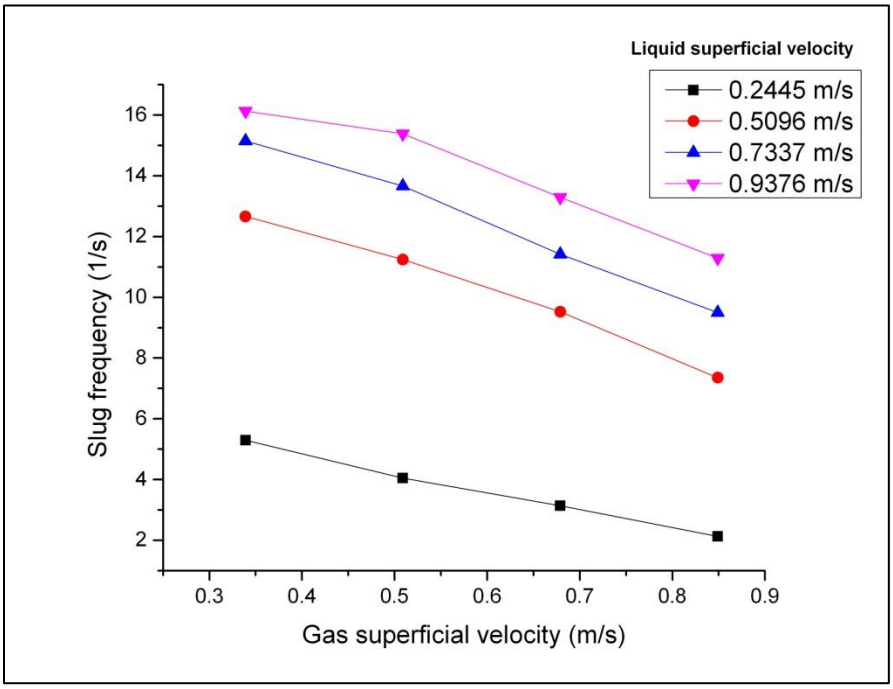

Figure 4.31 Effect of gas superficial velocity on slug frequency in viscous oil

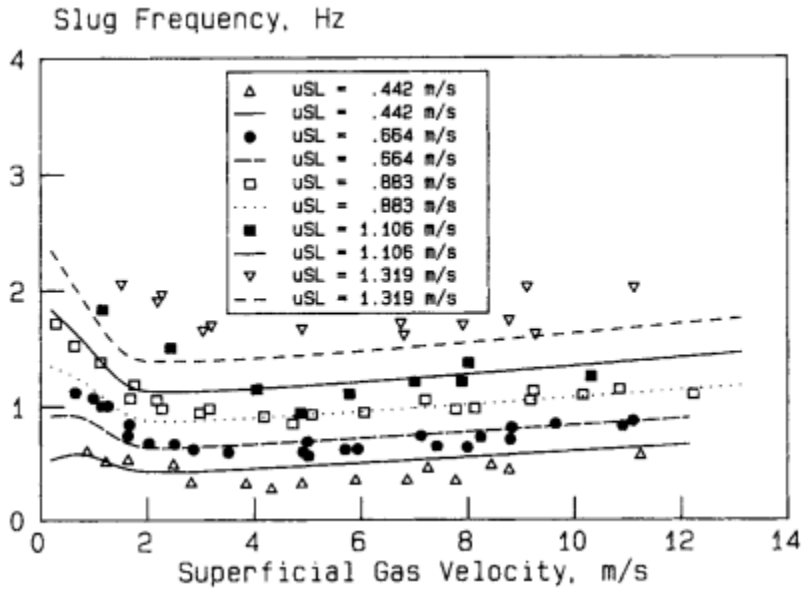

Figure 4.32 Variation of slug frequency w.r.t gas superficial velocity as reported by Tronconi (Trononi 1990)

Experimental result shows that slug frequency in vertical flow increases as the liquid superficial velocity is increased Fig (4.33). These results are similar to the previous works conducted in horizontal gas-liquid flows (J.Y.CAI 1999).

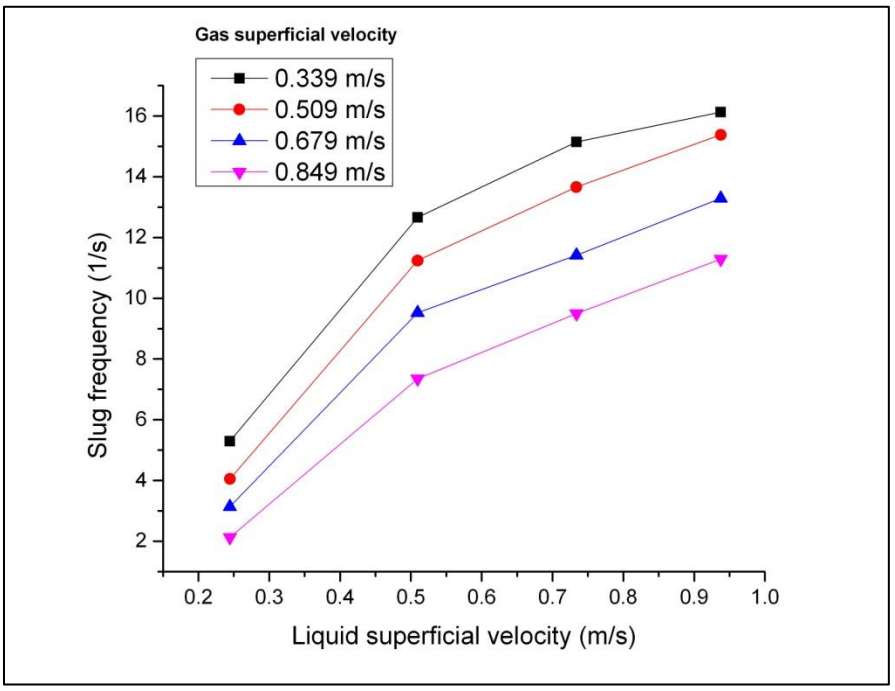

Figure 4.33 Effect of liquid superficial velocity on slug frequency in viscous oil

4.3.2 Identification of churn flow regime:

Unlike slug flow regime, churn flow regime does not have distinctive gas and liquid slug flowing alternatively. Churn flow regime is usually characterized by the presence of thick unstable liquid film. In addition to this although there is a net upward flow in this regime, the liquid film tends to be oscillatory (moving up and down intermittently). This phenomenon in particular is used for identification purpose. The characteristic oscillatory motion is show in Fig. 4.35 and Fig. 4.36. In addition to this phenomenon, according to observations of Barbosa Jr et al. (2001), large scale waves pass over the liquid film in oscillatory motion. This is

schematically explained in Fig. 4.34. Since this characteristic wave occur only in fully developed churn flow, and it has been visualized in the current experimental study (Fig. 4.35), the flow is assumed to be fully developed.

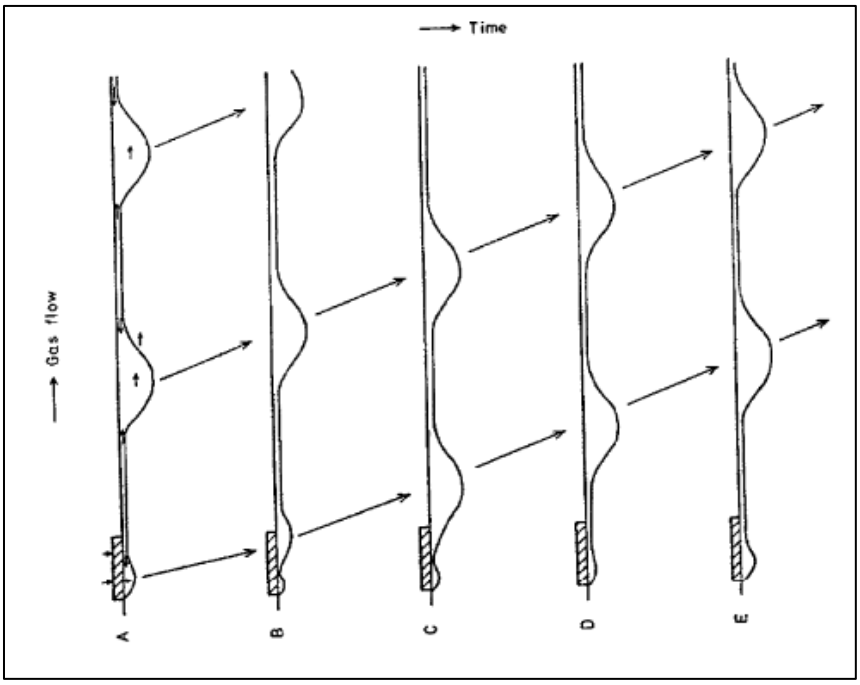

Figure 4.34 Postulated mechanism of churn flow (Barbosa Jr et al. 2001)

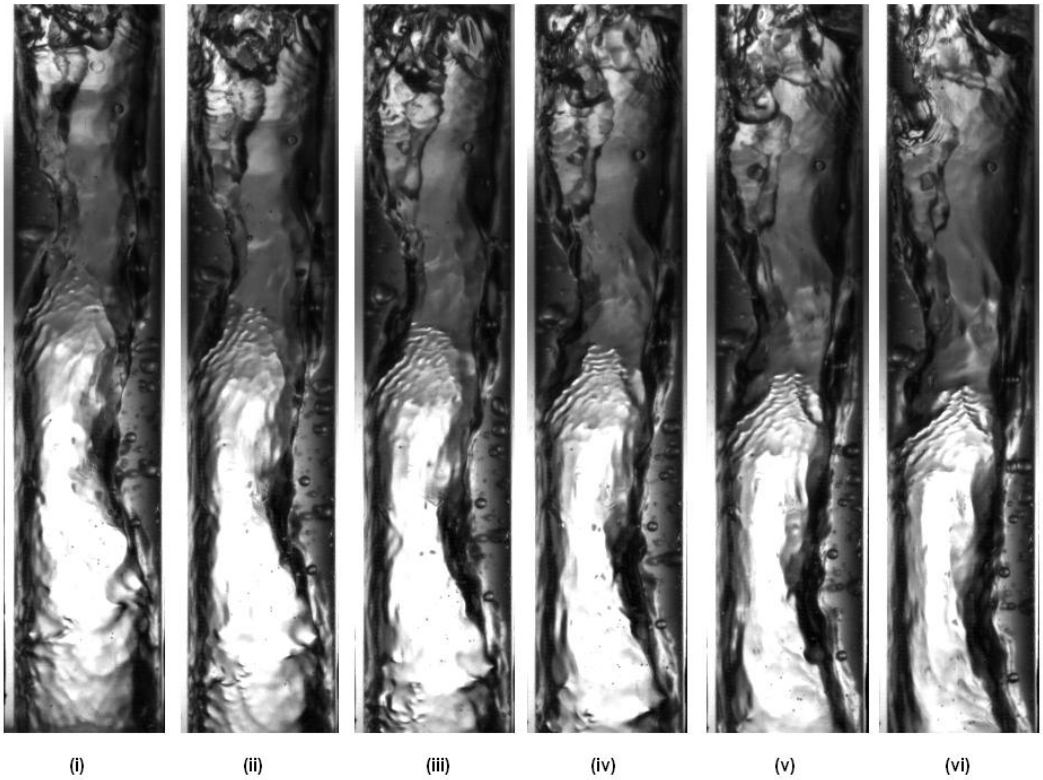

Figure 4.35 Churn flow visualization-downwash for V_{sl} = 0.244 m/s; V_{sg} = 1.359 m/s ((i) t = 0.0s; (ii) t = 0.005s; (iii) t = 0.010s; (iv) t = 0.015s; (v) t = 0.020s; (vi) t = 0.025s)

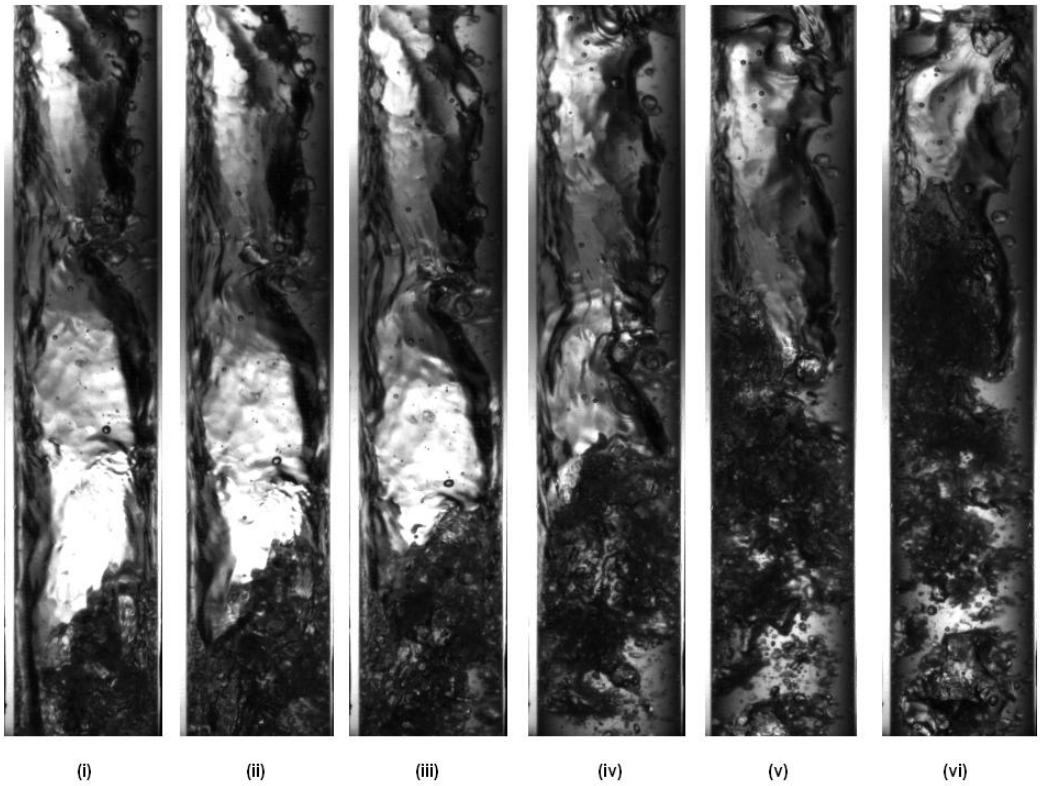

Figure 4.36 Churn flow visualization-up wash for V_{sl} = 0.244 m/s; V_{sg} = 1.359 m/s ((i) t = 0.900s; (ii) t = 0.905s; (iii) t = 0.910s; (iv) t = 0.915s; (v) t = 0.920s; (vi) t = 0.925s)

4.3.2.1 Results of three phase churn flow experiments

Churn flow regime is an intermediate flow regime which occurs between slug and annular flow regime. In this regime, the Taylor bubbles are destroyed due to high local gas concentration in the slug.

From Fig. 4.37, it can be seen that for a given oil concentration and given liquid superficial velocity, as the gas flow rate is increased, the frictional pressure drop increases. This is on contrary with slug flow regime. The reason behind this phenomenon is suspected due to the irreversible work done by gas on the liquid. Presence of the second fluid (gas in this case) reduces the effective cross sectional

area of first fluid (liquid), leading to reduction in hydraulic diameter. Detailed time history plot is presented in Appendix M and N.

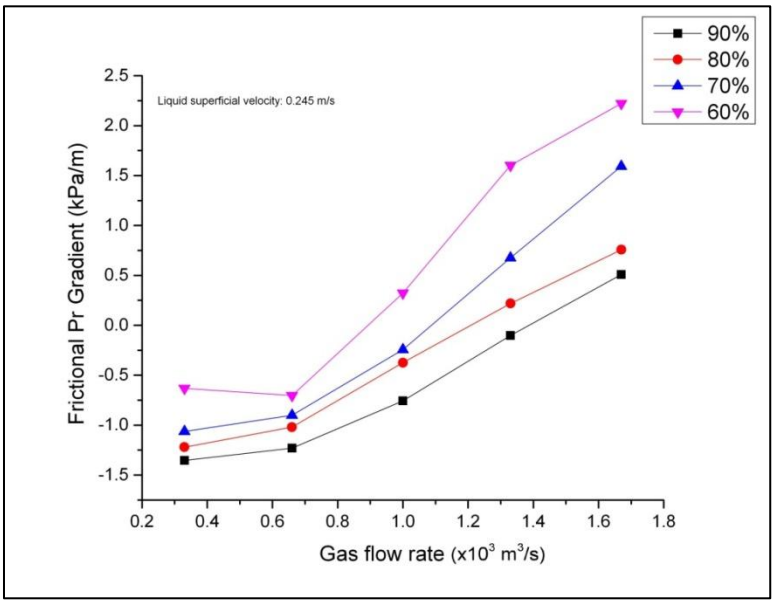

Figure 4.37 Effect of gas flow rate on frictional pressure drop in churn flow regime

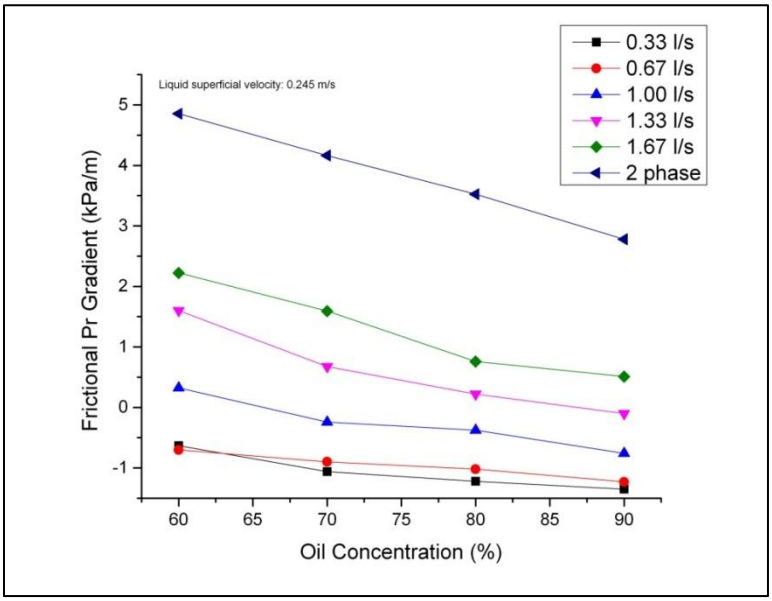

Figure 4.38 Effect of oil concentration on frictional pressure drop in churn flow regime

4.3.3 Comparison of results of slug flow and churn flow regime:

Resolving the piezometric pressure gradient into hydrostatic and frictional pressure gradient, in slug flow regime as the gas phase flow rate is increased, both hydrostatic and frictional pressure gradient decreases and hence piezometric pressure gradient also decreases. Also when it is oil continuous, frictional pressure gradient is more significant than hydrostatic pressure gradient. Another notable phenomenon is as the water concentration is increased, the dominance of frictional pressure gradient is also increased up to the phase inversion region and decreased thereafter, which is similar to two phase liquid –liquid flows. Refer Fig. 4.39.

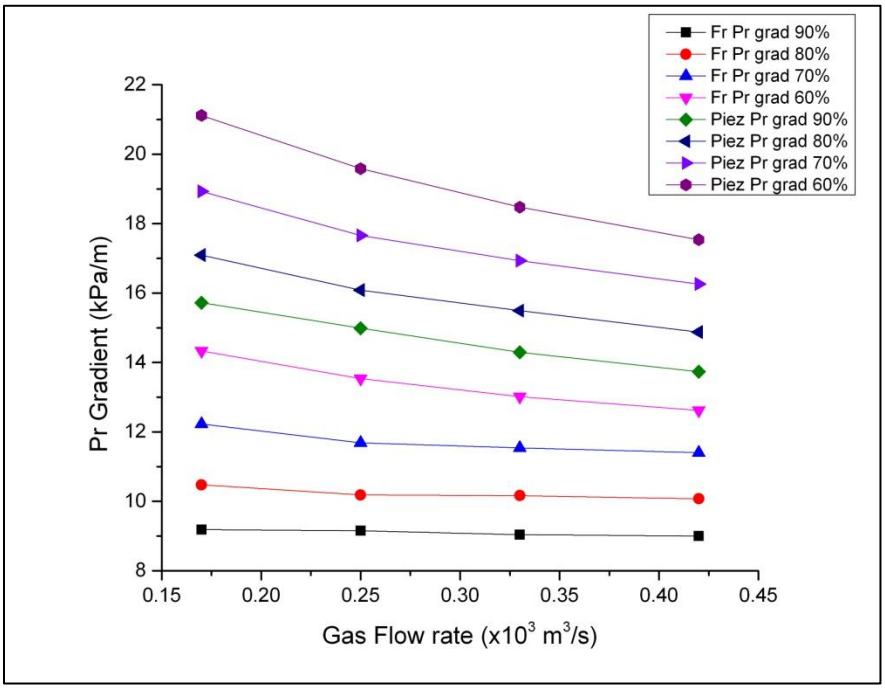

Figure 4.39 Variation of components of pressure drop w.r.t gas flow rate in slug flow regime

However on resolving the total pressure drop into hydrostatic and frictional pressure drop, in churn flow regime as the gas phase flow rate is increased,

hydrostatic pressure drop decreases while the frictional pressure drop and hence total pressure drop tend to increases significantly (Fig. 4.40). This factor should be considered seriously while designing gas lift equipment. In such cases, if the gas lift well is operated in churn flow regime, instead of increasing the productivity, it may actually decrease the production rate.

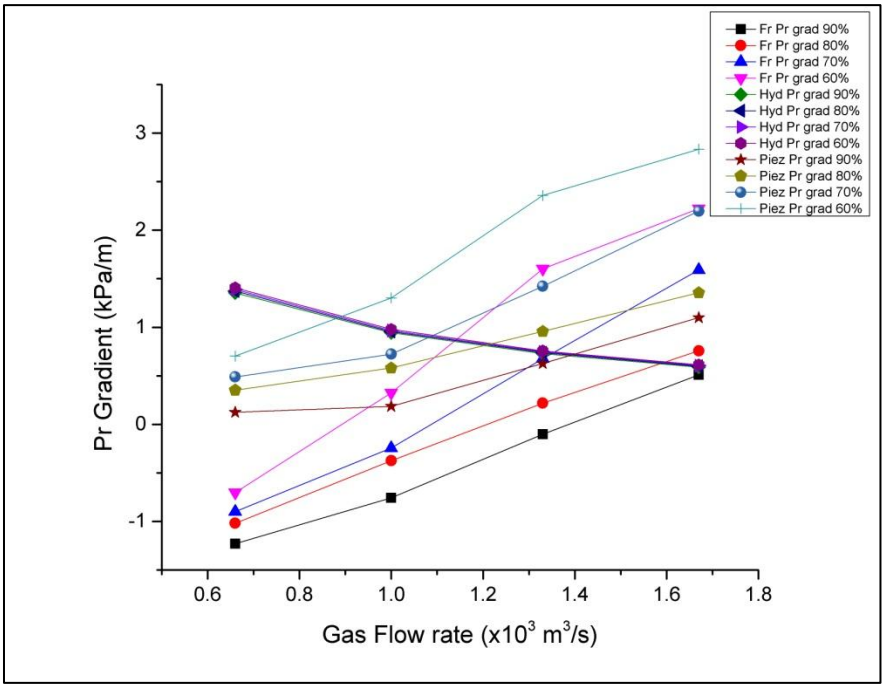

Figure 4.40 Variation of components of pressure drop w.r.t gas flow rate in churn flow regime

Chapter 5

Conclusion and Future work

5.1 Summary

In this thesis, an experimental study on multiphase flows was conducted in a small scale test loop constructed at Fluid Mechanics laboratory in NUS. The results of pressure drop measurements in vertical upward liquid-liquid and liquid-liquid-gas systems were analyzed by comparing them with empirical pressure drop models and available data in the literature.

Based on the two-phase pressure drop data, wall shear stress was derived by force balance equation. Wall shear rate was determined using Rabinowitsch-Mooney equation. Then apparent viscosity of two phase system is estimated using wall shear stress and wall shear rate. In addition to it, the liquid-liquid emulsion system with different phase volume fraction is characterized using the state-of-the-art HAAKE MARS III rheometer. The apparent viscosity data obtained from the rheogram is then compared with the apparent viscosity calculated using pressure drop data. Various viscosity prediction models developed in the past were analyzed and compared with the experimental viscosity data.

The effect of phase inversion phenomenon on wall shear stress, pressure drop and friction factor has been analyzed and discussed. The phase inversion models published in the literature were discussed in detail and evaluated with the measured data. Experimental data implies the existence of ambivalent region

where either of the phases can exist as continuous phase. None of the models discussed in the literature hints the very existence of such region. The exact mechanism for the existence of such region is still unclear. The phase inversion and viscosity prediction models discussed in the literature does not take into consideration about the effect of dispersed phase droplet size. This shall be the reason for over-prediction of oil holdup value at inversion point.

In three phase liquid-liquid-gas system, pressure drop experiments were restricted to slug flow and churn flow regimes and the results were presented. The flow regimes were identified by their distinct characteristics using high-speed photography technique. The slug flow regime is identified by the characteristic Taylor bubbles and the churn flow regime is identified using the characteristic up wash-downwash phenomenon postulated in the literature. The effects of liquid and gas superficial velocities on the components of pressure drop were examined and the results are presented. In slug flow regime, as the gas flow rate was increased, both frictional and hydrostatic pressure drop decreases and hence total pressure drop also decreases. However in churn flow regime, as the gas flow rate was increased, hydrostatic pressure drop decreases while frictional pressure drop tend to increase. This leads to an increase in total pressure drop too.

From the experimental results, it becomes evident that injection of third phase (air) does not necessarily decrease the total pressure gradient. Although in churn flow regime, injection of third phase decreases the hydrostatic gradient, the frictional pressure drop did not reduce. This is attributed to the increase in contact area between the liquid phase and gas phase, which increases the interfacial shear

stress eventually leading the increase in frictional pressure gradient. This aspect should be considered while designing gas lift wells.

5.2 Recommendations for future work

In the current work, the study was limited to upward vertical flow of two phase and three phase systems. The flow loop shall be slightly modified to conduct downward flow experiment as well. In the existing setup, instead of differential pressure transducer, two individual flush mounted pressure sensors could be utilized to capture the pressure drop signals. This would possibly eliminate the negative signals which arise due to the downward flow of thin annular film attached to the walls of the pipe.

Instead of T-junction, an inverted-Y junction can be used for better flow mixing with the third phase. In the current experimental setup, there was no control on the size of injected air bubble. This could be incorporated by using a ring type or needle type injector.

References

Abduvayt, P., Manabe, R., Watanabe, T., and Arihara, N. 2004. Analisis of Oil-Water Flow Tests in Horizontal, Hilly-Terrain, and Vertical Pipes. *In* SPE Annual Technical Conference and Exhibition.

Arirachakaran, S., Oglesby, K., Malinowsky, M., Shoham, O., and Brill, J. 1989. An analysis of oil/water flow phenomena in horizontal pipes, SPE Paper 18836, SPE Prof. *In* Prod. Operating Symp., Oklahoma.

Barbosa Jr, J., Govan, A., and Hewitt, G. 2001. Visualisation and modelling studies of churn flow in a vertical pipe. International journal of multiphase flow **27**(12): 2105-2127.

Bratland, O. 2010. Pipe Flow 2: Multi-phase Flow Assurance. Ove Bratland.

Brauner, N., and Ullmann, A. 2002. Modeling of phase inversion phenomenon in two-phase pipe flows. International journal of multiphase flow **28**(7): 1177-1204.

Brinkman, H. 1952. The viscosity of concentrated suspensions and solutions. The Journal of Chemical Physics **20**: 571.

Brown, R., Sullivan, G., and Govier, G. 1960. The upward vertical flow of air-water mixtures: III. Effect of gas phase density on flow pattern, holdup and pressure drop. The Canadian Journal of Chemical Engineering **38**(2): 62-66.

Davies, R., and Taylor, G. 1950. The mechanics of large bubbles rising through extended liquids and through liquids in tubes. Proceedings of the Royal Society of London. Series A. Mathematical and Physical Sciences **200**(1062): 375-390.

Descamps, M., Oliemans, R., Ooms, G., Mudde, R., and Kusters, R. 2006. Influence of gas injection on phase inversion in an oil–water flow through a vertical tube. International journal of multiphase flow **32**(3): 311-322.

Dukler, A., Wicks, M., and Cleveland, R. 1964. Frictional pressure drop in two-phase flow: B. An approach through similarity analysis. AIChE Journal **10**(1): 44-51.

Durst, F., Ray, S., Ünsal, B., and Bayoumi, O. 2005. The development lengths of laminar pipe and channel flows. Journal of Fluids Engineering **127**(6): 1154-1160.

Einstein, A. 1906. A new determination of molecular dimensions. Ann. Phys **19**(2): 289-306.

Farooqi, S., and Richardson, J. 1982. Horizontal flow of air and liquid (Newtonian and non-Newtonian) in a smooth pipe. Trans. Inst. Chem. Engrs **60**: 292-305.

Flores, J., Sarica, C., Chen, T., and Brill, J. 1998. Investigation of holdup and pressure drop behavior for oil-water flow in vertical and deviated wells. Journal of Energy Resources Technology-Transactions of The ASME **120**(1): 8-14.

Friedel, L. 1979. Improved friction pressure drop correlations for horizontal and vertical two-phase pipe flow. *In* European two-phase flow group meeting, Paper E. p. 1979.

Ghosh, R., and Cui, Z. 1999. Mass transfer in gas-sparged ultrafiltration: upward slug flow in tubular membranes. Journal of membrane science **162**(1): 91-102.

Govier, G., and Short, W.L. 1958. The upward vertical flow of air-water mixtures: II. Effect of tubing diameter on flow-pattern, holdup and pressure drop. The Canadian journal of chemical engineering **36**(5): 195-202.

Griffith, P., and Wallis, G.B. 1961. Two-phase slug flow. Journal of Heat Transfer (US) **83**.

Guth, E., and Simha, R. 1936. Untersuchungen über die viskosität von suspensionen und lösungen. 3. über die viskosität von kugelsuspensionen. Colloid & Polymer Science **74**(3): 266-275.

Haandrikman, G., Seelen, R., Henkes, R., and Vreenegoor, R. 1999. Slug control in flowline/riser systems. *In* Proc 2nd Int Conf: Latest Advances in Offshore Processing.

Hagedorn, A., and Brown, K. 1964. The effect of liquid viscosity in two-phase vertical flow. Journal of Petroleum Technology **16**(2): 203-210.

Hewitt, G., and Whalley, P. 1980. Advanced optical instrumentation methods. International Journal of Multiphase Flow **6**(1): 139-156.

Hinze, J. 1955. Fundamentals of the hydrodynamic mechanism of splitting in dispersion processes. AIChE Journal **1**(3): 289-295.

Hu, B., and Angeli, P. 2006. Phase Inversion and Associated Phenomena in Oil-Water Vertical Pipeline Flow. The Canadian Journal of Chemical Engineering **84**(1): 94-107.

J.Y.CAI, R.W.W., T.HONG W.P.JEPSON 1999. SLUG FREQUENCY AND LENGTH INCLINED LARGE DIAMETER MULTIPHASE PIPELINE. *In* Multiphase Flow and Heat Transfer Proc. of the Fourth International Symposium'.

Jana, A.K., Ghoshal, P., Das, G., and Das, P.K. 2007. An Analysis of Pressure Drop and Holdup for Liquid-Liquid Upflow through Vertical Pipes. Chemical engineering & technology **30**(7): 920-925.

Jayanti, S., and Hewitt, G. 1992. Prediction of the slug-to-churn flow transition in vertical two-phase flow. International journal of multiphase flow **18**(6): 847-860.

Kolmogorov, A. 1949. On the breakage of drops in a turbulent flow. *In* Dokl. Akad. Navk. SSSR. pp. 825-828.

Krieger, I.M., and Dougherty, T.J. 1959. A mechanism for non-Newtonian flow in suspensions of rigid spheres. Journal of Rheology **3**: 137.

Liu, H., Vandu, C.O., and Krishna, R. 2005. Hydrodynamics of Taylor flow in vertical capillaries: flow regimes, bubble rise velocity, liquid slug length, and pressure drop. Industrial & engineering chemistry research **44**(14): 4884-4897.

Lockhart, R., and Martinelli, R. 1949. Proposed correlation of data for isothermal two-phase, two-component flow in pipes. Chem. Eng. Prog **45**(1): 39-48.

Luo, Y., Chen, T., and Cai, J. 1997. Frictional pressure loss and phase inversion point for oil–water emulsion in vertical tube. *In* Proceedings of International Symposium on Multiphase Fluid non-Newtonian Fluid & Physico-Chemical Fluid Flows. pp. 3.53-53.58.

Meriem-Benziane, M., and Bou-Saïd, B. 2013. Determination of Friction Factor of Algerian Crude Oil During Flow in Pipe-lines. Flow Measurement and Instrumentation.

Mooney, M. 1951. The viscosity of a concentrated suspension of spherical particles. Journal of Colloid Science **6**(2): 162-170.

Mukherjee, H., Brill, J., and Beggs, H. 1981. Experimental study of oil-water flow in inclined pipes. Journal of Energy Resources Technology **103**: 56.

Müller-Steinhagen, H., and Heck, K. 1986. A simple friction pressure drop correlation for two-phase flow in pipes. Chemical Engineering and Processing: Process Intensification **20**(6): 297-308.

Nädler, M., and Mewes, D. 1997. Flow induced emulsification in the flow of two immiscible liquids in horizontal pipes. International journal of multiphase flow **23**(1): 55-68.

Orkiszewski, J. 1967. Predicting two-phase pressure drops in vertical pipe. Journal of Petroleum Technology **19**(6): 829-838.

Pal, R. 2000. Viscosity–concentration equation for emulsions of nearly spherical droplets. Journal of colloid and interface science **231**(1): 168-175.

Pal, R. 2001. Novel viscosity equations for emulsions of two immiscible liquids. Journal of Rheology **45**: 509.

Pal, R., and Rhodes, E. 1989. Viscosity/ Concentration Relationships for Emulsions. Journal of Rheology **33**: 1021.

Phan-Thien, N., and Pham, D. 1997. Differential multiphase models for polydispersed suspensions and particulate solids. Journal of Non-Newtonian Fluid Mechanics **72**(2): 305-318.

Poesio, P., and Beretta, G. 2008. Minimal dissipation rate approach to correlate phase inversion data. International Journal of Multiphase Flow **34**(7): 684-689.

Richardson, E. 1933. Über die Viskosität von Emulsionen. Kolloid-Zeitschrift **65**(1): 32-37.

Russell, T., Hodgson, G., and Govier, G. 1959. Horizontal pipeline flow of mixtures of oil and water. The Canadian Journal of Chemical Engineering **37**(1): 9-17.

Schmidt, Z., Brill, J., and Beggs, H. 1979. Choking can eliminate severe pipeline slugging. Oil and gas journal: 230-238.

Skogestad, S., and Havre, K. 1996. The use of RGA and condition number as robustness measures. Computers & chemical engineering **20**: S1005-S1010.

Storkaas, E., Skogestad, S., and Alstad, V. 2001. Stabilization of desired flow regimes in pipelines. *In* AIChE Annual Meeting.

Street, J.R., and Tek, M.R. 1965. Unsteady state gas-liquid slug flow through vertical pipe. AIChE Journal **11**(4): 601-607.

Taitel, Y., Bornea, D., and Dukler, A. 1980. Modelling flow pattern transitions for steady upward gas-liquid flow in vertical tubes. AIChE Journal **26**(3): 345-354.

Taylor, G.I. 1932. The viscosity of a fluid containing small drops of another fluid. Proceedings of the Royal Society of London. Series A **138**(834): 41-48.

Tek, M. 1961. SPE-001657-G-Multiphase Flow of Water, Oil and Natural Gas Through Vertical Flow Strings. Journal of Petroleum Technology **13**(10): 1029-1036.

Thien, N.P., and Tanner, R.I. 1977. A new constitutive equation derived from network theory. Journal of Non-Newtonian Fluid Mechanics **2**(4): 353-365.

Trononi, E. 1990. Prediction of slug frequency in horizontal two-phase slug flow. AIChE journal **36**(5): 701-709.

Ueda, T. 1958. Studies on the flow of air-water mixtures. Bull JSoc Mech Eng(1:): 139-145.

Vand, V. 1948. Viscosity of solutions and suspensions. I. Theory. The Journal of Physical Chemistry **52**(2): 277-299.

Wallis, G.B., and Dodson, J.E. 1973. The onset of slugging in horizontal stratified air-water flow. International Journal of Multiphase Flow **1**(1): 173-193.

Wilkens, R., and Jepson, W.P. 1996. Studies of multiphase flow in high pressure horizontal and+ 5 degree inclined pipelines. *In* Proc 6th Int Offshore and Polar Eng Conf. Los Angeles. pp. 139-147.

Xu, Z., Gayton, P., Hall, A., and Rambæk, J. 1997. Simulation study and field measurement for mitigation of slugging problem in The Hudson Transportation Lines. *In* BHR GROUP CONFERENCE SERIES PUBLICATION. MECHANICAL ENGINEERING PUBLICATIONS LIMITED. pp. 497-514.

Yeh, G.C., Haynie, F.H., and Moses, R.A. 1964. Phase-volume relationship at the point of phase inversion in liquid dispersions. AIChE journal **10**(2): 260-265.

APPENDICES

Appendix A: Experimental setup (top)

Appendix B: Experimental setup (bottom)

Appendix C: Pressure loss data sheet for non-return valve

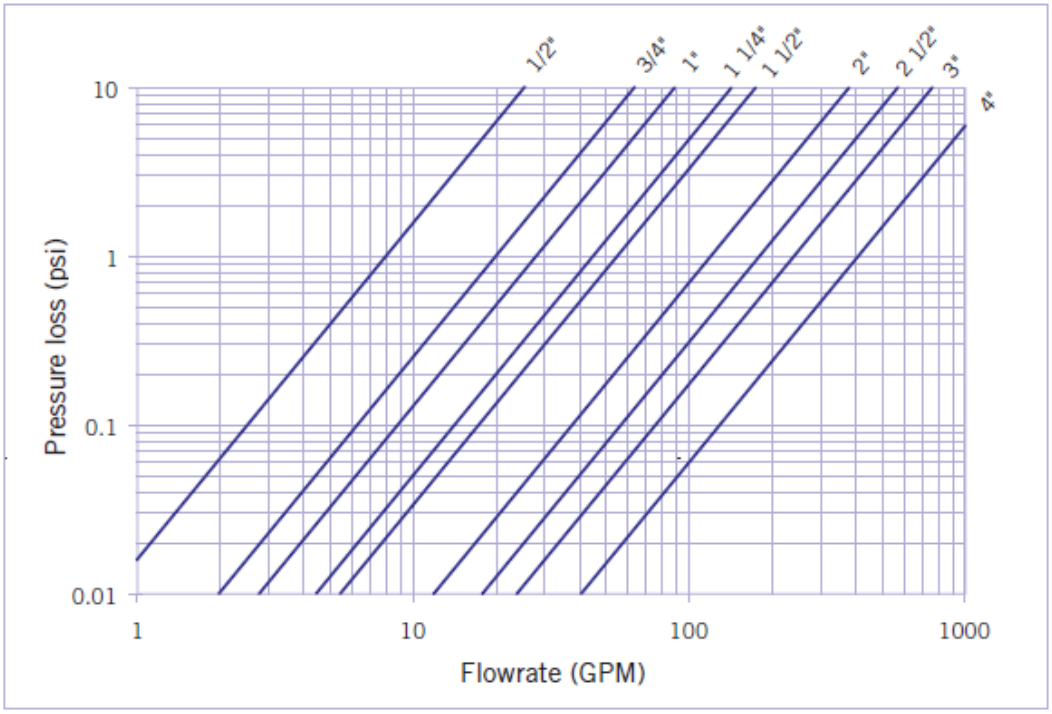

Appendix D: Moody's Chart

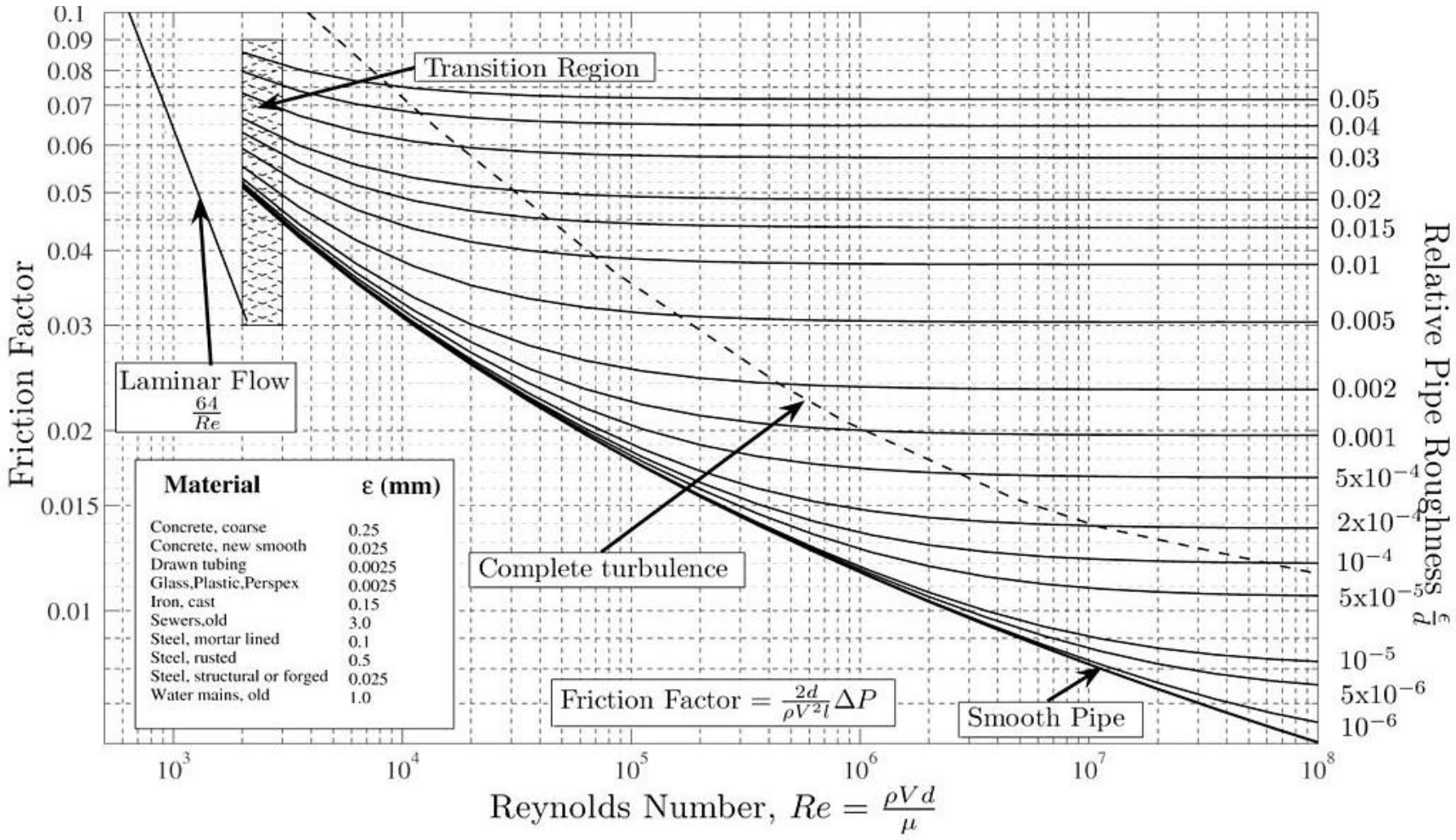

Appendix E: Time history of slug flow experiment (60% oil concentration; (a) V_{sg} = 0.339 m/s; (b) V_{sg} = 0.509 m/s)

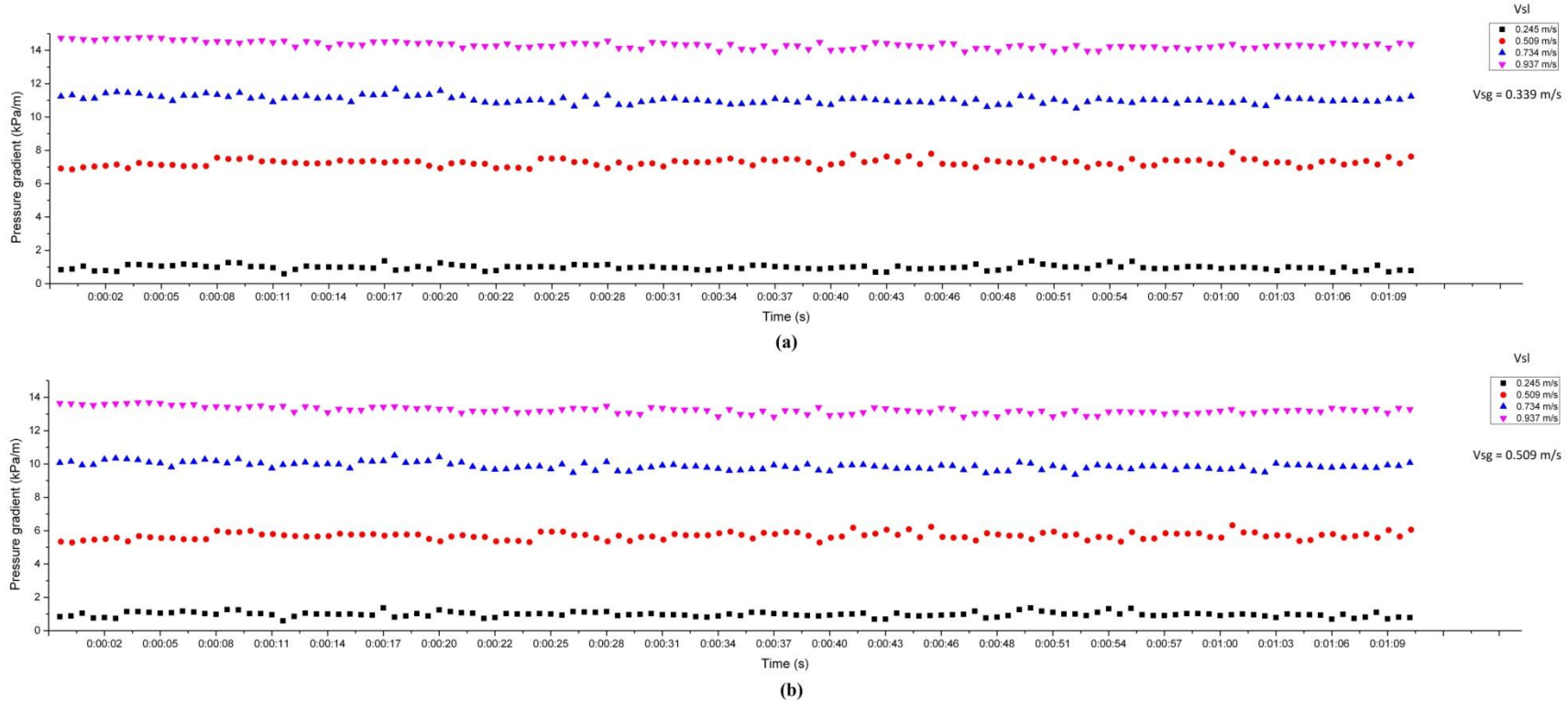

Appendix F: Time history of slug flow experiment (60% oil concentration; (a) V_{sg} = 0.679 m/s; (b) V_{sg} = 0.849 m/s)

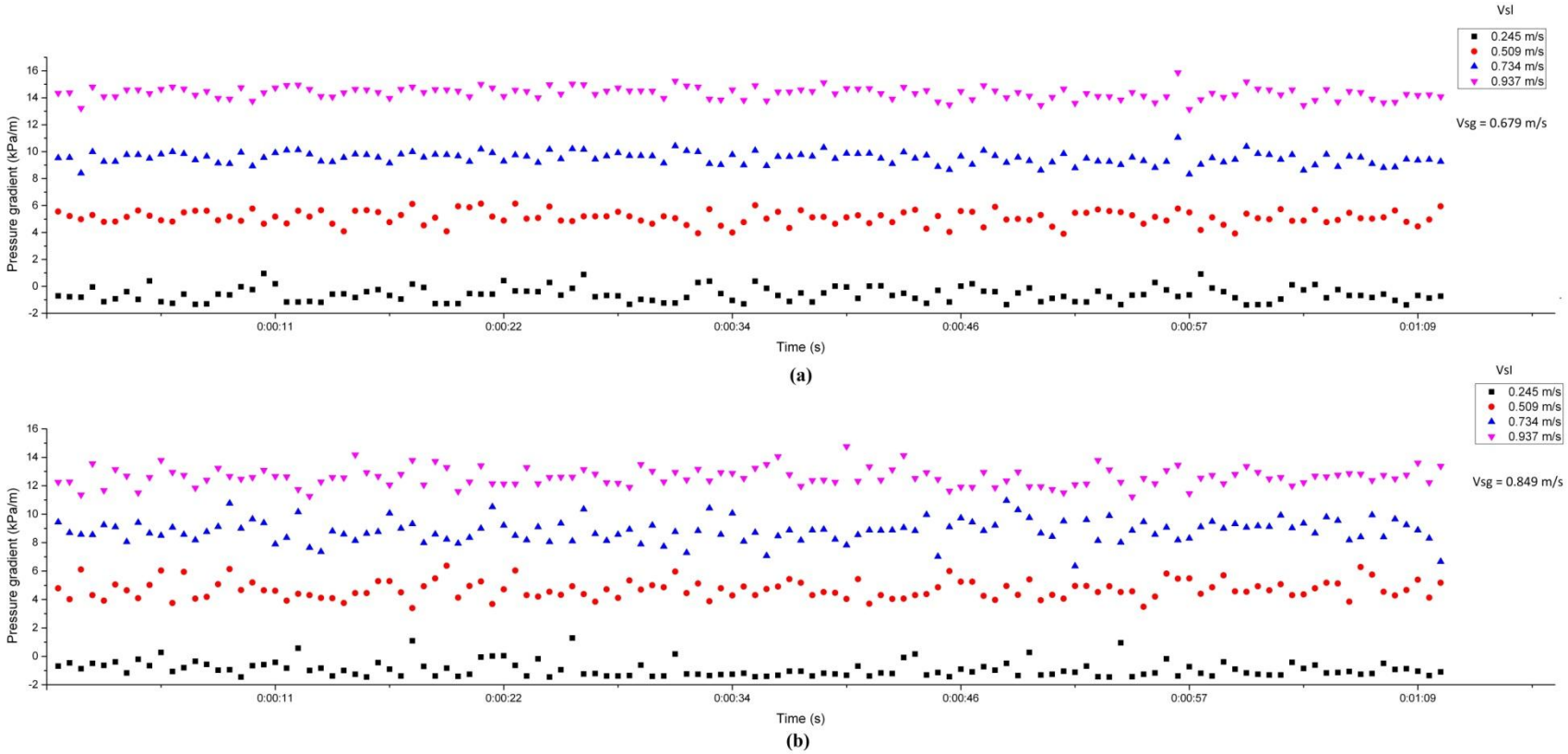

Appendix G: Time history of slug flow experiment (70% oil concentration; (a) V_{sg} = 0.339 m/s; (b) V_{sg} = 0.509 m/s)

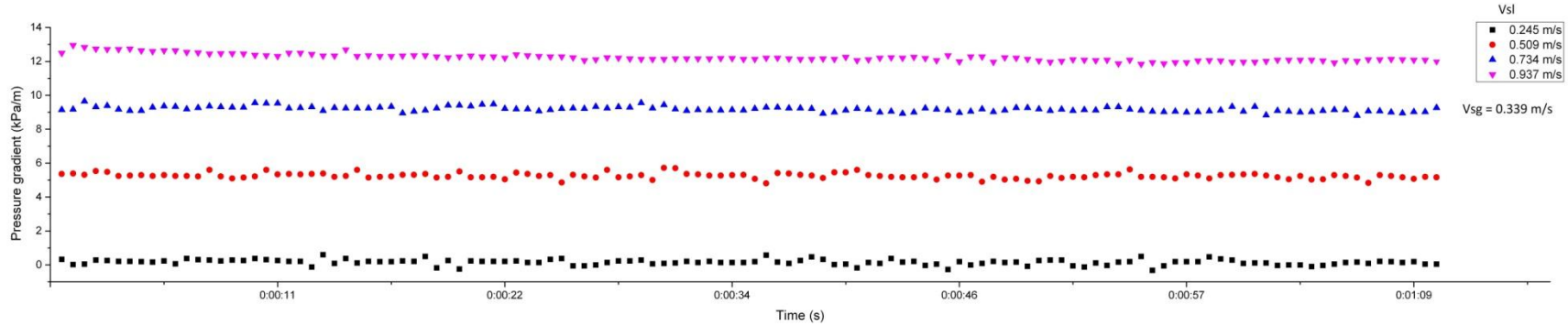

(a)

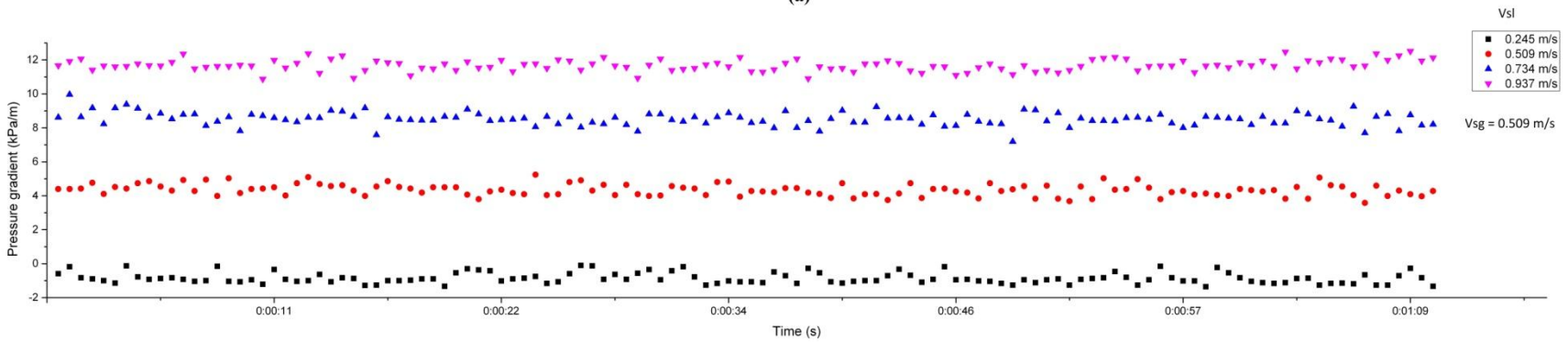

(b)

Appendix H: Time history of slug flow experiment (70% oil concentration; (a) V_{sg} = 0.679 m/s; (b) V_{sg} = 0.849 m/s)

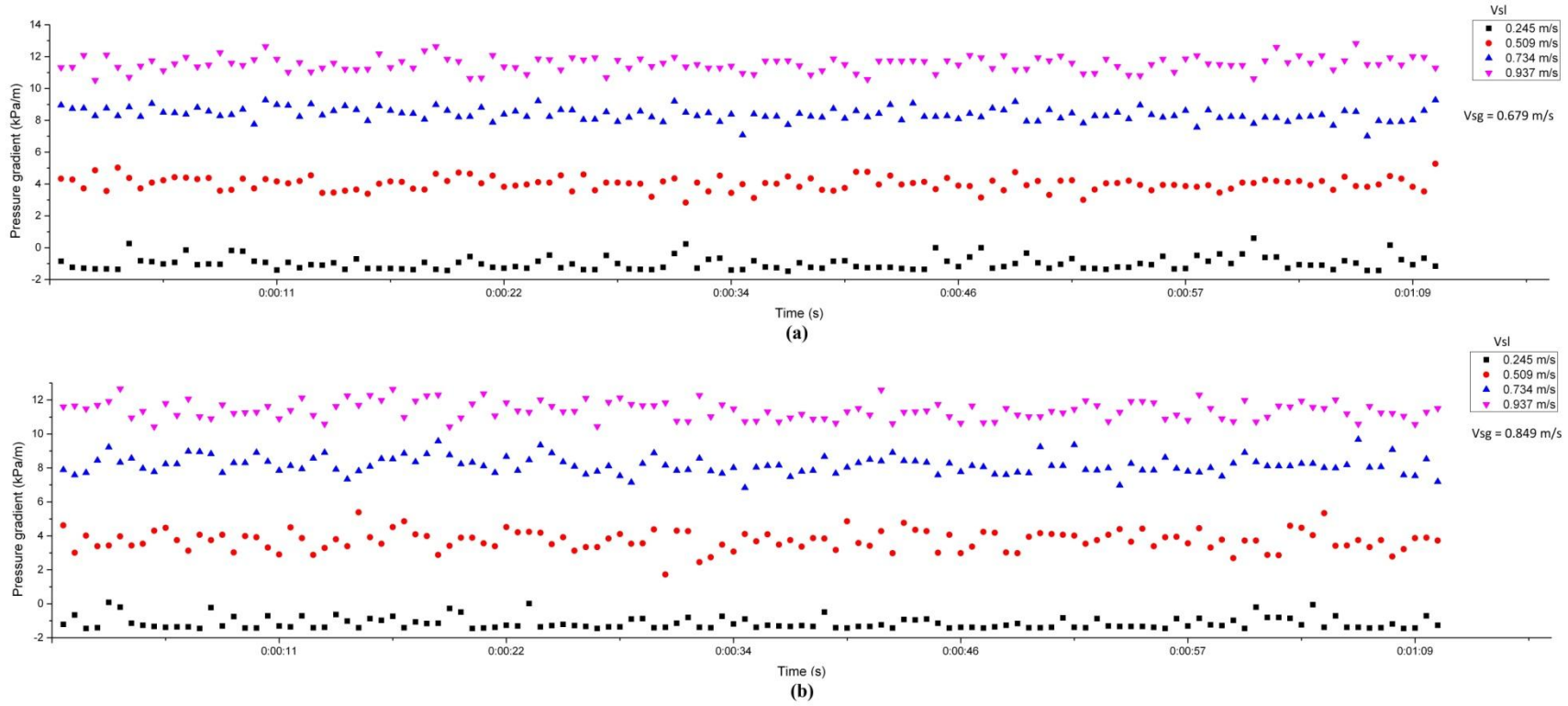

Appendix I: Time history of slug flow experiment (80% oil concentration; (a) V_{sg} = 0.339 m/s; (b) V_{sg} = 0.509 m/s)

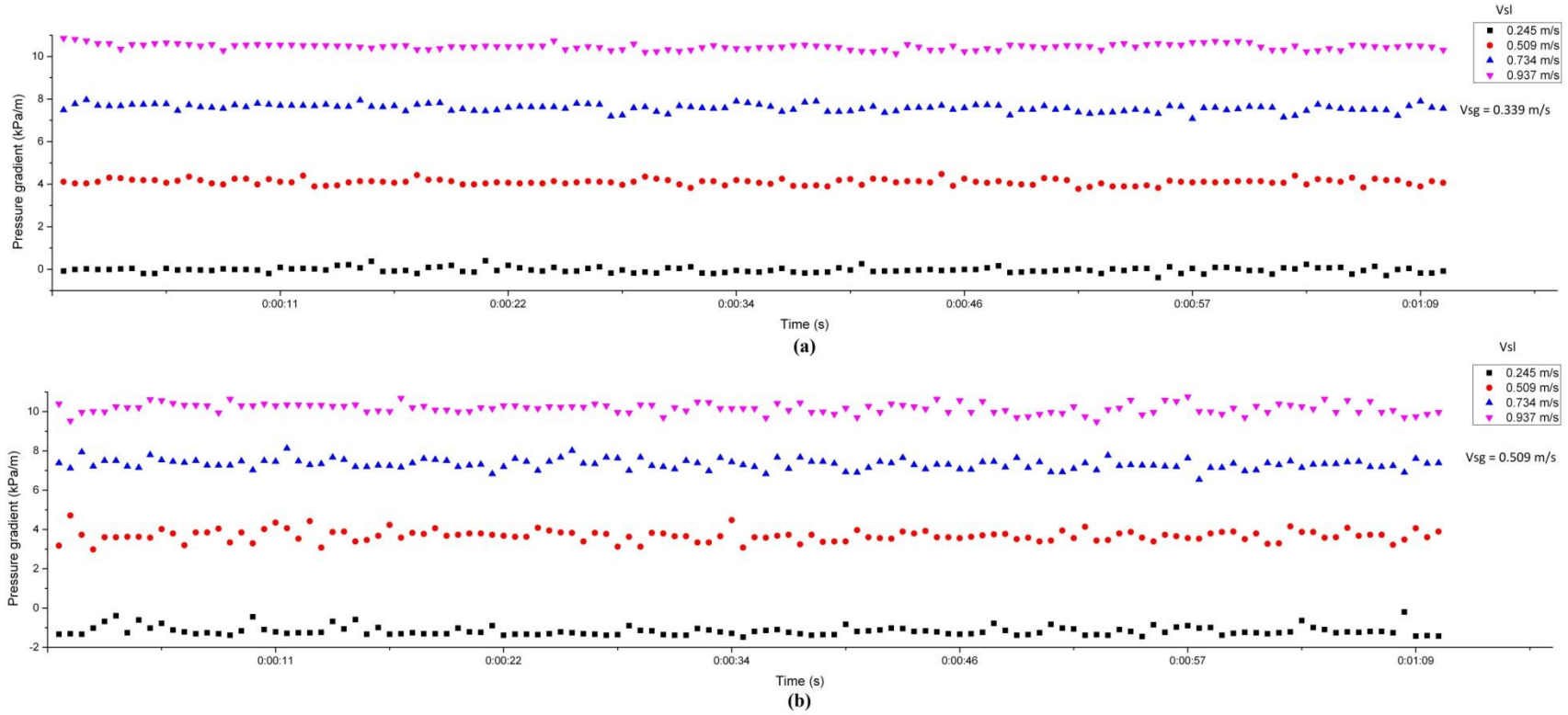

Appendix J: Time history of slug flow experiment (80% oil concentration; (a) V_{sg} = 0.679 m/s; (b) V_{sg} = 0.849 m/s)

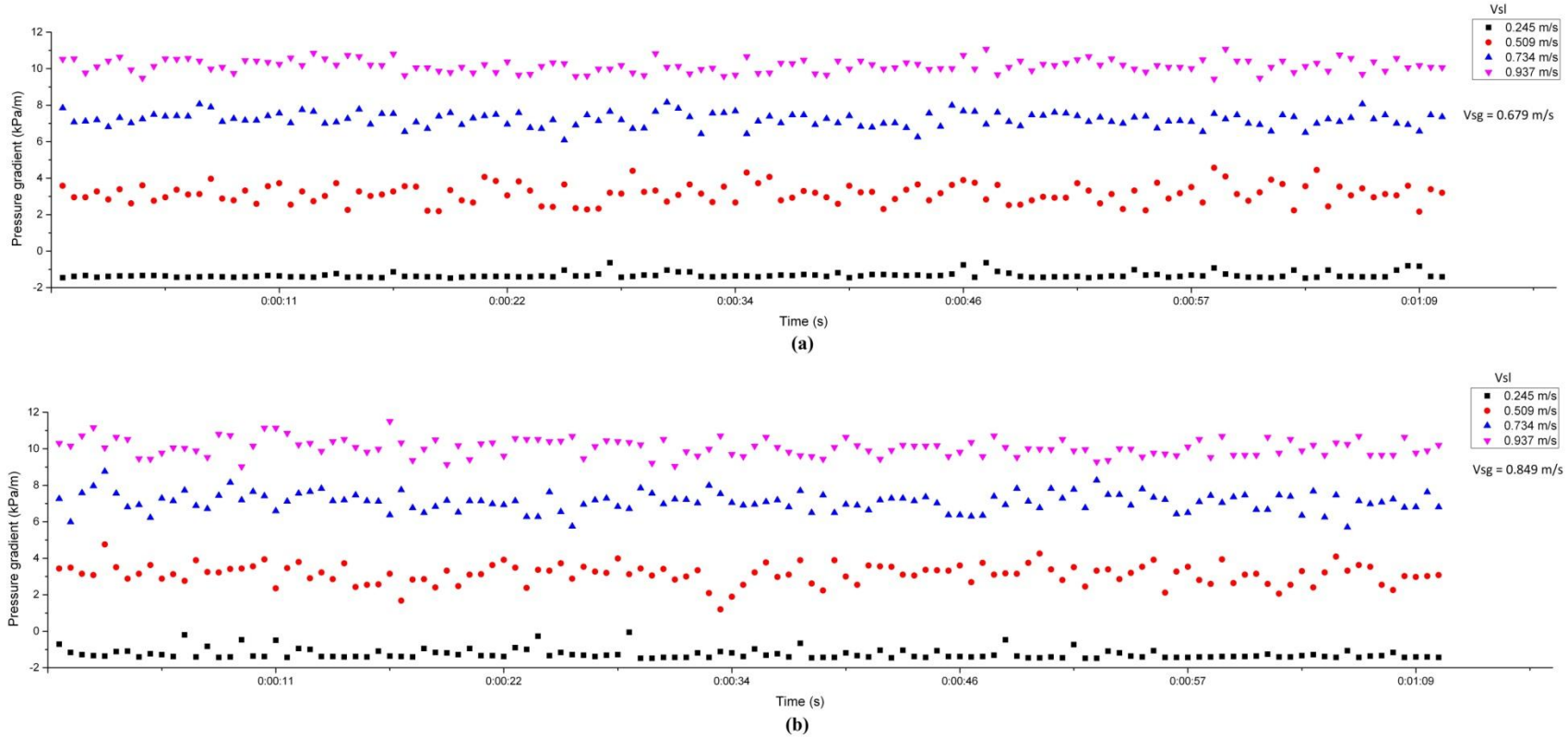

Appendix K: Time history of slug flow experiment (90% oil concentration; (a) V_{sg} = 0.339 m/s; (b) V_{sg} = 0.509 m/s)

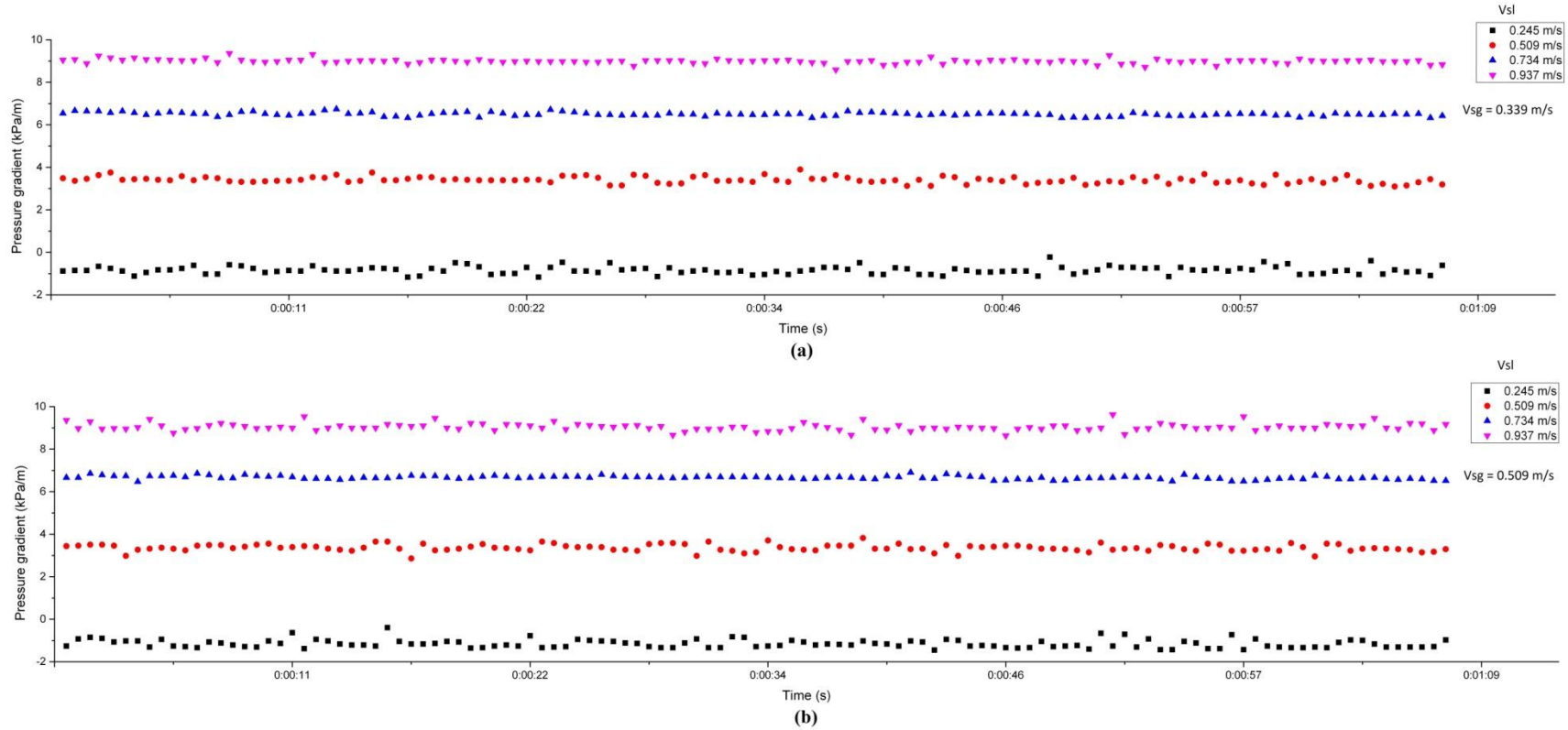

Appendix L: Time history of slug flow experiment (90% oil concentration; (a) V_{sg} = 0.679 m/s; (b) V_{sg} = 0.849 m/s)

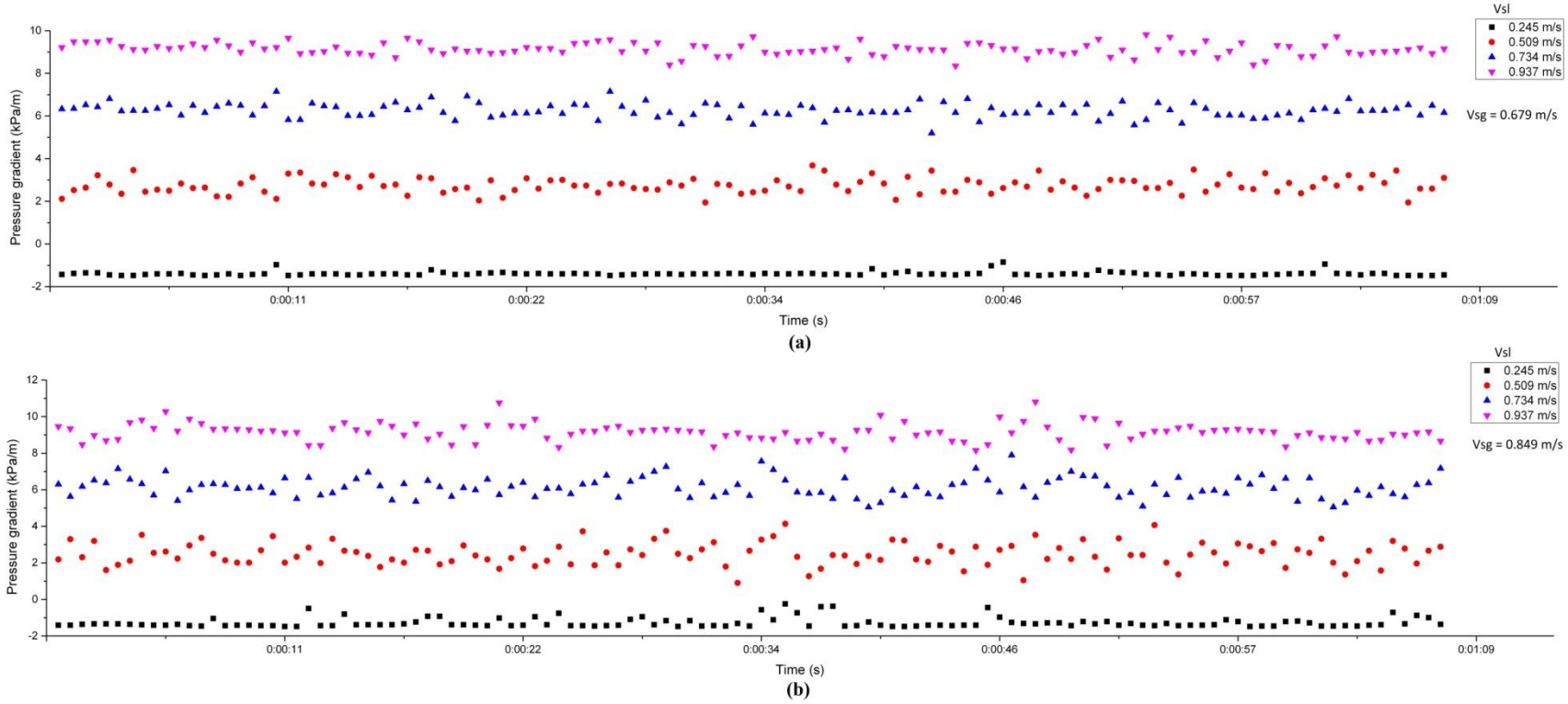

Appendix M: Time history of churn flow experiment (60% oil concentration; V_{sl} = 0.245 m/s (a) V_{sg} = 1.359 m/s; (b) V_{sg} = 2.038 m/s)

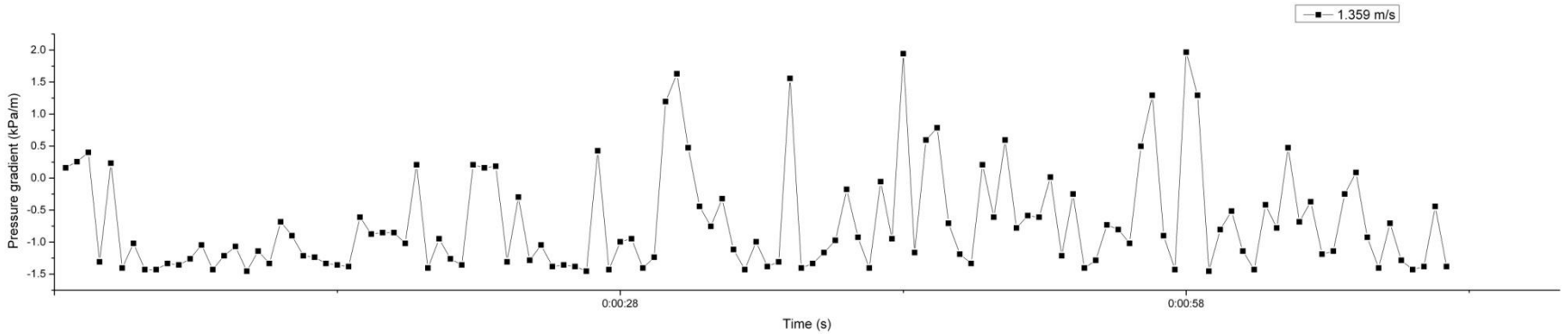

(a)

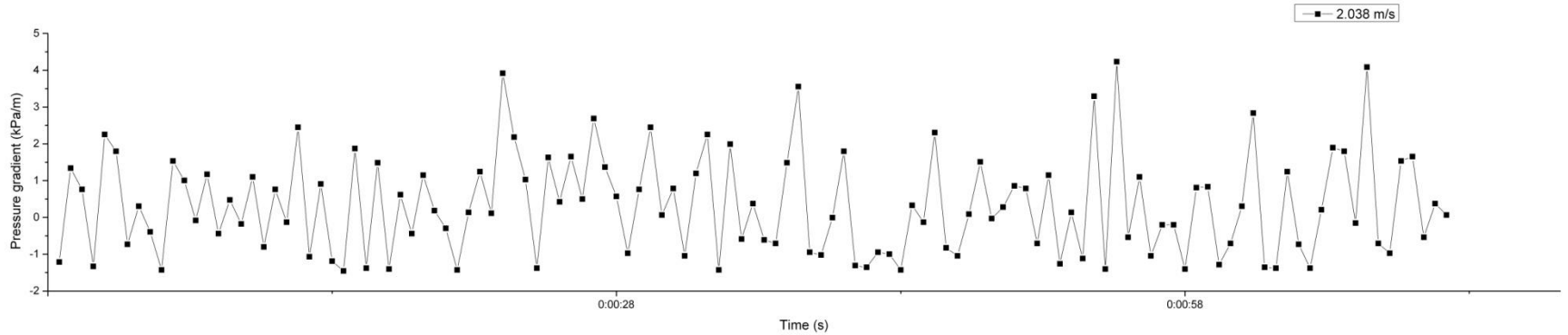

(b)

Appendix N: Time history of churn flow experiment (60% oil concentration; V_{sl} = 0.245 m/s (a) V_{sg} = 2.718 m/s; (b) V_{sg} = 3.397 m/s)

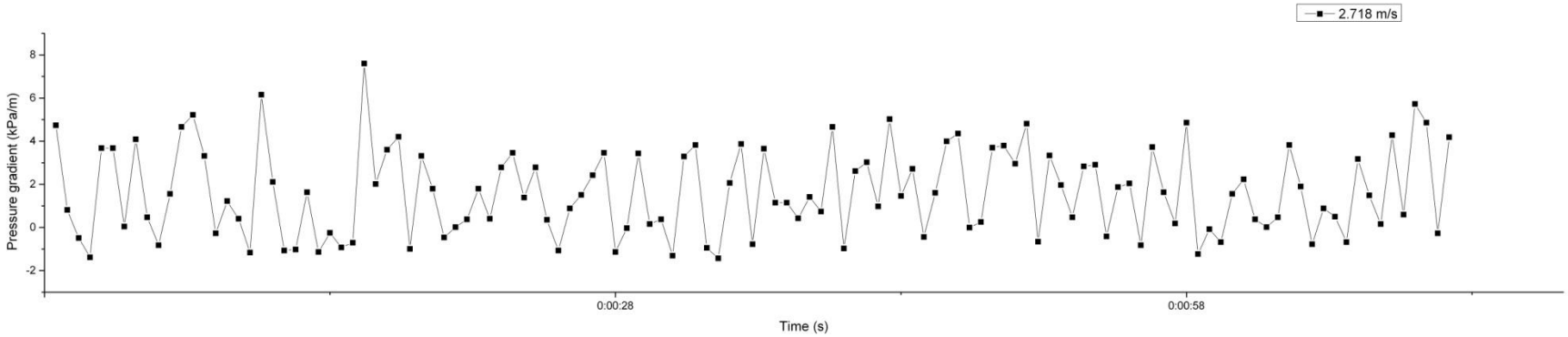

(a)

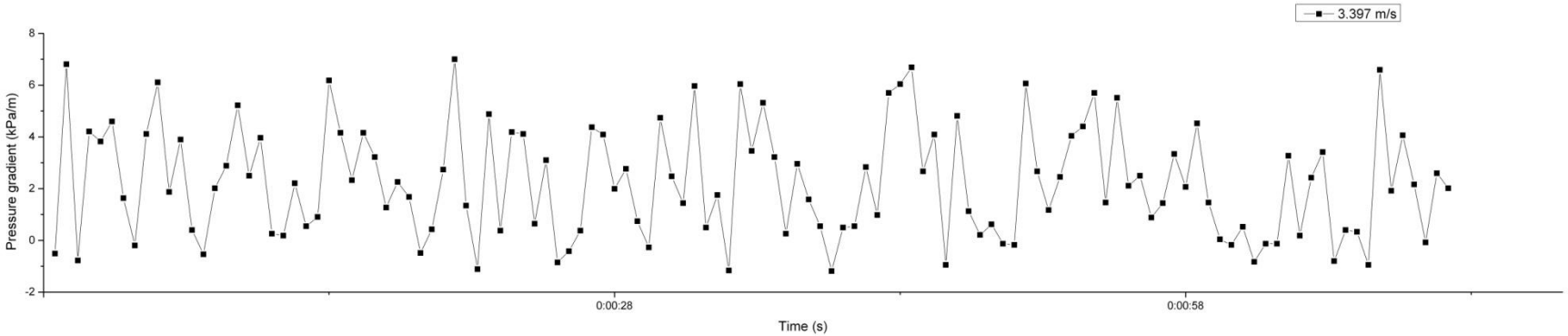

(b)